Cosmic Neutrinos as a Probe of TeV-Scale Physics

Dissertation
zur Erlangung des Doktorgrades
des Departments Physik
der Universität Hamburg

vorgelegt von
Markus Ahlers
aus Sögel

Hamburg
2006

Gutachter des Dissertation:	Dr. A. Ringwald
	Prof. Dr. J. Louis
Gutachter der Disputation:	Dr. A. Ringwald
	Prof. Dr. J. Bartels
Datum der Disputation:	06. 02. 2007
Vorsitzende des Prüfungsausschusses:	Prof. C. Hagner
Vorsitzender des Promotionsausschusses:	Prof. Dr. G. Huber
Dekan der Fakultät MIN:	Prof. Dr. A. Frühwald

Abstract

Ultra-high energy cosmic neutrinos are versatile probes of astrophysics, astronomy, and particle physics. They represent the messengers of hadronic processes in cosmic accelerators and survive the propagation through the interstellar medium practically unscathed. We investigate the neutrino fluxes associated with optically thin proton sources which provide a diagnostic of the transition between galactic and extragalactic cosmic rays. The center of mass energies in collisions of these cosmic neutrinos with atomic nuclei in the atmosphere or the Earth's interior easily exceed those so far reached in man-made accelerators. We discuss the prospects of observing supersymmetric neutrino interactions with Cherenkov telescopes and speculate about a neutrino component in extremely high energy cosmic rays from exotic interactions in the atmosphere.

Zusammenfassung

Ultrahochenergetische kosmische Neutrinos sind vielseitig einsetzbare Tester der Astrophysik, Astronomie und Teilchenphysik. Sie bilden die Boten hadronischer Prozesse in kosmischen Beschleunigern und bleiben praktisch unangetastet während ihrer Ausbreitung im interstellaren Medium. Wir untersuchen die Neutrinoflüsse in Verbindung mit optisch dünnen Quellen, anhand derer eine Diagnose bezüglich des Übergangs zwischen galaktischen und extragalaktischen kosmischen Strahlen erstellt werden kann. Die Schwerpunktsenergien in Kollisionen dieser kosmischen Neutrinos mit Atomkernen in der Atmosphäre oder im Erdinnern überschreiten spielend die bisher in Teilchenbeschleunigern erreichbaren Energien. Wir diskutieren die Aussichten, supersymmetrische Neutrinowechselwirkungen in Cherenkov-Teleskopen zu beobachten, und spekulieren über einen Neutrinobeitrag in extrem hochenergetischer Strahlung von exotischen Wechselwirkungen in der Atmosphäre.

Contents

I. Introduction

The Earth is constantly bombarded with a flux of particles causing nuclear reactions in the upper atmosphere. Most of these cosmic rays (CRs) consist of protons and light nuclei with a kinetic energy per nucleon of a few GeV and a total power density of about 1 Watt per square-kilometer. The most energetic of these particles initiate extended air showers of secondary particles which may even reach sea-level. Cosmic rays were first discovered by Victor Hess in 1912 measuring the ionization rate at high-altitude with balloon-borne experiments. Since then this natural source of high energy particle collisions has played an important role in the discovery of particles and as a source of unexpected phenomena even in the very recent past.

Historic examples are the discovery of the positron in 1932 and the muon in 1937 by cloud chamber experiments. The pions emerging in hadronic particle cascades were discovered later in 1947 with photo-plates located on top of high-altitude mountains in the Pyrenees and Andes. After recovery these plates revealed joint tracks of charged particles corresponding to the pion's decay chain $\pi^- \to \mu^- + \bar{\nu}_\mu \to e^- + \bar{\nu}_e + \nu_\mu + \bar{\nu}_\mu$. In the recent years, the effect of flavor oscillations have become apparent. The anisotropy of atmospheric muon neutrinos from zenith to nadir is interpreted as an oscillation between neutrino flavors induced by a mis-alignment of flavor and mass eigenstates [1]. These flavor oscillations provide also a solution for the deficit of solar electron neutrinos, which is the only flavor produced by nuclear fission processes in the Sun: Whereas the total flux of solar GeV-neutrinos is in good agreement with theoretical predictions [2], electron neutrinos contribute only about 1/3 of this amount [3].

High energy cosmic particles with energies from 10^6 GeV up to at least 10^{11} GeV interact with nuclei in the Earth's interior or atmosphere at center of mass energies above the TeV scale. This easily surpasses the energies so far attained by man-made accelerators. For comparison, the Large Hadron Collider (LHC) at CERN starting its operation in 2007 is designed for center of mass energies of about 14 TeV. The limitations of CR interactions as a particle laboratory arise from their fairly unclean initial state concerning their chemical composition, arrival direction, and flux normalization. Thus, the study of CR interactions is intrinsically tied to the study of their production, propagation and cosmic history.

The production mechanism of CRs, in particular those at *ultra-high energies* (UHE) exceeding 10^9 GeV is a source of many speculations. The energy of these particles is of the order of 1 Joule, a scale one usually encounters in macroscopic particle systems. Even if we succeed in modeling their production, limitations of their life-time in the cosmic environment require a close-by production. We may improve our picture of CRs if we also take into account other particle types associated with CR production and

propagation mechanisms, in particular photons and neutrinos. Taking this more general point of view, high energy CRs are just one particular type of messenger from the non-thermal Universe.

This *multi-messenger approach* is framed by experimental data and theoretical predictions and can be used in two directions. If our knowledge on secondary messenger fluxes is sufficient we may use this as an argument against a model hypothesis. The other way round, if the event statistics of one type of messenger is fairly bad one may use multi-messenger data to improve the predictions. This is typically done for neutrinos, which have a feeble interaction with matter over a wide range of neutrino energies together with a large background from secondary processes. If neutrinos are associated with the production and propagation of UHE CRs we may derive model dependent predictions by the normalization to CR data. Guided by this multi-messenger approach we derive in this thesis neutrino fluxes associated with CR production. Based on these neutrino fluxes we then investigate the prospects of new physics contributions in neutrino-nucleon interactions.

The thesis is organized as follows. Chapter II discusses neutrino fluxes associated with CR production. As a preparation we present a brief overview on the spectrum of UHE CRs in section II.1 discussing various aspects of their production (Sec. II.1.1), propagation (Sec. II.1.2), and observation (Sec. II.1.3) and experimental ambiguities at the highest energies (Sec. II.1.4). This also provides the necessary tools and ideas for the subsequent section II.2 where we discuss the "low crossover" scenario, a particular model for CRs above 5×10^8 GeV using extragalactic proton sources. We repeat the analysis of our Ref. [4] and provide further insight in model dependencies regarding variations w.r.t. CR data samples and their calibrations. The results are applied in section II.3 in the discussion of the flux of neutrinos from optically thin proton sources (Secs. II.3.1 and II.3.2) and cosmogenic neutrinos (Secs. II.3.3), which we compare with experimental upper limits in section II.3.4.

In chapter III we then use these neutrino fluxes motivated by the multi-messenger analysis for predictions of neutrino-induced events in various extensions of the Standard Model (SM). As a warm-up we discuss the neutrino-nucleon interactions of the SM in section III.1. After a brief introduction of the parton model we compare our calculation of charged and neutral current interactions with results stated in the literature (Secs. III.1.1 and III.1.2). We conclude this section with a short overview of detection methods relevant for the discussion of UHE neutrinos.

Following our Ref. [5] (see also Ref. [6]) we will apply these methods in section III.2 to supersymmetric (SUSY) neutrino-nucleon interactions. In $\mathcal{R}$-parity conserving SUSY extensions of the SM there exists a stable lightest SUSY particle (LSP) and the next-to-lightest SUSY particle (NLSP) may be long-lived (Sec. III.2.1). We focus on the production of a stau NLSP, the scalar SUSY partner of the tau, (Sec. III.2.2) and its energy loss properties in matter (Sec. III.2.3). We discuss the signals of these type of SUSY events in the context of Cherenkov telescopes in section III.2.4 and compare this with the prospects of their detection at the LHC in section III.2.5.

The last section III.3 is devoted to more speculative interactions. We give a brief review on exotic models of neutrino interactions which may have a branching ratio comparable to or even larger than SM predictions (Sec. III.3.1). This discussion is guided by the idea that neutrinos may contribute to events beyond the Greisen-Zatsepin-Kuzmin cutoff [7, 8] (Sec. III.3.2). Qualitatively, this requires a rapid rise in the neutrino-nucleon cross section to nucleonic values of a few milli-barn. We have studied this idea on a quantitative level in Ref. [9] (see also Ref. [10, 11, 12]) by a statistical comparison of CR data and neutrino upper limits with event rates predicted by strongly interacting neutrinos. In addition, we will show the results on variations of the fit w.r.t. CR data samples, normalization, energy calibration, neutrino fluxes and close-by CR sources (Sec. III.3.3).

As a support for the reader we provide brief summaries of the results and further steps at the end of each section. Our final conclusions and outlook are then given in chapter IV. Unless otherwise stated or obvious from the context we use natural units with $c = \hbar = k_B = 1$.

II. Cosmic Neutrino Sources

1. Cosmic Rays

The spectrum of cosmic rays (CRs) follows a remarkably featureless power-law $\propto E^{-\gamma}$ over several orders of magnitude. The small changes in the power index γ are conveniently visualized taking the product of the flux with some power of the energy. In this case the spectrum reveals a leg-like structure as it is sketched in Fig. II.1 (from Ref. [13]). The anatomy of this "cosmic leg" – its changes in slope, mass composition or arrival direction – reflects the various aspects of CR propagation, production and source distribution. In the following paragraphs we will give a brief overview of characteristic features in the CR spectrum above 1 PeV and their possible relation to astrophysical aspects (for reviews see e.g. [14, 15, 16, 17, 18]).

A steepening of the spectrum from $\gamma \approx 2.7$ to $\gamma \approx 3.1$ at the energy $E_{\rm kn} \approx 3 \times 10^6$ GeV is known as the cosmic *knee*. Measurements from the KASCADE [19] and EAS-TOP [20] experiments indicate that this feature of the spectrum is composed of the subsequent fall-off of galactic nuclear components with maximal energy $Z \times E_{\rm kn}$. This scaling with the atomic number Z can be understood in terms of the maximal energy a charged particle may attain in a magnetically confining cosmic accelerator according to its Larmor Radius, which is inversely proportional to the particle's charge. We will discuss this in more detail in section II.1.1. If this interpretation holds the galactic contribution in CRs can not extend much further than 10^8 GeV assuming iron ($Z = 26$) as the heaviest component [21]. However, the observational data at these energies is inconclusive and the end-point of galactic CRs has not been pinned down so far. The continuation of observation and future experiments like KASCADE-Grande [22] and IceTop [23] are expected to clarify this issue.

The *second knee* is a further steepening of the spectrum from $\gamma \approx 3.1$ to $\gamma \approx 3.3$ at the energy $E_{\rm 2kn} \approx 5 \times 10^8$ GeV. This small break in the data could indicate the on-set of an extragalactic dominance in CRs. This interpretation is fueled by recent measurements from the HiRes Collaboration [24] which seem to indicate a composition change at the second knee from about 50% protons just below to 80% protons just above. Extragalactic CRs are subject to collisions with the interstellar medium during their propagation over cosmological distances. Depending on the initial chemical composition these particle specific interactions will be imprinted in the spectrum observed on Earth. We will discuss the corresponding energy loss effects of extragalactic proton sources in section II.1.2.

The *ankle* at $E_{\rm ank} \approx 3 \times 10^9$ GeV is a flattening in the spectrum from $\gamma \approx 3.3$ to $\gamma \approx 2.7$. It has been shown [25] (see also Refs. [26, 27, 4, 28]) that this feature could result from

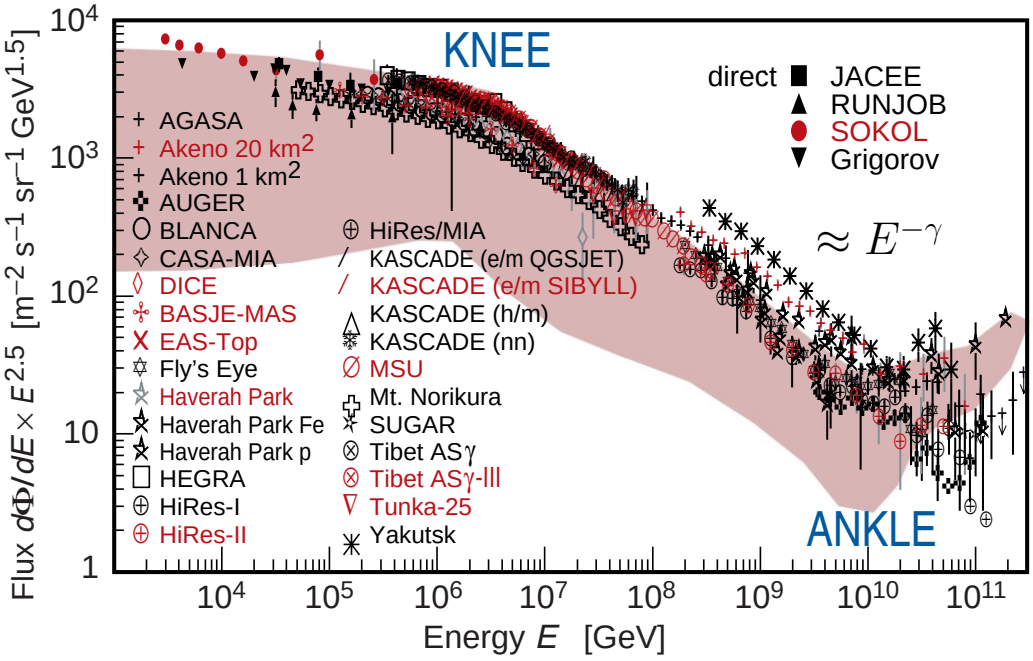

Figure II.1: *The "Cosmic Leg" provided by Ref. [13] (modified for illustration). The flux of CRs is multiplied by $E^{2.5}$.*

inelastic collisions of extragalactic protons in the cosmic microwave background (CMB). In this case the ankle can be identified as a *dip* from e^+e^- pair production together with a *pile-up* of protons from pion photo-production. A statistical test shows that the CR spectrum between 10^9 GeV and 4×10^{10} GeV is in excellent agreement with a propagated flux of extragalactic protons using a simple injection spectrum of their sources with only two free parameters [25]. This can be taken as a further evidence for the on-set of proton-dominance in the CR spectrum in the region of the 2nd knee: Heavier candidates like helium or iron have different energy loss properties in the CMB and will in general not reproduce the spectral features [29]. A crossover at larger energies towards the ankle is feasible and would allow for a more general mass composition of extragalactic CRs (*e.g.* Ref. [30, 31]). This requires, however, an extension of galactic CRs by three orders of magnitude beyond the knee and might be in conflict with the interpretation of a universal rigidity cutoff.

In any case, the large-scale isotropy [32, 33] of CRs above 10^9 GeV - so called *ultra high energy* (UHE) CRs - is a strong evidence that an extragalactic component is dominating above the ankle.[1] Soon after the discovery of the CMB in 1965 it was pointed out by Greisen [7], Zatsepin, and Kuzmin [8] (GZK) that resonant pion photo-production of extragalactic protons above about 5×10^{10} GeV limits their propagation range to less than 50 Mpc. For heavier nuclei, photo-disintegration in the CMB gives a comparable or even stronger attenuation above this energy. Hence, the presence of extragalactic

[1] We follow the notation of Ref. [18] and use the term "ultra high energy" for $E > 10^9$ GeV and "extremely high energy" for $E > 10^{11}$ GeV.

UHE CRs should be reflected by an effective *GZK cutoff* in the spectrum, irrespective of the particular CR production mechanism. So far the experimental resolution of this feature is limited by the low event statistics and systematic uncertainties in energy calibration. Different experiments seem to imply conflicting results w.r.t. a continuation of the spectrum beyond the GZK cutoff and the appearance of small-scale clustering of events. We will comment on the experimental results in more detail in section II.1.4.

1.1. Production

"Bottom-Up" Scenarios

The production mechanism of UHE CRs is still an open question. For an effective electro-magnetic acceleration charged particles have to encounter large potential drops, but since the interstellar medium is mostly ionized, *i.e.* a good conductor it should short-circuit any potential difference immediately [17]. In fact, in the magneto-hydrodynamical description of cosmic plasma each infinitesimal volume element does not see any electric field in its own rest frame. One possible exception to this "no-go" argument is *Fermi acceleration* of charged particles by repeated encounters with plasma shocks in astrophysical environments (*1st order*) or with interstellar magnetic clouds (*2nd order*). This process is analogous to the acceleration principle of man-made cyclotrons where a particle gains its energy gradually in a storage ring. We will give a brief description of these mechanisms in the following paragraphs.

Fermi's original version of CR acceleration – so-called *2nd order Fermi acceleration* in modern terms – is based on the idea that charged particles bounce off moving magnetic inhomogeneities, acting as magnetic mirrors, which may appear in interstellar molecular clouds. The right panel of Fig. II.2 shows a sketch of these encounters. The collisionless scattered particle will gain energy in a head-on collision ($\theta > \pi/2$) and lose energy by tail-end ($\theta < \pi/2$) scattering. The net increase of its energy is a statistical effect: averaging over θ and θ' the particle will gain energy $\Delta E/E$ proportional to β^2_{cloud}, the square of the velocity of the magnetic cloud in the isotropic reference frame of the ensemble [15]. This model is very similar to a thermodynamical system of two gases, which tries to come into thermal equilibrium [17]. Correspondingly, the spectrum of CRs should follow a thermal spectrum which might be in conflict with the observed power-law. Also, due to its dependence on $\beta^2_{\text{cloud}} \ll 1$ this mechanism might not be efficient on realistic acceleration time scales.

A more efficient acceleration may occur in astrophysical environments like supernova remnants (SNR). In a simplified version one may consider a non-relativistic shock traveling through plasma with some speed $v = c\beta_{\text{shock}}$ as sketched in the left panel of Fig. II.2. Seen from the rest frame of the shock the downstream plasma with low density ρ_{down} enters the shock with velocity $v_{\text{down}} = v$ and exits it into the upstream region with higher density ρ_{up}. The exit velocity is determined by particle conservation, *i.e.* $\rho_{\text{up}} v_{\text{up}} = \rho_{\text{down}} v_{\text{down}}$, and is smaller than the shock velocity: $v_{\text{up}} < v_{\text{down}} = v$. As a result,

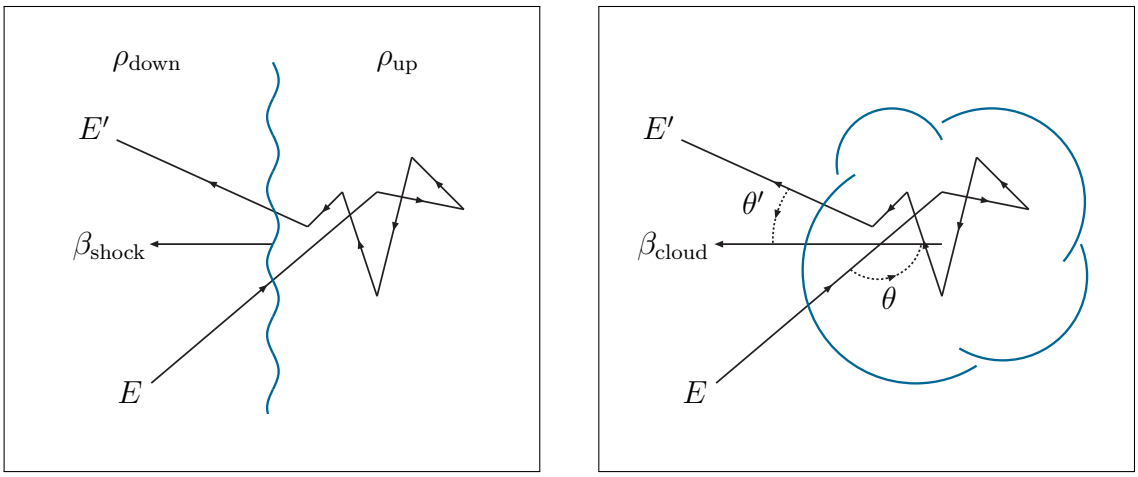

Figure II.2: *A sketch of 1st and 2nd order Fermi acceleration by scattering off plasma shocks (right) and magnetic clouds (left), respectively.*

particles in the rest frame of the upstream region see particles from downstream moving towards the shock boundary with velocity $v - v_{\text{up}}$ and vice versa. If a charged particle diffuses across the shock boundary from one side it will bounce back into its region from head-on collisions with magnetic mirrors. This process is repeated each time the particle crosses the plasma shock front.

As in the case of 2nd order Fermi acceleration the net increase of the energy will be a result of a statistical process. In this model the encounter with the plasma shock is always in head-on collision ($\theta > \pi/2$ and $\theta' > \pi/2$ and following cycles) and it turns out that the average energy gain depends linearly on β_{shock}. Hence, this so-called *1st order Fermi acceleration* is expected to be a much more efficient way to accelerate particles. In addition, the CR spectrum does not necessarily follow a thermal spectrum. However, a realistic description of plasma shock acceleration is complicated due to the effects of the shock geometry, back-reaction of the particles, relativistically moving shocks and questions concerning the creation and orientation of the magnetic inhomogeneities [18].

Other candidate accelerators may be searched for in astrophysical environments which cannot be described by the laws of magnetohydrodynamic. This may be the case for *pulsars*, rapidly rotating neutron stars with strong magnetic fields, or rotating accretion disks threaded by magnetic fields [14, 16]. The pulsar acts like a disc dynamo in its magnetic field where charged particles are pulled towards the pole due to their orbital motion. Such an environment may act analogously to a van der Graaf accelerator where a charged particle receives its energy by one large potential drop. Other suggestions for *one-shot* accelerators are magnetars and magnetic reconnections. The latter is thought to be the driving mechanism for solar flares. [17]. Again, it is unclear, how the observed power law spectrum may emerge from this kind of accelerators.

Remarkably, it is possible to give an estimate for the maximal energy a particle may gain in such environments from simple geometric arguments. For the efficiency of a "cosmic cyclotron" particles have to be confined in the accelerator by its magnetic field

B over a sufficiently long time scale compared to the characteristic cycle time. The Larmor radius of a particle with charge Z increases with its energy E according to

$$\left(\frac{R_{\mathrm{Larmor}}}{1\,\mathrm{kpc}}\right) \approx 1.1\,\frac{1}{Z}\left(\frac{E}{10^9\,\mathrm{GeV}}\right)\left(\frac{B}{1\,\mu\mathrm{G}}\right)^{-1} \quad . \tag{II.1}$$

Clearly, the maximal energy is limited by the case when the Larmor radius encounters the characteristic radial size R_{source} of the source. In fact, one can derive a stronger bound which takes into account the velocity of the scattering centers β. According to Ref. [34] this gives a maximal energy of

$$\left(\frac{E_{\mathrm{max}}}{10^9\,\mathrm{GeV}}\right) \approx 0.9\,\beta\,Z\left(\frac{B}{1\,\mu\mathrm{G}}\right)\left(\frac{R_{\mathrm{source}}}{1\,\mathrm{kpc}}\right) \quad . \tag{II.2}$$

This limitation in energy is conveniently visualized by the "Hillas plot" [14] shown in Fig. II.3 (from Ref. [35]) where the characteristic magnetic field B of candidate cosmic accelerators is plotted against their characteristic size R. The contours of constant maximal energy (assuming $\beta = 1$) are given by dash-dotted lines according to Eq. (II.2). Also shown by solid curves are upper limits of realistic sources taking into account energy losses from synchrotron radiation and interactions in the CMB, which will be discussed in more detail in the following sections. It turns out that Eq. (II.2) is even applicable as an order of magnitude estimate for the case of one-shot accelerators. In the case of a pulsar R_{source} is the radius of the neutron star and β the velocity of its outer layers.

An attractive feature of Fermi acceleration is its prediction of a power-law flux of CRs with, typically, $\gamma \gtrsim 2$. If the energy gain of a particle per time is proportional to its energy, $\dot{E} = E/t_{\mathrm{gain}}$, and if the loss of particles from the acceleration region is proportional to their number, $\dot{N} = N/t_{\mathrm{loss}}$ than it is straightforward to see that $\mathrm{d}N/\mathrm{d}E \propto E^{-\gamma}$ with $\gamma = 1 + t_{\mathrm{gain}}/t_{\mathrm{loss}}$. For relativistic plasma shocks one finds $\gamma \approx 2$, for slower shock centers $\gamma > 2$. The steeply falling spectrum of CRs with $\gamma \approx 3$ seems to disfavor relativistically moving plasma shocks. In addition, the encounters of magnetic clouds (2nd order Fermi acceleration) with different velocities will distort this spectrum. However, for the comparison of these injection spectra with the flux of CRs observed on Earth one has to consider particle interactions in the source and in the interstellar medium. This can have a great impact on the shape as we will discuss in the next section.

It is currently believed that SNRs with shock velocities $\beta \approx 0.03$ are the origin of galactic CRs up to the knee at 3×10^6 GeV depending on charge. The necessary energy budget could be achieved by three SNe per century with a conversion of 1/6 of the energy into CRs [36]. The scaling of containment with charge could explain the subsequent falloff of different atomic nuclei at the knee with cutoff $E_{\mathrm{max}} = Z \times 3 \times 10^6$ GeV. There are only very few astrophysical sources that have the necessary properties to accelerate particles to energies above the ankle as can be seen from Fig. II.3 (see e.g. Ref. [37] for a review). So far none of the candidate sources have been confirmed.

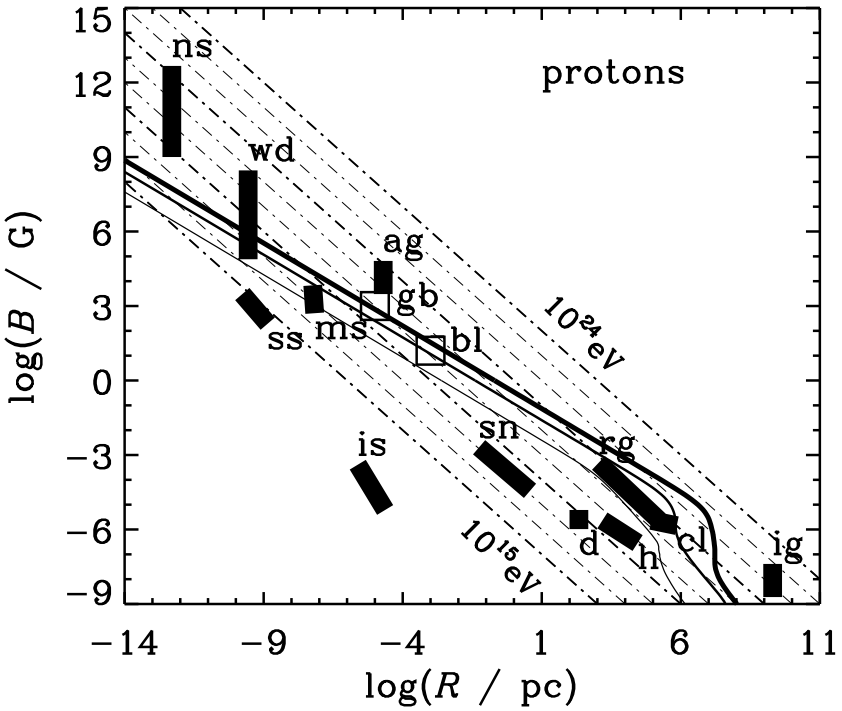

Figure II.3: *The "Hillas plot" (from Ref. [35]) for protons ($Z = 1$): The dashed-dotted lines refer to different maximal energies of an accelerated proton from Eq. (II.2) assuming a source with characteristic size R, magnetic field B, and shock velocity $\beta = 1$. The solid curves correspond to an upper limit of plausible sources considering scattering effects in the CMB and synchrotron losses explained in section II.1.2. The candidate sources are: neutron stars (ns), white dwarfs (wd), sunspots (ss), magnetic stars (ms), active galactic nuclei (ag), interstellar space (is), supernova remnants (sn), galactic disk (d), halo (h), radio galaxy lobes (rg), clusters of galaxies (cl) and intergalactic medium (ig). Also shown as open squares are jet-frame parameters for blazers (bl) and gamma ray bursts (gb).*

"Top-Down" Scenarios

The models described in the previous section used conventional physics, *i.e.* collective electro-magnetic interactions of particles to accelerate nuclei. Instead, UHE CRs could be produced by the decay or annihilation of topological defects or super-heavy dark matter particles. In this case the energy of the fragments will only be limited by the mass of the initial particle which can easily lie beyond the GZK cutoff.

Grand unified theories (GUTs) extend the local gauge symmetry of the Standard Model (SM) by embedding it into a higher dimensional gauge group. The reduction to the SM may proceed by a phase transition of a Higgs scalar to a vacuum configuration, which breaks a part of the symmetry. Topological defects are the result of a mis-alignment of the continuous Higgs field in theories with topologically non-trivial vacuum manifolds. Depending on the GUT breaking scheme these defects can be monopoles, (cosmic) strings, domain walls or textures, or combinations of these (see e.g. Refs. [38, 18] for a review).

Topological defects could be formed in a phase transition of the hot early Universe or non-thermally in the preheating stage after inflation [39, 40]. The energy density

of the defect, associated with "trapped" quanta of massive gauge and Higgs fields, is thereby larger than in the symmetry breaking configuration and may be released by their annihilation with anti-defects [18]. The particles that finally emerge in fragmentation spectra may reach GUT-scale energies of the order of 10^{16} GeV.

Other candidates are metastable superheavy relic particles, which could be formed non-thermally during the reheating phase of the early Universe after inflation [40]. These superheavy particles could be some form of the cold dark matter which contribute about 30% to the total energy budget of the present Universe [41]. If their life-time is larger than the age of the Universe these particles may release EHE CRs on decay or annihilation processes.

The fragmentation spectrum of these heavy states will produce mainly pions with only a 3% to 10% admixture of baryons [18]. Thus, if the high energy spectrum of CRs is connected to a top-down mechanism one should expect a large bolometric flux of neutrinos and gamma rays. In particular, photons will cascade down to the MeV-GeV range by electron-positron pair production in the CMB and subsequent synchrotron radiation in magnetic fields. These fluxes typically exceed measurements of the GeV gamma ray spectrum [42].

Cold dark matter (CDM) particles, by definition, are expected to accumulate in our galactic halo. For the metastable relics this may lead to an anisotropic distribution of UHE CRs on their decay and annihilation due to our off-center position in the Milky Way. So far experiments do not observe such an anisotropy w.r.t. the galactic center, but the limited statistics still leave some room for speculations. If future high exposure experiments should observe a large scale anisotropy of EHE CRs this would provide a strong evidence against a "top-down" contribution from metastable CDM [18].

1.2. Propagation

After injection from an astrophysical source a cosmic particle is exposed to interactions with the interstellar medium and magnetic fields. The spectrum and arrival directions of CRs observed on Earth will reflect these interactions and may depart from the spectrum on injection and the proper position of the sources, respectively. We will discuss the interactions that dominate UHE CRs in the following sections. This will also provide an additional criterion for the maximal injection energy of cosmic sources which will further reduce the number of plausible candidate sources.

Attenuation in the Interstellar Medium

For the discussion of propagation effects it is convenient to define propagation functions $P_{a|b}(E; E_\mathrm{i}, r)$ which were introduced in Ref. [43]. Starting from a particle of type b at "propagation distance"[2] r with energy E_i the function $P_{a|b}$ gives the expected number of

[2]The propagation distance r is defined as $\mathrm{d}r \equiv c\,\mathrm{d}t = c\,\mathrm{d}z\,(1+z)^{-1}H^{-1}$ and corresponds to the age of a particle created in the Universe at red-shift z.

CRs of particle type a above an energy E created ($a \neq b$) or surviving ($a = b$) during the propagation towards the Earth ($r = 0$). The CR source of the particle type b at propagation distance r is described by the luminosity per co-moving volume $\mathcal{L}_b$. The number N_a of particles a arriving at Earth with energy E per units of energy, area A, time t and solid angle Ω reads

$$J_a \equiv \frac{\mathrm{d}^4 N_a}{\mathrm{d}E\,\mathrm{d}A\,\mathrm{d}t\,\mathrm{d}\Omega} = \frac{1}{4\pi} \sum_b \int_0^\infty \mathrm{d}E_i \int_0^\infty \mathrm{d}r \left| \frac{\partial P_{a|b}(E; E_i, r)}{\partial E} \right| \mathcal{L}_b \ . \tag{II.3}$$

The propagation distance r and the redshift z are related by $c\,\mathrm{d}z = \mathrm{d}r\,H(z)(1+z)$ where $H(z)$ is the Hubble expansion rate at a redshift z. The expansion of the Universe is determined by its energy content Ω relative to the critical energy density $\rho_{\mathrm{cr}} \equiv 3H^2/(8\pi G_{\mathrm{N}})$. For a flat ($\Omega_{\mathrm{tot}} = 1$) Universe dominated by vacuum energy Ω_Λ and cold (dark) matter Ω_{M} the present Hubble expansion $H_0 = 71 \mathrm{kms}^{-1}\mathrm{Mpc}^{-1}$ [44] is related to the expansion at earlier times through $H^2(z) = H_0^2\,[\Omega_{\mathrm{M}}(1+z)^3 + \Omega_\Lambda]$. Here we take $\Omega_{\mathrm{M}} = 0.3$ and $\Omega_\Lambda = 0.7$, in agreement with WMAP observations [41].

The relevant interactions of UHE protons during propagation are pion photo-production and electron-positron pair production in the cosmic microwave background (CMB). The photon spectrum (observed today) follows that of a black body radiator with a temperature of about 2.7 K giving an average photon energy $\langle E_\gamma \rangle_{2.7\mathrm{K}} \approx 0.6$ meV. For average proton energies larger than the threshold

$$E_{\mathrm{th},\gamma\pi} = \frac{m_\pi(2m_p + m_\pi)}{2E_\gamma} \approx 6.8 \times 10^{10} \left(\frac{\mathrm{meV}}{E_\gamma}\right) \mathrm{GeV} \ , \tag{II.4}$$

pion photo-production in the CMB is kinematically possible. Resonant production via $\Delta^+(1232)$ occurs at energies

$$E_{\mathrm{res},\Delta^+} = \frac{m_{\Delta^+}^2 - m_p^2}{2E_\gamma} \approx 3.2 \times 10^{11} \left(\frac{\mathrm{meV}}{E_\gamma}\right) \mathrm{GeV} \ . \tag{II.5}$$

At lower energies where meson production is kinematically excluded e^+e^- pair production is the dominating process with a production threshold

$$E_{\mathrm{th},e^+e^-} = \frac{m_e(m_e + m_p)}{E_\gamma} \approx 4.8 \times 10^8 \left(\frac{\mathrm{meV}}{E_\gamma}\right) \mathrm{GeV} \ . \tag{II.6}$$

For even smaller energies adiabatic energy loss due to the expansion of the Universe dominate with $E(z) = E/(1+z)$.

Remarkably, for meV photons the energy threshold of e^+e^- pair production is close to the 2nd knee of the CR spectrum. This provides an interesting possibility: The transition between two components in the CR spectrum can "naturally" be explained by a flattening of the spectrum corresponding to the sum of two spectra with different power index and normalization. This is one motivation for models which explain the cosmic

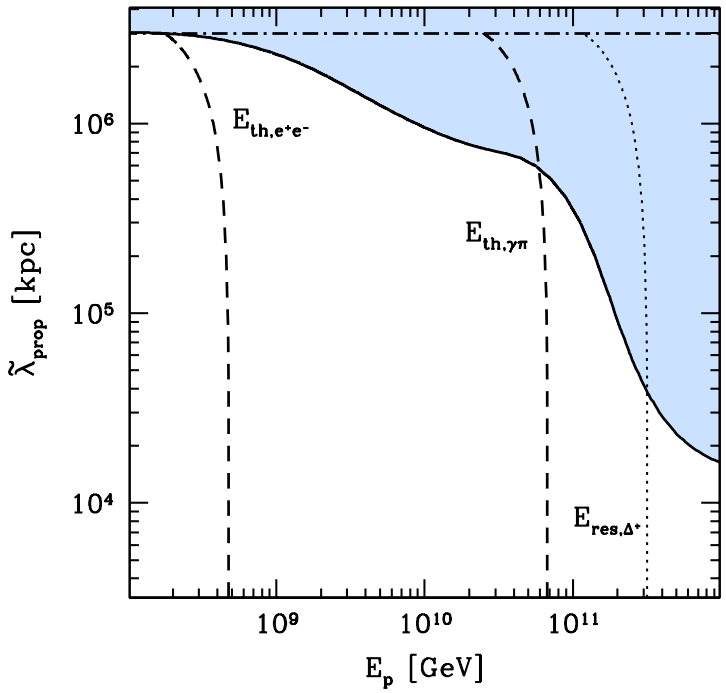

Figure II.4: *The effective energy loss length $\widetilde{\lambda}_{prop}$ as a solution to Eq. (II.9) vs. the energy of the proton E_p at the CR source. The dashed lines show the threshold for pair production and photomeson production given in Eqs. (II.6) and (II.4), respectively, with $E_\gamma = (1+z)$ meV. Also shown as a dotted line is the proton energy corresponding to the Δ^+ resonance given in Eqs. (II.5). The dash-dotted line shows $\widetilde{\lambda}_{red}$ from redshift losses corresponding to Eq. (II.10).*

ankle as the crossover between the galactic and extragalactic component. However, the propagation of extragalactic CRs will produce a broken power-law spectrum even in the case of a single source with a simple power law injection. Hence, it is also possible that the breaks in the CR spectrum are the result of a single component and a transition to a different component may also occur as a steepening. We have already indicated in the introduction that CRs above the 2nd knee may result from extragalactic proton sources and we will further explore the implications of this idea in section II.2 and II.3.

The discussion of propagation effects is greatly simplified by the introduction of the energy loss length λ defined as

$$\frac{1}{\lambda} \equiv -\frac{1}{E}\frac{\mathrm{d}E}{\mathrm{d}r} \ . \tag{II.7}$$

For $\lambda \approx$ const the energy loss length is the propagation distance (or cosmic period) of a particle before it loses an e-folding of its energy. In the case of adiabatic losses we have simply

$$-\frac{1}{E}\frac{\mathrm{d}E}{\mathrm{d}r} = -\frac{1}{E}\frac{\mathrm{d}E}{\mathrm{d}z}\frac{\mathrm{d}z}{\mathrm{d}r} = \frac{1}{1+z}\frac{\mathrm{d}z}{\mathrm{d}r} = \frac{H}{c} = \frac{1}{\lambda_{\mathrm{red}}} \ . \tag{II.8}$$

This result stems from the fact that the Hubble length c/H sets the effective red-shift horizon scale of our Universe.

We can make use of the propagation functions $P_{p|p}$ introduced earlier and define an *effective* energy loss length $\widetilde{\lambda}_{\rm prop}$ of the protons as a solution to the equation

$$\frac{E}{\mathrm{e}} = \int_0^E \mathrm{d}E' P_{p|p}(E'; E, \widetilde{\lambda}_{\rm prop}(E)) \ . \tag{II.9}$$

Below the threshold of e^+e^- pair production and pion photo-production redshift losses dominate. In this case $P_{p|p}(E; E_i, r) = \Theta\left(E_i - (1+z(r))E\right)$ and $\widetilde{\lambda}_{\rm prop}$ reduces to

$$\widetilde{\lambda}_{\rm red} = \int_0^{\widetilde{z}} \frac{c\,\mathrm{d}z}{(1+z)H(z)} \approx 2.9\,\mathrm{Gpc} \quad \text{with} \quad \widetilde{z} = e - 1 \approx 1.72 \ . \tag{II.10}$$

Note that the previous Eq. (II.10) reduces to $\widetilde{\lambda} = c/H_0$ in the case of a constant Hubble expansion rate. We will take $\widetilde{z} \approx 1.72$ in the following calculations as an upper bound $z_{\rm max}$ in redshift for the evolution of extragalactic proton sources.

Figure II.4 shows the solution to Eq. (II.9) in the general case together with the production threshold of e^+e^- pairs and pions for an photon energy of 1 meV. Since the CMB temperature increases as $(1+z)$ the threshold energy proportional to E_γ^{-1} decreases as $(1+z)^{-1}$. The proton energy E_p shown in Fig. II.4 corresponds to the initial energy at the source. One clearly sees the dominance of adiabatic losses (dash-dotted line) for energies below the e^+e^- threshold according to Eq. (II.10).

For our calculation we made use of propagation functions which were already calculated in Ref. [43, 26] with the SOPHIA [45] Monte-Carlo program. The program exploits a continuous energy loss approximation to describe the e^+e^- pair production process. For the calculation of the propagation functions we join infinitesimal propagation steps of $\delta r = 1 \div 10$ kpc depending on the local redshift z from a source at $r(z)$ to the earth $r = 0$.

Attenuation in the Source

The effective attenuation length shown in Fig. II.4 can be used as an additional constraint on plausible proton sources. According to the authors of Ref. [35] the acceleration of relativistic particles by moving magnetic fields can be written as

$$\frac{1}{E}\frac{\mathrm{d}E}{\mathrm{d}r} = \frac{\xi}{R_{\rm Larmor}} = -\frac{1}{\lambda_{\rm gain}} \ , \tag{II.11}$$

where $\xi < 1$ depends on the details of the acceleration mechanism.[3] The energy gain per propagation distance has to compete with energy losses due to interactions with the

[3] From the discussion of Fermi acceleration we have $\lambda_{\rm gain} = ct_{\rm gain}$.

background radiation, mostly the CMB, and also synchrotron radiation which yields an attenuation length of

$$\left(\frac{\lambda_{\rm sync}}{1\,{\rm kpc}}\right) \approx 41\,\frac{A^4}{Z^5}\,\left(\frac{R}{1\,{\rm kpc}}\right)^{-1}\left(\frac{B}{1\,{\rm mG}}\right)^{-3}\ . \tag{II.12}$$

Again, R and B are the characteristic radius and magnetic field of a cosmic cyclotron, respectively. This formula is for the general case of a particle with atomic mass number A and charge Ze. Note, that the synchrotron loss of iron $^{56}_{26}$Fe is almost the same as for protons ($A^4/Z^5 \approx 1.2$) for fixed Larmor radius and magnetic field, but with an iron energy larger by a factor 26. For a positive acceleration one has to require

$$0 > \lambda_{\rm acc}^{-1} + \lambda_{\rm prop}^{-1} + \lambda_{\rm sync}^{-1}\ . \tag{II.13}$$

This limits the parameters R and B of candidate acceleration sites by the solution of the equation[4]

$$\frac{\xi}{R} = \lambda_{\rm prop}^{-1}(E(R,B)) + \lambda_{\rm sync}^{-1}(R,B)\ , \tag{II.14}$$

which is shown for the case of proton sources as the solid lines in Fig. II.4. The upper line correspond to an optimal acceleration mechanism with $\xi = 1$, the lower lines are more plausible accelerations of $\xi = 0.04$ and $\xi = 1.5 \times 10^{-4}$, respectively [35]. We have checked, that Eq. (II.14) together with Eqs. (II.9) and (II.12) reproduces the limits shown in Fig. (II.3).

A look at Fig. II.4 reveals that the number of sources for the extremely high energy CRs above 10^{11} GeV is very sparse. For protons only radio galaxy lobes and clusters of galaxies seem to be plausible candidates. Exceptions may occur for sources which move relativistically in the host-galaxy frame [35], in particular jets from active galactic nuclei (AGN) and gamma ray bursts (GRB). In this case the maximal energy might be increased due to a Doppler boost by a factor ~ 30 or ~ 1000, respectively. As already noted, the synchrotron loss for fixed R and B is almost independent of the particle, whereas the maximal energy scales with Z according to Eq. (II.2). In the case of iron sources the group of candidates might be extended *e.g.* by the galactic halo.

Deflection in Magnetic Fields

Charged nuclei are also deflected by galactic and intergalactic magnetic fields during their propagation. Within a magnetic field region of constant field strength B the maximal deflection of a particle after a propagation distance d is given by $\delta\theta_{\rm cor} = d/R_{\rm Larmor}$ or

$$\left(\frac{\delta\theta_{\rm cor}}{1^\circ}\right) \approx 5\,Z\left(\frac{d}{10\,{\rm Mpc}}\right)\left(\frac{B}{1\,{\rm nG}}\right)\left(\frac{E}{10^{11}\,{\rm GeV}}\right)^{-1}\ . \tag{II.15}$$

[4]Our definition $\lambda_{\rm prop}$ includes also red-shift losses in contrast to the treatment of Ref. [35]. The difference is only relevant for very large candidate sources extending 3 Gpc like the intergalactic medium (see Fig. II.4) and is appropriate for objects that follow the expansion of the Universe.

The previous equation assumes that the correlation length $\lambda_{\rm cor}$ of the magnetic field is larger than the propagation distance d. If instead $d \gg \lambda_{\rm cor}$ a particle will accumulate a deflection angle $\delta\theta_{\rm dec}$ as the result of a random walk over $d/\lambda_{\rm cor}$ regions with different field orientations giving [46]

$$\delta\theta_{\rm dec} \approx \sqrt{\frac{2}{9}}\sqrt{\frac{\lambda_{\rm cor}}{d}}\ \delta\theta_{\rm cor}\ . \tag{II.16}$$

The disk of the Milky Way with an average magnetic field of the order of $3\,\mu$G has a diameter of about 30 kpc and a thickness of 300 pc. Our solar system has a distance of about 8 kpc to the galactic center. Within the disk ($d < 300$ pc) and for energies less than 10^9 GeV we get typical deflections $\delta\theta \gg 1^\circ$ from Eq. (II.15). Cosmic rays below the ankle are thus expected to show an isotropic arrival distribution as it is indicated by experiments [47, 48].

An upper limit of about 1 nG has been estimated for intergalactic magnetic fields from measurements of the Faraday rotation of radio signals from distant radio galaxies [49]. The attenuation length of extremely high energy (EHE) nuclei above 10^{11} GeV is less than 50 Mpc. If we assume a coherent intergalactic field over distances similar to the diameter of our local Virgo supercluster (~ 10 Mpc) the typical deflection according to Eq. (II.16) is only a few degrees. Hence CRs in correlation with galaxies of the Virgo cluster could be observed.

The deflections in magnetic fields should not have any effect on the CR spectrum if the source distribution is spatially isotropic and homogenous. The large-scale homogeneity of the Universe implies that CR sources can be treated as homogenous on distances which are large compared to a characteristic sources separation $\lambda_{\rm sep}$. One would expect that if this is larger than, say, the Larmor radius corresponding to particle propagation in intergalactic magnetic fields, the standard approximation of a homogenous source distribution breaks down. In this case our relative position to CR sources is important. However, it was shown by the authors of Ref. [50] that as long as characteristic propagation scales like Larmor radii or attenuation lengths the spectrum of CRs seen at Earth is universal. Such a universality is implicitly assumed in the following.

1.3. Observation

The primary flux of CRs consisting of protons and heavier nuclei initiates showers of secondary particles in the atmosphere. Most of these particles will be highly relativistic and the cascade will develop as a thin disk around the shower axis until the process of particle multiplication stops. Above the knee the rate of CR primaries is less than one particle per square meter per year and a direct observation in the upper layers of the atmosphere (balloon or aircraft) or even above (spacecraft) is inefficient. As a lucky coincidence particle cascades of PeV CRs may reach the sea-level if the arrival direction is not far from the zenith and an observation of extensive air showers (EAS) at ground arrays is possible. In particular, there are two detection methods which have

been successfully used in high exposure experiments which we will describe in the next sections.

The size of an EAS on sea-level depend on the primary energy and arrival direction. For showers of UHE CRs the cascade is typically several hundreds of meters in diameter and contains millions of secondary particles. Secondary electrons and muons produced in the decay of pions may be observed in scintillation counters or alternatively by the Cherenkov light emitted in water tanks. The separation of these detectors may range from 10 m to 1 km depending on the CR energy and the optimal cost-efficiency of the detection array. The analysis of the data proceeds in several steps. The shower core and hence arrival direction can be estimated by the relative arrival time and density of particles in the grid of detectors. The first estimate using a plane shower front can be refined in a second step by a χ^2-fit to a more realistic profile. The particle density at a certain distance from the core may then be used to calibrate the primary energy. It turns out that the density at about 600 m from the core is rather insensitive to the primary mass and may be used for calibration (e.g. [34]).

The atomic mass number A of the initial particle may be estimated from the topology of the cascade. At an early stage, the number of particles N in a cascade increases exponentially in the atmosphere until it reaches its maximum. To first order a particle with mass A can be treated as a hadronic cascade from a proton ($A = 1$) with the same initial energy which has already reached a shower particle multiplicity of $N = A$, but without an electro-magnetic component. Thus the shower from a heavy nucleus will reach its maximum earlier in the atmosphere and with a larger muon to electron ratio N_μ/N_e. The muon number can be measured separately from the electrons with an appropriate shielding of the detectors, *e.g.* by a deployment underground.

This detection of EASs have been successfully used by a large number of CR experiments over the years. Those with the largest exposure at UHE (see Fig. II.1) are the Akeno giant air shower array (AGASA) [51] operating since 1990, Haverah Park [52] array from 1967 to 1987 and the Yakutsk [53] array since 1971.

Alternatively, the excitation of nitrogen molecules in the atmosphere by the CR cascade and the resulting fluorescence emission of light in the near ultra-violet (300 nm to 400 nm) may be used for CR detection. An experimental implementation of this method consists of a spherical arrangement of photomultipliers covering different segments of the night sky. This *Fly's Eye* technique uses the Earth's atmosphere as a calorimeter, since the luminosity of fluorescence light is proportional to the energy of the primary. The projection of the shower trajectory onto the night sky and the position of the detector determines the *shower plane*. Similar to the data analysis of ground arrays one can estimate the arrival direction inside the shower plane by the relative hit time of the photomultipliers. However, a better resolution is obtained by multiple Fly's Eyes where the arrival direction is simply determined by the best fitting intersection of the respective shower planes. The energy can be estimated by the total fluorescence yield from the shower. From this and the longitudinal profile of the shower one can estimate the chemical composition of the primary.

Since the detection of fluorescence light requires clear moonless nights the experimental exposure time is smaller than those of EAS arrays, but the effective detection volume for these events is much larger. Experiments using fluorescence light operate at the UHE end of the CR spectrum. The original Fly's Eye experiment located in Utah has operated from 1981 to 1993. In the following we will use binocular data ("Fly's Eye Stereo") collected from 1986 to 1992 [54]. Its successor experiment, the High Resolution Fly's Eye (HiRes) [55, 56] is operating since 1994 both in binocular and in monocular mode. For our fit we use the monocular data samples "HiRes-I" ('97-'03) and "HiRes-II" ('99-'01), respectively.

1.4. Puzzles

The measurements of UHE CRs shown in Fig. II.5 are in reasonably good agreement. We focus here on data sets from the experiments AGASA [57] and HiRes [58] having the largest exposure at these energies. Supplementary data sets are shown in Fig. II.1 from Ref. [13], where also references can be found. At first glance the data samples seem to have a relative systematic shift – either in energy calibration [59] or in absolute normalization. A relative error in energy determination of 30% may account for the "excess" of eleven events above 10^{11} GeV [57] reported by the AGASA Collaboration, which is in contrast to the findings of the HiRes Collaboration [58]. This interpretation is fueled by a recent re-analysis of the AGASA data [60]. The preliminary results indicate that the energy of highly inclined showers has previously been over-estimated. If verified, this would result in a re-calibration of the spectrum according to a relative energy shift of -10% to -15%. Remarkably, this energy shift agrees with predictions from a matching procedure of CR spectra assuming an early onset in extragalactic proton dominance at about 10^9 GeV [29]. The calibration by the "dip" in these proton spectra resulting from electron-positron pair production on the CMB predicts a -10% and $+20\%$ energy shift of the AGASA and HiRes data, respectively. In the following sections we will use both the original and a re-calibrated data set according to the predictions of Ref. [29]. This provides an estimate of the systematic errors involved in the statistical analysis.

An additional puzzle is the statistical relevance of clusters of UHE CRs. The AGASA Collaboration reports observations of event clusters above 4×10^{10} GeV which have a chance probability smaller than 1% to arise from a random distribution [61, 32, 62, 63], whereas the recent analysis reported by the HiRes Collaboration showed that their data are consistent with no clustering among the highest energy events [33]. Further discrepancy arises from the findings of large-scale anisotropy in UHE CRs. The AGASA Collaboration has reported a 4% dipole-like enhancement oriented towards the galactic center for UHE events [64]. In contrast, the HiRes Collaboration finds no significance of this dipole orientation in their data above 3×10^9 GeV [65].

Note, that these conflicting experimental results are derived using different experimental techniques: AGASA estimates the primary energy by the charged particle density at fixed distance from the shower core observed in water Cherenkov tanks. Instead, HiRes

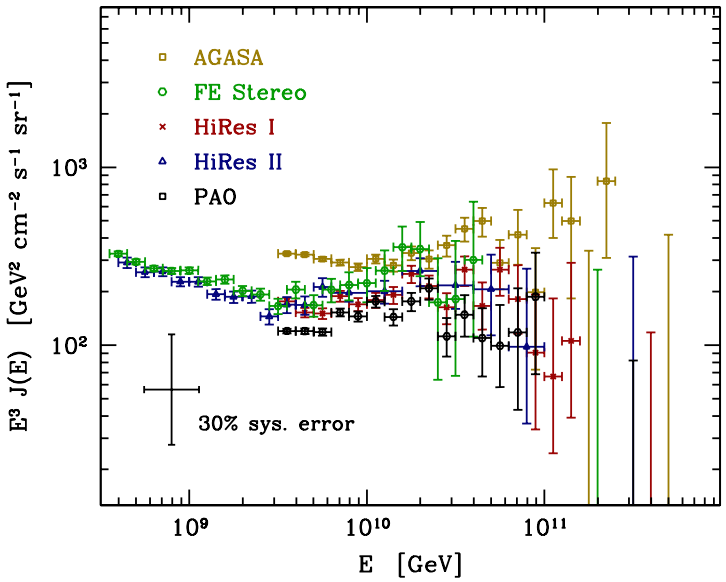

Figure II.5: *A selection of UHE CR data samples. The flux of CRs is multiplied by E^3. Also indicated is the effect of a relative energy shift of* $\pm 30\%$.

uses an calorimetric technique observing the fluorescence light emitted by excited nitrogen atoms along the trajectory of the extensive air shower. For a disentanglement of the physics results from the limitations of systematic errors it is desirable to cross-calibrate the detection methods by a simultaneous detection of the same UHE CR event. This is realized by the Pierre Auger Observatory (PAO) [66, 67] currently under construction in western Argentina. On completion it will combine a 3000 km^2 array of 1600 water Cherenkov detectors separated by about 1.5 km with 24 fluorescence detectors. By the time of writing there are more than 1000 water Cherenkov tanks deployed and 18 of the 24 fluorescence detectors are operating.

The Pierre Auger Collaboration has already published a preliminary data set [66, 67] with an exposure similar to the HiRes detector. The data points are also included in Fig. II.5. We will see in the following sections that the implementation of this preliminary data weakens the goodness of our statistical tests using extragalactic proton sources as CRs above the 2nd knee. This could be held against the hypothesis, but a judgment on the basis of a preliminary data set might be inappropriate. It is expected that PAO will soon have the necessary statistics at the highest energies to resolve these uncertainties. Since the detector is located in the southern hemisphere it is also well-suited for a detailed study of a hypothetic excess of CRs from the galactic center predicted in certain top-down scenarios of CRs. So far, the results are consistent with an isotropic distribution on large scales [68, 67].

Summary

Ultra high energy (UHE) cosmic rays (CRs) are a source of speculations involving the production mechanisms and the cosmic distribution of production sites (Sec. II.1.1). Even in the presence of cosmic sources with energy exceeding 10^{11} GeV, the interactions of CR with the interstellar medium (Sec. II.1.2) leave characteristic features in the spectrum, in particular the Greisen-Zatsepin-Kuzmin cutoff for nuclei, which might be in conflict with CR data (Sec. II.1.4). Solutions to these problems may be guided by new precision data on UHE CRs with both a higher statistics and a better energy calibration (Sec. II.1.3).

In the next section II.2 we will discuss the statistical goodness of a model which describes the spectrum of CRs above the 2nd knee by extragalactic proton sources. We have already argued in section II.1.2 that proton-photon interactions in the cosmic microwave background may reproduce the "ankle" as a "dip" from e^+e^- pair production together with a "pile-up" of protons from pion photo-production. We will analyse the requirements for the cosmic proton sources which follows closely the analysis of Ref. [4]. In addition to previous estimates we will check the effect of variations of the data sets, in particular a hypothetic re-calibration of the energies and the inclusion of preliminary data from the Pierre Auger Observatory. These informations are necessary for the estimation of neutrino fluxes from optically thin proton sources (Sec. II.3).

2. Low Crossover to Extragalactic Cosmic Rays

The large-scale isotropy of UHE CRs above the ankle is evidence of their extragalactic origin. We have argued in section II.1 that the transition between the galactic and extragalactic component is so far inconclusive. A recent analysis of the HiRes data [24] indicates a change in the CR composition at around 5×10^8 GeV from heavy nuclei to a light component, which is an order of magnitude lower in energy than the previous transition deduced from the Fly's Eye data [69]. This can be interpreted as an early onset of extragalactic proton dominance at the 2nd knee. It was shown by many authors [25, 26, 27, 4, 28] that this low crossover to protons can account for the ankle in the CR spectrum due to scattering effects in the cosmic microwave background (CMB).[5] In preparation for the following sections we will derive the requirements on the injection spectrum, evolution, and luminosity of extragalactic proton sources by a goodness-of-fit test to CR data samples from AGASA [57], Fly's Eye [69, 54], HiRes [58], and the Pierre Auger Observatory [66, 67] (preliminary data).

Without having a detailed knowledge on the dynamical properties of CR sources we will assume that their luminosity can be approximated by

$$\mathcal{L}_{\rm CR}(z, E_i) = \Theta(z - z_{\rm min})\,\Theta(z_{\rm max} - z)\,\mathcal{L}_0\,(1+z)^n\,E_i^{-\gamma}\,e^{-E_i/E_{\rm max}}\ . \tag{II.17}$$

This simple ansatz describes a source distribution which is spatially homogenous and isotropic with an injection spectrum following a single power-law $\propto E_i^{-\gamma}$ with an exponential cutoff at $E_{\rm max}$. We do also consider the possibility that the source density and intensity evolves with redshift $\propto (1+z)^n$ excluding early ($z_{\rm max}$) and close-by ($z_{\rm min}$) sources.

Goodness-of-Fit Test

The flux of extragalactic protons incident on Earth is determined from the source luminosity (Eq. II.17) by propagation functions (Eq. II.3) which were introduced in section II.1.2. A statistical comparison of this proton flux with CR data can be carried out by a *goodness-of-fit test* which was already used in Ref. [70] in the same context. In frequentist statistics the level of agreement of a particular hypothesis $\mathcal{H}$ with the experimental data can be represented [13] by

$$\mathcal{G}(\mathcal{H}) = \sum_{N'|P(N')<P(N_{\rm exp})} P(N'|\mathcal{H})\ , \tag{II.18}$$

the integrated probability of those samples N' which have a smaller probability P than the actual experimental result $N_{\rm exp}$. In general, $\mathcal{H}$ is then accepted (or rejected) at a chosen significance level $\mathcal{G}$ corresponding to a confidence level (CL) $1-\mathcal{G}$ [13]. As it is standard in statistics, we choose 68%, 90%, 95% and 99% CLs as benchmarks for

[5] We use the term "low crossover" for a transition at 5×10^8 GeV compared to a "high crossover" in the vicinity of the ankle, $E_{\rm ank} \sim 3 \times 10^9$ GeV.

Table II.1: *Parameters of the source luminosity associated with different CR intervals and data sets. The first two rows show the best fit parameters of the goodness-of-fit test in the "low crossover" scenario. The last two rows correspond to the set-up of Ref. [71] for a "high crossover" scenario.*

Data Set	(E_-, E_+) [GeV]	γ	n	$\dot{\epsilon}_{\rm CR}$ [erg Mpc^{-3} yr^{-1}]
Akeno & AGASA	$(10^{8.7}, 10^{11})$	2.55	3.65	2.1×10^{45}
Fly's Eye & HiRes	$(10^{8.7}, 10^{11})$	2.55	3.45	1.1×10^{45}
Akeno & AGASA	$(10^{10}, 10^{11})$	2	3	4.4×10^{44}
Fly's Eye & HiRes	$(10^{10}, 10^{11})$	2	3	2.3×10^{44}

the acceptance of our model. The minimum of a goodness-of-fit test is equivalent to the outcome of a χ^2-fit in the case of large samples N. In this case the minimal value $1 - \mathcal{G}$ corresponds to the minimal χ^2 normalized to the number of degrees of freedom. For the low number of events at the upper end of the CR spectrum the goodness-of-fit test is more reliable and, by construction, it has also an intuitive interpretation as a probability.

In the case of the low crossover scenario, the probability P in Eq. (II.18) is made up by Poisson distributions of CR event rates per energy bin. The expectation values are determined by the hypothesis $\mathcal{H}(\gamma, n)$, i.e. by the particular model for the source luminosity given by an injection index γ and an evolution index n. The unknown constant $\mathcal{L}_0$ in Eq. (II.17) is fixed by a normalization of the propagated proton fluxes to the particular data sample. We also account in the probability P for the systematic error in energy calibration of about $\pm 30\%$ by a Gaussian distribution for an energy shift of the spectra by a multiple of the bin-size $\Delta E/E = 10\%$ [26].

Results

We follow the analysis outlined in Ref. [4] and use CR data in the energy interval from $E_- = 5 \times 10^8$ GeV to $E_+ = 10^{11}$ GeV to search the statistically allowed regions for the evolution index n and power index γ. All other input parameters are kept fixed during the fit. In particular, we take a maximal injection energy $E_{\rm max} = 10^{12}$ GeV and use only sources at redshift $0 < z < z_{\rm max} = 1.72$.[6] We comment on a change in $E_{\rm max}$, $z_{\rm min}$, and $z_{\rm max}$ later.[7]

Figure II.6 shows the results of the goodness-of-fit test for joint CR data samples observed by Akeno [72, 73] & AGASA [57] and Fly's Eye [69, 54] & HiRes [58], respectively. The fitting results for the Akeno & AGASA are worse compared to Fly's Eye & HiRes which result largely from a "spurious" bump[8] in the region around $10^{9.4}$ GeV and a slight

[6] We choose $z_{\rm max} = \widetilde{z}$ from Eq. (II.10).

[7] Note, that we change the parameters $z_{\rm min}$, $z_{\rm max}$, E_- and $E_{\rm max}$ w.r.t. Ref. [4]. This has only a marginal effect on the results.

[8] This stems from combining the data of the Akeno array and the full AGASA experiment.

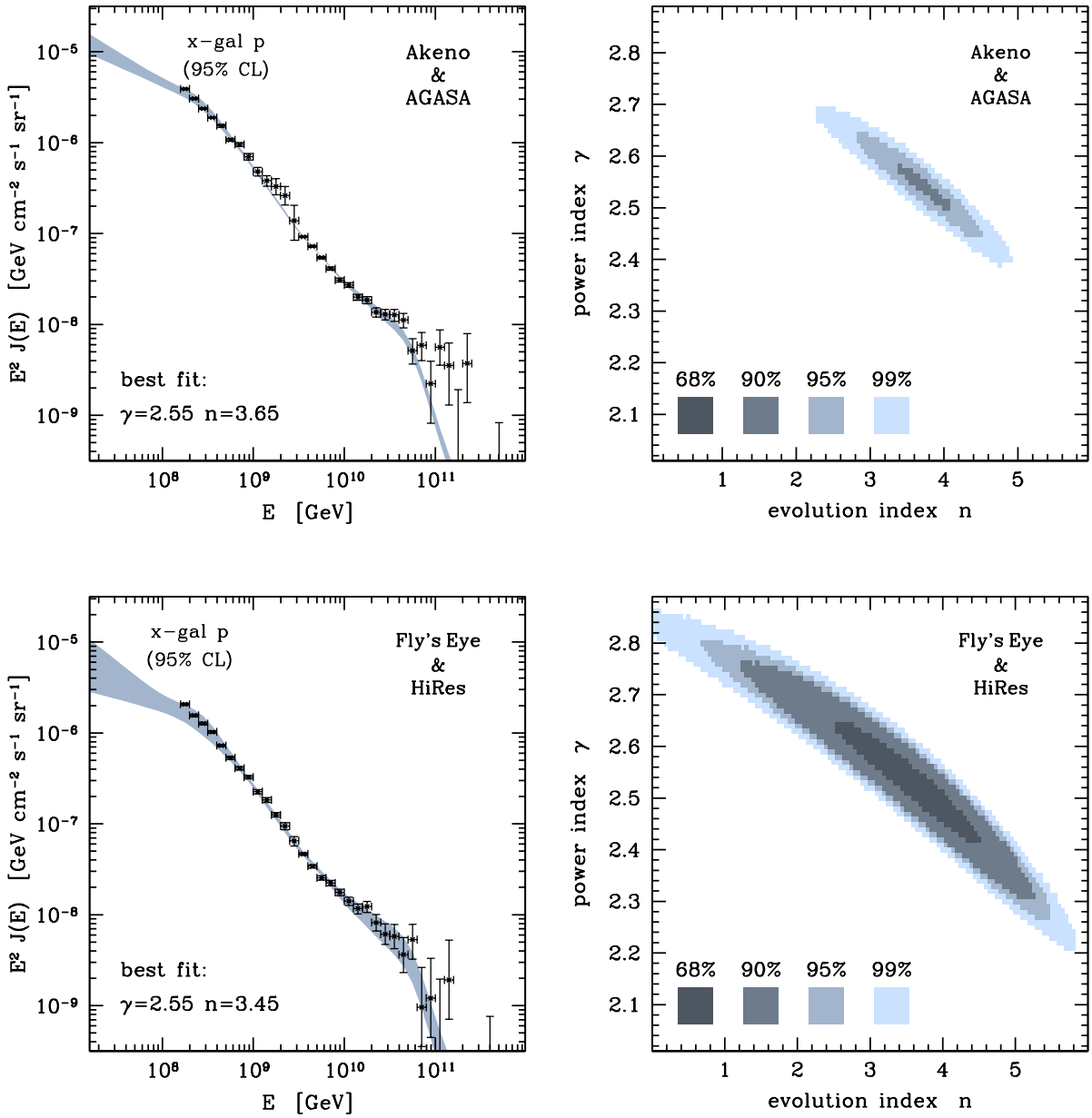

Figure II.6: *The goodness-of-fit test of the low crossover scenario. The upper panels show the results of the joint Akeno and AGASA data and the lower panels the joint Fly's Eye and HiRes data following the analysis of Ref. [70]. The error bars of the data points correspond to one standard deviation. In the fitting procedure we used data in the energy interval from* $E_- = 5 \times 10^8$ *GeV to* $E_+ = 10^{11}$ *GeV and a source evolution between* $z_{min} = 0.0$ *and* $z_{max} = 1.72$.
Left panels: *The 95% confidence level of the extragalactic proton flux as a blue shaded band.*
Right panels: *The allowed parameter regions of the evolution index* n *and power index* γ *according to the 68%, 90%, 95%, and 99% confidence level of the goodness-of-fit test.*

Table II.2: *Results from a goodness-of-fit test to data samples from AGASA, Fly's Eye Stereo, and Hires-I/II, which independently accounts for systematic errors in energy calibration and normalization. The "shifted" data accounts for the energy re-calibration method of Ref. [29].*

"dip"-calibration	(E_-, E_+) [GeV]	γ	n	$\dot{\epsilon}_{\rm CR}$ [erg Mpc^{-3} yr^{-1}]
no	$(10^{8.7}, 10^{11})$	2.48	3.20	1.4×10^{45}
yes	$(10^{8.7}, 10^{11})$	2.47	3.25	1.6×10^{45}

excess of data above the GZK cutoff.

The parameters for the best fit, shown in Fig. II.6, are quite similar and are summarized in Table II.1. In particular, the best fit of the power index is $\gamma = 2.55$ in both cases. The exclusion contours in the n-γ plane for the two data samples predict significantly steeper power indices than the standard E_i^{-2} expected from Fermi engines [71]. Additionally, $\gamma < 2.4$ is disfavored at 68% CL by Fly's Eye [69, 54] & HiRes [58] data and at 95% CL by Akeno [73] & AGASA [57] data.

As we will show in the next section this result has consequences for neutrino observation: predictions for both the cosmogenic fluxes (produced via interactions of super-GZK cosmic-rays on the CMB) and the direct neutrino luminosity from optically thin sources can be significantly modified.

In Tab. II.1 we also show the absolute scale of the source luminosity $\mathcal{L}_0$, which is conveniently expressed by the CR power density

$$\dot{\epsilon}_{\rm CR}(E_-, E_+) = \mathcal{L}_0 \int_{E_-}^{E_+} dE_i \, E_i^{1-\gamma} \ , \tag{II.19}$$

of the fitting interval (E_-, E_+). We have verified the consistency of the simulations with the results obtained in [71] by fitting the data above 10^{10} GeV and comparing the CR power density $\dot{\epsilon}_{\rm CR}$ with our results. Our best fits of the CR interval between 10^{10} GeV and 10^{11} GeV, using Eq. (II.19) with $\gamma = 2$ and $n = 3$, are shown in the last two rows of Tab. II.1 and are in excellent agreement with the results in [71].

The results turn out to be rather insensitive to the precise values of the cosmological parameters within their uncertainties. We have checked that our results are robust against variations of $z_{\rm min} \lesssim 0.01$ and $z_{\rm max} \gtrsim 1.5$. In particular, a larger value of $z_{\rm max}$ could increase the flux of extragalactic protons if the evolution index n is large. But this does only effect the region below the second knee, which we have excluded from the fit. Similarly, as long as $E_{\rm max} \gtrsim 5 \times 10^{11}$ GeV the results of the goodness-of-fit test are practically unchanged.

The injection spectrum of realistic CR sources will not extend to arbitrarily low energies. In optically thin sources, which we will discuss in the next section, CRs are

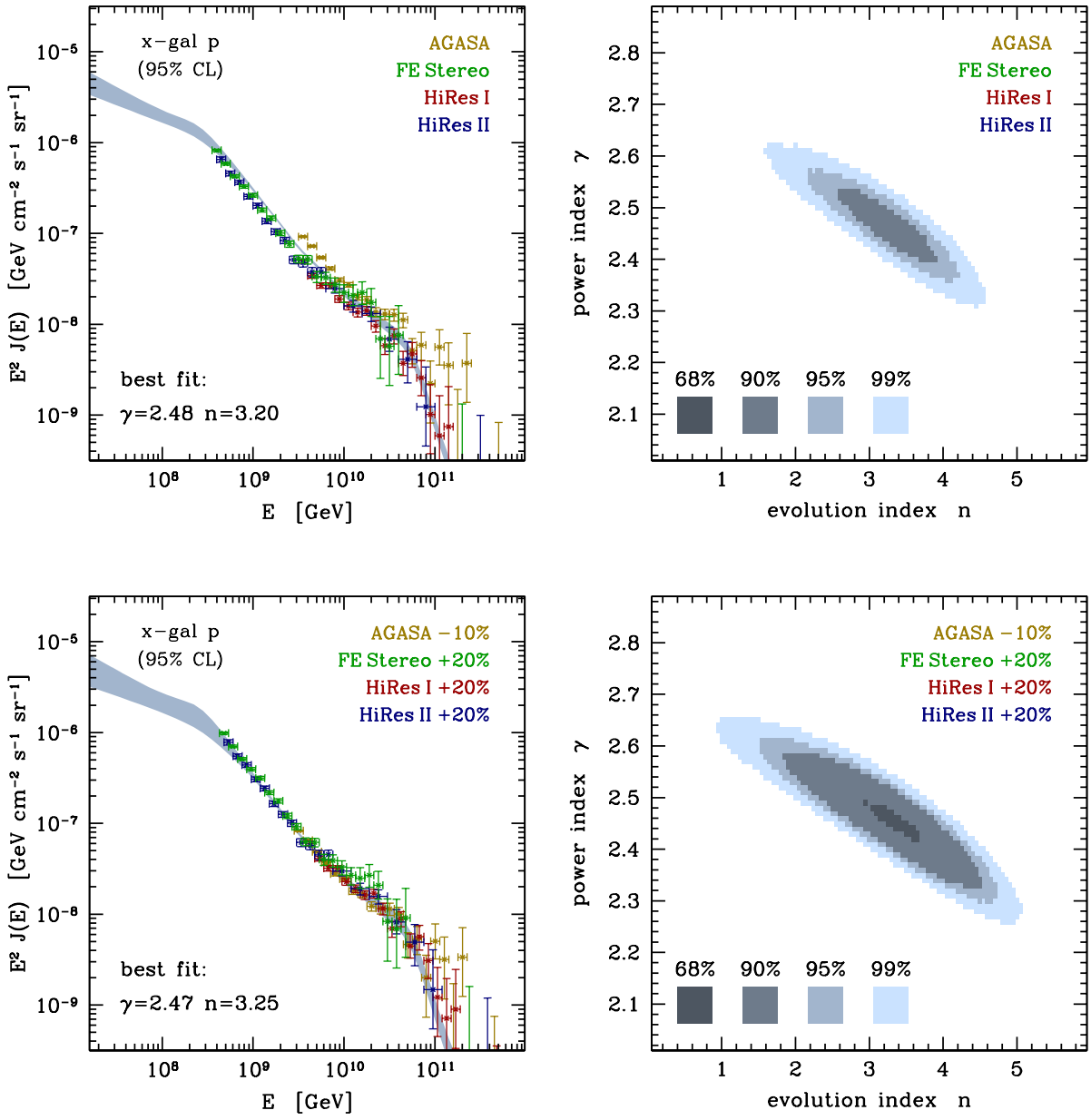

Figure II.7: *The goodness-of-fit test of the low crossover scenario with independent normalization of the AGASA, Fly's Eye Stereo, HiRes-I, and HiRes-II data. The error bars of the data points correspond to one standard deviation. The uppers panels use the data as quoted by the experiments which seem to have a relative error in energy calibration. The lower panels use the procedure of Ref. [29] to re-calibrate the data. In the fitting procedure we used data in the energy interval from* $E_- = 5 \times 10^8$ *GeV to* $E_+ = 10^{11}$ *GeV and a source evolution between* $z_{min} = 0.0$ *and* $z_{max} = 1.72$.
Left panels: *The 95% confidence level of the extragalactic proton flux as a blue shaded band.*
Right panels: *The allowed parameter regions of the evolution index* n *and power index* γ *according to the 68%, 90%, 95%, and 99% confidence level of the goodness-of-fit test.*

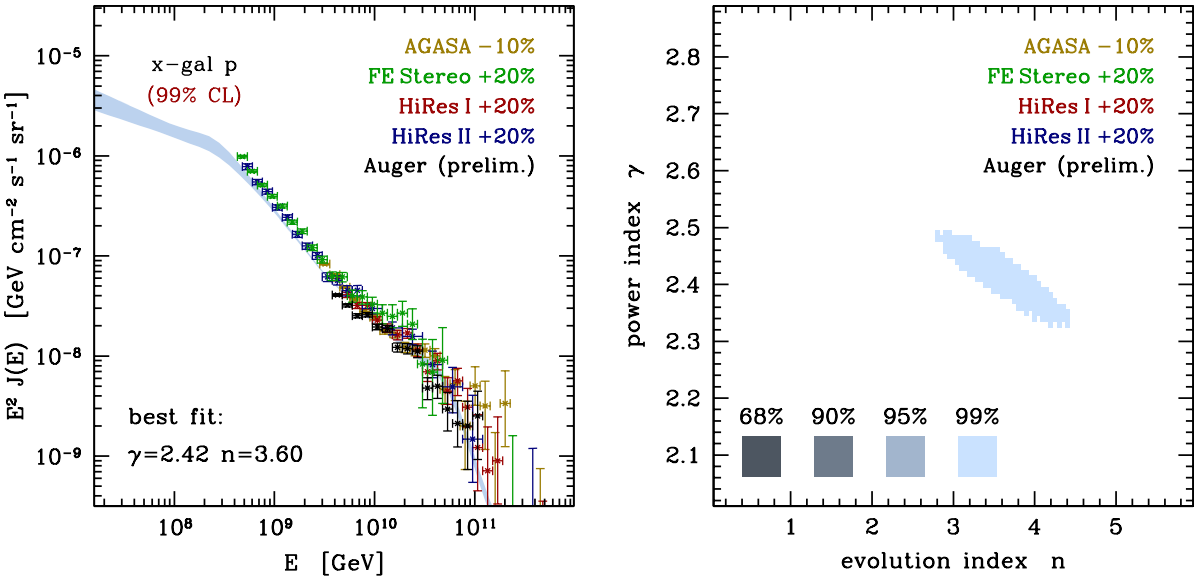

Figure II.8: *The goodness-of-fit test of the low crossover scenario with re-calibrated data and the preliminary data of the Pierre Auger Observatory.*
Left panel: *The 99% confidence level of the extragalactic proton flux as a blue shaded band.*
Right panel: *The allowed parameter regions of the evolution index n and power index γ according to the 68%, 90%, 95%, and 99% confidence level of the goodness-of-fit test.*

associated with pion production in $p\gamma$ or pp scattering processes. In this case we should take into account a production threshold depending on the parameters of the astrophysical environment [74]. This could result in a changeover to a flat spectrum at lower energies or even a low energy cutoff in the injection spectrum, which should reduce the extragalactic contribution in the CR data below the second knee.

The CR data samples which were used in the goodness-of-fit test so far are combinations of results from different Collaborations, experimental techniques, and analysis methods. In order to estimate the systematic effects we have considered separate data samples from AGASA, Fly's Eye, and HiRes where we idependently account for systematic errors in energy calibration and normalization to the data. The normalization of the proton and neutrino fluxes is accomplished by weighting the different experimental exposures in each data bin. The results of the goodness-of-fit test is shown in left panels of Fig. II.7. In a second step, we have used the results of Ref. [29] to re-calibrate the data samples by the position of the e^+e^- dip. This is shown in the right panels of the same figure. Qualitatively, the results predict slightly lesser values of γ and n. The independent normalization of AGASA and HiRes data to the spectrum predict a variations of the best fit parameters within 10%. The combined fit of the re-calibrated data excludes power indices below $\gamma < 2.3$ at the 95% CL.

The power density of extragalactic proton sources is much larger in the low crossover scenario using data in the energy range between $E_- = 5 \times 10^8$ GeV and $E_+ = 10^{11}$ GeV. This is shown for the best fit values in Tab. II.1. This large power density of a few 10^{45} erg Mpc^{-3} yr^{-1} together with the high energy cutoff $E_{\rm max} \gtrsim 5 \times 10^{11}$ GeV of the

injection spectrum is a crucial point of our analysis. If we return to the Hillas diagram of Fig. II.3 the only possible sources seem to be radio galaxy lobes (rg) and clusters of galaxies (cl) or boosted environments like blazers (bl) and gamma ray bursts (gb). The experimental validation of these sources has yet to come.

Finally, we also show the results of the goodness-of-fit test for the re-calibrated data with the additional inclusion of preliminary data from the Pierre Auger Observatory [66, 67] in Fig. II.8. In this case, the goodness of the fit gets weaker and reaches only a 99% CL.[9] However, we have already argued in section II.1.4 that an exclusion of the low crossover scenario based on this preliminary data set is untimely. The high exposure data of PAO expected in the near future will certainly have a great impact on this scenario.

Summary

The "low crossover" model describes the cosmic ray (CR) data well in the data range from 5×10^8 GeV to 10^{11} GeV. We have reviewed our analysis of Ref. [4] and showed the statistically allowed regions of the parameter space of cosmic proton sources. The performance of this statistical test is the main contribution to Ref. [4] by the author of this thesis. In addition, we have shown here the effect of variations w.r.t. the data samples, so far unpublished in the literature. The independent normalization of AGASA and HiRes data to the spectrum predict a variation for the best fit parameters within 10% . The power index γ is significantly (95%) larger than 2.3, in contrast to standard Fermi acceleration in relativistic plasma shocks. The re-calibration of the data according to Ref. [29] optimizes the data samples for the fluxes of extragalactic proton sources, as intended by the authors, and correspondingly our fit improves. The preliminary data set of the Pierre Auger Collaboration worsens the overall fit, but a conclusive judgment of the low crossover scenario has to wait until large exposure data has been published.

We will use these results in the following section II.3 to derive the neutrino fluxes predicted from optically thin proton sources. This analysis will extend the results of Ref. [4] w.r.t. the variation of the data samples and the comparison with new experimental bounds on diffuse neutrino fluxes.

[9] Note, that our statistical approach focuses on the goodness of the low crossover hypothesis and not on confidence intervals of the parameters.

3. Cosmic Ray Associated Neutrino Production

Cosmic rays originating in cosmic accelerators will typically be accompanied by gamma-rays and neutrinos. This is a consequence of the inelastic hadronic processes which are involved in their production mechanism [75]. We have already discussed in section II.1.1 that candidate sources such as blazers, gamma-ray bursts or radio galaxy lobes (see e.g. [37] for a nice review) may accelerate charged particles by their scattering off moving magnetic inhomogeneities which appear in the vicinity of plasma shock fronts (1st order Fermi acceleration). For an efficient acceleration of the nuclei up to energies observed at experiments this scattering process has to be repeated many times. Therefore, it is necessary that the magnetic field confines the charged particle in the source over a time $\tau_{\rm conf}$ much larger then the time-scale of repetition of the acceleration cycle $\tau_{\rm cycle}$.[10]

Accelerated electrons will loose their energy in the magnetic field due to synchroton radiation. The resulting photons provide a target for protons and heavier nuclei to undergo meson photo-production and photo-disintegration, respectively. A neutron produced in this process may diffuse out of the magnetically confining source before it β-decays into a proton. For efficiency of the diffusion process and consistency with the acceleration mechanism these interactions should take place on time scales $\tau_{\rm int}$ much smaller than the period of confinement $\tau_{\rm conf}$ and larger than the $\tau_{\rm cycle}$, respectively. Charged and neutral pions decay into high energy neutrinos and gamma rays, respectively, which are also not confined to the source. The relative mix and luminosity of these particles depend on the details of the source such as the densities of the target photons and the ambient gas [75].

3.1. Optically Thin Sources

In the following we will focus on cosmic proton accelerators. Depending on the relative ambient gas and photon densities, charged pion production proceeds either through inelastic *pp* scattering [76], or photopion production predominantly through the resonant process $p + \gamma \rightarrow \Delta^+ \rightarrow n + \pi^+$ [77]. We will assume in the following that photopion production is the dominating process and comment on the possibility of inelastic *pp* scattering later on. Since the interaction time scale of the emerging high energy neutrons n with photons is similar to $\tau_{\rm int}$ the relative luminosity of CRs and neutrinos will depend on the density of the ambient photon gas as it is sketched in Figure II.9. In the case of an *optically thin* source, *i.e.* $\tau_{\rm cycle} \ll \tau_{\rm int} \ll \tau_{\rm conf}$ each neutron produced by $p\gamma$ interactions will escape the source[11] as it is sketched in the left panel of Figure (II.9). A desirable property of this low-damping scenario is that a single source will produce neutrons with a smooth spectrum across a wide range of energy. In the following β-decay most of the neutrons energy is transfered to the proton whereas the electron neutrino gets a maximal energy of $(1 - m_p/m_n)E_n \approx 10^{-3} \times E_n$.

[10] This may be compared to the time of circumference in a cyclotron.
[11] The life-time $\tau_{\rm n}$ of the neutron is assumed to be larger than its interaction time scale $\tau_{\rm int}$

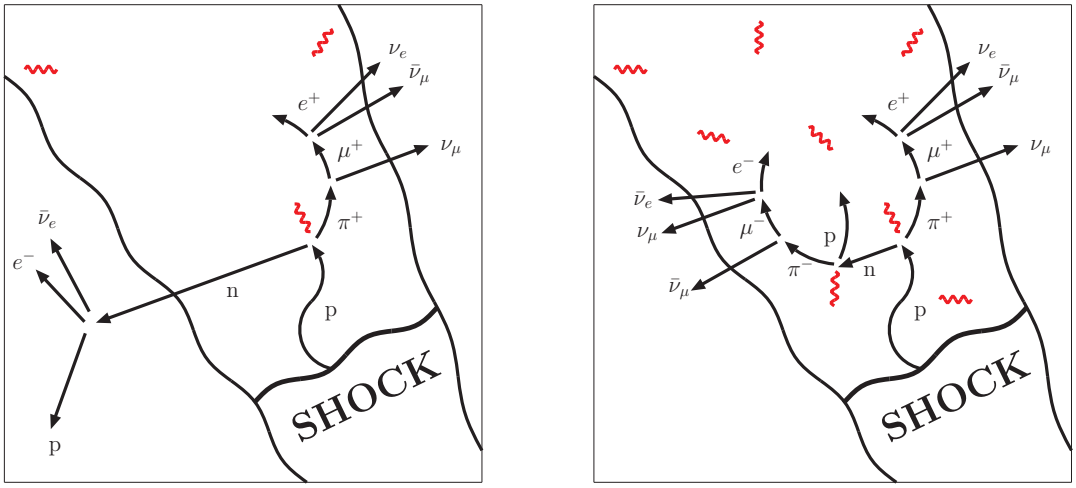

Figure II.9: *Sketch of the neutrino production associated with CRs. The relative fluxes depend on the optical thickness of the magnetic confinement region indicated by wavy lines.*
Left panel: *An optically thin source with ultra-high energy neutrino to proton ratio of 3:1.*
Right panel: *In optically thicker sources some neutrons may scatter inelastically off the photon gas before they escape the region of magnetic confinement.*

The charged pions which are simultaneously produced decay via $\pi^+ \to \mu^+ + \nu_\mu \to e^+ + \nu_e + \overline{\nu}_\mu + \nu_\mu$ and constitute the flux of high energy neutrinos emitted from the source. This production mechanism predicts an initial flavor ratio $\nu_e : \nu_\mu : \nu_\tau$ of $1:2:0$. For neutrino sources distributed over cosmological distances the flavor mix after propagation should be similar to $1:1:1$ due to large mixing between ν_μ and ν_τ.

The energy budget of the scattering process is estimated as follows. Following the treatment of Ref. [77] we introduce the quantity ϵ_π as the average pion energy ratio relative to the average neutron energy on production in $p\gamma$ interactions

$$\epsilon_\pi \equiv \frac{\langle E_\pi \rangle}{\langle E_n \rangle} \ . \tag{II.20}$$

For photo-production via the $\Delta^+(1232)$ resonance, $p + \gamma \to \Delta^+ \to n + \pi^+$, the inelasticity is kinematically determined by requiring equal boosts for the decay products of the Δ^+ [78], giving $\epsilon_\pi \approx 0.28$. In the decay of the pion the emerging muon neutrino carries on average $\langle E_{\nu_\mu} \rangle_\pi \approx (m_\pi^2 - m_\mu^2)/(2m_\pi)\gamma_\pi \approx (1-r)E_\pi/2 \approx 0.22 E_\pi$ with $r = m_\mu^2/m_\pi^2$.[12] The muon which takes $\langle E_\mu \rangle_\pi \approx (1+r)E_\pi/2 \approx 0.78 E_\pi$ is much heavier than the emerging electron and neutrinos. Hence, we can assume that the muon energy is equally distributed between e^+, $\overline{\nu}_e$ and $\overline{\nu}_\mu$, i.e. $\langle E_{\nu_e} \rangle_\mu \approx \langle E_{\overline{\nu}_\mu} \rangle_\mu \approx (1+r)E_\pi/6 \approx 0.26 E_\pi$. In summary, each of the three neutrinos takes about $1/4$ of the pion energy and each pion takes ϵ_π of the neutron energy. We will use in the following the flavor universal ratio

$$\epsilon_\nu \equiv \frac{\langle E_\nu \rangle}{\langle E_n \rangle} = \frac{\epsilon_\pi}{4} \ . \tag{II.21}$$

[12] This follows simply from 4-momentum conservation: $E_\nu^2 \approx E_\mu^2 - m_\mu^2$ and $m_\pi = E_\nu + E_\mu$.

The absolute normalization of the neutrino flux can be inferred from the CR luminosity in the following way. Consider the differential rate of CRs emitted into the energy interval from E_1 to E_2 at a source at redshift z. In the previous section we concluded that in an optically thin source this rate of CRs equals 1/3 of the rate of neutrinos which are emitted in the energy interval[13] between $\epsilon_\nu E_1$ and $\epsilon_\nu E_2$, i.e.

$$\mathcal{N}_\nu \equiv \int_{\epsilon_\nu E_1}^{\epsilon_\nu E_2} \mathrm{d}E \mathcal{L}_\nu^{\mathrm{thin}}(z,E) \tag{II.22}$$

$$= 3\,\mathcal{N}_{\mathrm{CR}} \equiv 3\int_{E_1}^{E_2} \mathrm{d}E \mathcal{L}_{\mathrm{CR}}(z,E) = 3\int_{E_1}^{E_2} \mathrm{d}E \mathcal{L}_{\mathrm{CR}}(z,E) = \int_{\epsilon_\nu E_1}^{\epsilon_\nu E_2} \mathrm{d}E \frac{3}{\epsilon_\nu}\mathcal{L}_{\mathrm{CR}}(z,E/\epsilon_\nu)\ .$$

Since the previous equation should hold for an arbitrary energy interval the neutrino luminosity is given by

$$\mathcal{L}_\nu^{\mathrm{thin}}(z,E) = \frac{3}{\epsilon_\nu}\mathcal{L}_{\mathrm{CR}}(z,E/\epsilon_\nu)\ . \tag{II.23}$$

In an optically thick source the neutron interaction time τ_{int} can be comparable to the cycle time τ_{cycle}. In this case a fraction η of the neutrons is converted back to a proton as sketched in the right panel of Fig. (II.9) and increases the flux of neutrinos relative to CRs. Since the flux of neutrons $\propto (1-\eta)$ is normalized to the spectrum of CRs this will increase the flux of neutrinos and we have to modify Eq. (II.23) as

$$\mathcal{L}_\nu^{\mathrm{thick}}(z,E) = \left(\frac{1}{1-\eta}\right)\frac{3}{\epsilon_\nu}\mathcal{L}_{\mathrm{CR}}(z,E/\epsilon_\nu) + \left(\frac{\eta}{1-\eta}\right)\frac{3}{\widetilde{\epsilon}_\nu}\mathcal{L}_{\mathrm{CR}}(z,E/\widetilde{\epsilon}_\nu)\ . \tag{II.24}$$

The average relative energy $\widetilde{\epsilon}_\nu$ of neutrinos from the second process is necessarily smaller than ϵ_ν and we get a bound[14] of

$$\mathcal{L}_\nu^{\mathrm{thin}}(z,E) \;<\; \mathcal{L}_\nu^{\mathrm{thick}}(z,E) \;<\; \left(\frac{1+\eta}{1-\eta}\right)\mathcal{L}_\nu^{\mathrm{thin}}(z,E)\ . \tag{II.25}$$

Except for resonant interactions in the cosmic neutrino background [79, 80, 81] the neutrinos, once emitted from the source, will only undergo redshift losses. The corresponding propagation function is simply $P_{\nu|\nu}(E;E_i,z) = \Theta\left(E_i - (1+z)E\right)$. From Eqs. (II.3) and (II.23) this results in a flux of extragalactic neutrinos of

$$J_\nu(E) \;=\; \frac{1}{4\pi}\frac{3}{\epsilon_\nu}\int_0^\infty \frac{\mathrm{d}z}{H(z)}\mathcal{L}_{\mathrm{CR}}(z,(1+z)E/\epsilon_\nu)\ . \tag{II.26}$$

In summary, the preceding equation expresses the total flux of UHE neutrinos from optically thin sources with $\mathcal{N}_\nu = 3\,\mathcal{N}_n$ and a fixed ratio $\epsilon_\pi = \langle E_\pi\rangle/\langle E_n\rangle$. The initial flavor composition $\nu_e:\nu_\mu:\nu_\tau$ of $1:2:0$ will be converted to $1:1:1$ after propagation due to mass oscillations.

[13] The quantity ϵ_ν is defined in Eq. (II.21)

[14] This is true for realistic sources with a power index $\gamma > 1$.

3.2. Low Crossover Neutrinos

The treatment of the previous section was used by Waxman and Bahcall [77] to estimate neutrino fluxes from optically thin sources. In their analysis they assumed an extragalactic proton flux with power index $\gamma = 2$ with a high crossover in the CR spectrum at 10^{10} GeV. The expected total neutrino flux (all flavor $\nu + \bar{\nu}$) is [77]

$$J_{\rm WB}(E) \approx 2 \times 10^{-8}\, \epsilon_\pi\, \xi_z \left(\frac{E}{\rm GeV}\right)^{-2} {\rm GeV}^{-1}\, {\rm cm}^{-2}\, {\rm s}^{-1}\, {\rm sr}^{-1}\ , \tag{II.27}$$

where ξ_z depends on the cosmic evolution and ranges between $\xi_z \approx 0.6$ for no evolution and $\xi_z \approx 3$ for strong power-law evolution with $n = 3$. In this section we will extend the treatment of Waxman and Bahcall [77] for the neutrino emissivity of optically thin sources for a general power index γ and evolution index n for the low crossover scenario.

The goodness-of-fit test of the low crossover scenario discussed in section II.2 sets the absolute scale of the extragalactic CR luminosity from the normalization of the propagated flux to CRs above the 2nd knee. The best fit power densities shown in the first two rows of Tab. II.1 and II.3 exceed the estimates for the high crossover scenario (last two rows of Tab. II.1) by one order of magnitude. Since the neutrino power density scales linearly with the CR power density $\dot{\epsilon}_{\rm CR}$ [77] the flux of neutrinos from optically thin sources is expected to be much larger than the predictions of the previous treatment. For our particular parameterization of the source luminosity given in Eq. (II.17) we obtain from Eq. (II.26)

$$J_\nu(E) \;\approx\; 3 \left(\frac{\epsilon_\pi}{4}\right)^{\gamma-1} \frac{\mathcal{L}_0}{4\pi}\, E^{-\gamma} \int\limits_{z_{\rm min}}^{z_{\rm max}} \frac{{\rm d}z}{H(z)}\, (1+z)^{n-\gamma} \qquad \text{for } E \ll \epsilon_\nu E_{\rm max}\ . \tag{II.28}$$

The neutrino fluxes corresponding to Eq. (II.17) and the 95% confidence level of the low crossover model shown in Fig. (II.6) are summarized in Fig. (II.10). For neutrino energies $E_\nu \gtrsim 10^{10}$ GeV the neutrino flux follows the power-law injection of the source. The best fit fluxes below this neutrino energy are summarized in Table (II.3). For larger neutrino energies Eq. (II.28) has to be modified corresponding to effect of the energy cutoff.

The CR production in optically thin sources is associated with pion production, either in pp or in $p\gamma$ interactions. The latter process is only effective in sufficiently hot environments corresponding to center-of-mass energies above the pion production threshold Eq. (II.4). From this perspective it is natural to assume that the CR injection has a broken power-law behavior associated with the transition between different production mechanisms. For the fit of the low crossover scenario in the preceeding section we have used CR data above 5×10^8 GeV. The results of the fit are not sensitive to a broken power-law injection as long as the transition occurs below this energy. For simplicity, we can account for this transition by introducing a low-energy cutoff $E_{\rm min}$ in CR injection.

Table II.3: *Best fit neutrino fluxes*

Data Set	γ	n	$J_{\text{all flavor}}\,[\text{GeV}^{-1}\text{cm}^{-2}\text{s}^{-1}\text{sr}^{-1}]$
Akeno & AGASA	2.55	3.65	$4.9 \times 10^{-3}\,(E/\text{GeV})^{-2.55}$
Fly's Eye & HiRes	2.55	3.45	$2.6 \times 10^{-3}\,(E/\text{GeV})^{-2.55}$

A cutoff $E_{\min}$ in the CR spectrum translates into a cutoff $\epsilon_\nu E_{\min}$ for the neutrinos and we can easily incorporate this effect in Eq. (II.28) by introducing an energy dependent minimal redshift

$$E_\nu(1+z) > \epsilon_\nu E_{\min} \qquad \Rightarrow \qquad z_{\min} = \epsilon_\nu \frac{E_{\min}}{E_\nu} - 1 < z_{\max}\ . \tag{II.29}$$

If we set $E_{\min} = 5 \times 10^8$ this results in a smooth cutoff in the neutrino spectrum observed on Earth at $\epsilon_\nu E_{\min}/(1+z_{\max}) \approx 10^{7.1}$ GeV. As a result, the low crossover scenario does not necessarily constrain neutrino fluxes below $10^{7.1}$ GeV.

The fit of the low crossover scenario to CRs above the 2nd knee does not depend on an increase of the maximal redshift $z_{\max}$ beyond 1.72. In fact, as long as $z_{\max}$ is larger than about 1.5 there is practically no change in the goodness-of-fit test. However, Eq. (II.28) indicates that a change in $z_{\max}$ can effect the normalization of the neutrino flux if $n - \gamma > 1/2$ since $H(z) \sim (1+z)^{3/2}$ for large z. For a change of $z_{\max}$ in the redshift region $1.5 - 2.0$ this corresponds to a change of about $\pm 10\%$ of the extragalactic neutrino flux.

The total neutrino flux of Eq. (II.26) does not include electron anti-neutrinos from the β-decay of neutrons escaping the optically thin source. This is an additional contribution of cosmic neutrinos. We have already estimated (Sec. II.3.1) that the energy is three orders of magnitude below the energy of the emerging proton. Hence, the flux of UHE neutrinos is dominated by the neutrinos from pion decay.

3.3. Cosmogenic Neutrinos

The opacity of the cosmic photon background to ultra-high energy protons propagating over cosmological distances guarantees a cosmogenic flux of neutrinos, originated in the reaction $p + \gamma \rightarrow n + \pi^+$ [89]. This flux of *cosmogenic* neutrinos has recently been estimated in a very general context using different initial nuclei and the photon background in the ultra-violet, optical and infra-red as well as the CMB [90, 91]. At neutrino energies larger than 10^8 GeV the flux of cosmogenic neutrinos originating from extragalactic protons is dominated by interactions with the CMB photons. In analogy with the proton propagation function this cosmogenic flux is obtained by replacing $P_{p|n}$

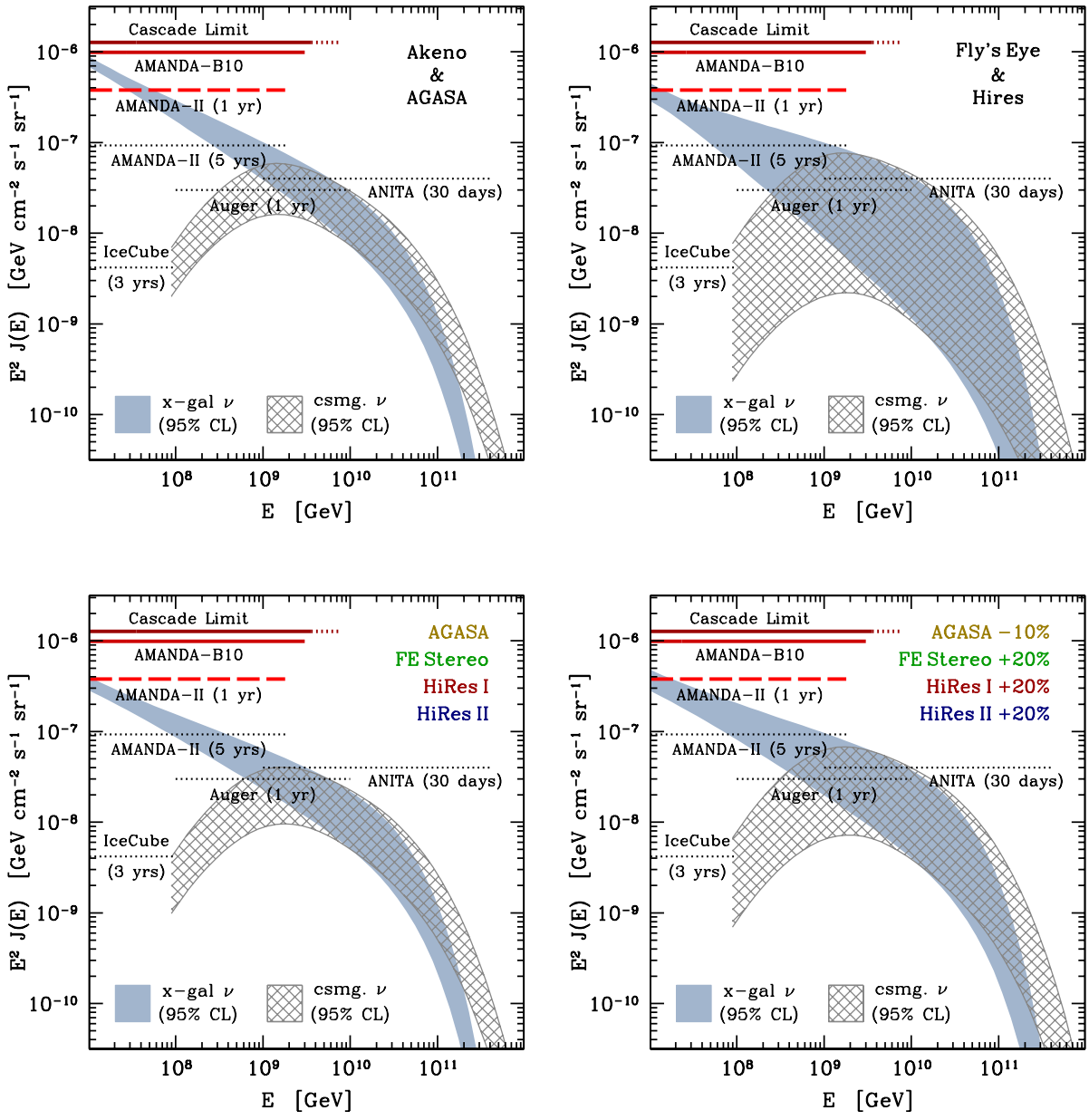

Figure II.10: *Cosmic neutrino fluxes (summed over all flavors) corresponding to the 95% CL of the low crossover model. The blue shaded band shows the neutrino flux from pion decay in optically thin sources with a relative pion energy $\epsilon_\pi = 0.28$. The gray cross-hatched band correspond to the flux of cosmogenic neutrinos above 10^8 GeV. Also shown are the cascade limit [82, 83] (see text for details) and upper bounds (90% CL) of the total diffuse neutrino flux from AMANDA-B10 [84]. The red dashed line indicate the preliminary limit from the AMANDA-II 1-year analysis [85]. The dotted lines show the predicted sensitivities of AMANDA-II [85] (5 years), IceCube [86] (3 years), Auger [87] (1 year), and ANITA [42, 88] (30 days).*

in Eq. (II.3) with $P_{\nu|n}$,

$$J_\nu = \frac{1}{4\pi} \int_0^\infty dE_i \int_0^\infty dr \left| \frac{\partial P_{\nu|n}(E; E_i, r)}{\partial E} \right| \mathcal{L}_n \ . \tag{II.30}$$

The results are shown in Fig. II.10 in comparison with neutrinos from the source. The cosmogenic neutrino flux corresponding to the standard E_i^{-2} injection spectrum has been previously obtained in Ref. [92] for several assumed source evolution indices. A comparison with the WB flux shows that these (the cosmogenic and source fluxes) are comparable at energies above 10^8 GeV. This is in striking contrast with the fluxes resulting from the low crossover scenario. As can be seen in Fig. II.10, the source flux dominates the cosmogenic flux at energies below 10^9 GeV in the low crossover scenario. [15] Thus, the neutrinos below this energy behave as "unscathed messengers" of the source injection spectrum. The observation of a neutrino flux with a power law spectral index > 2.4 can provide strong support for the low crossover scenario.

3.4. Confrontation with Experimental Results

Currently, the AMANDA neutrino telescope sets the strongest bounds on the diffuse neutrino flux in the low crossover scenario with optically thin sources. The corresponding limits (published or preliminary) on the diffuse neutrino fluxes are shown in the panels of Fig. II.10 together with extragalactic and cosmogenic neutrino fluxes at the 95% CL of our fit [84, 85]. The dotted lines show the predicted sensitivities of AMANDA-II [85] (5 years), IceCube [86] (3 years), Auger [87] (1 year), and ANITA [42, 88] (30 days).

At this statistical level the neutrino fluxes are all consistent with the AMANDA-B10 upper limit.[16] The preliminary limit of the the 2-year AMANDA-II analysis seems to be inconsistent with the 95% CL neutrino flux derived with the Akeno & AGASA data in the energy range below 5×10^7 GeV. However, the combined analysis of the data shown in the lower panels of Fig. II.10 is consistent at the 95% CL. Moreover, the results of the preliminary AMANDA-II analysis is based on a Monte-Carlo fit of the data assuming an E^{-2}-flux of neutrinos incident on Earth. We have checked that the total neutrino flux in the overlap interval from 10^7 GeV to 1.8×10^9 GeV is consistent with the bound. Clearly, the sensitivity of AMANDA-II (5 years) or Auger (1 year) is sufficient to rule out this model. In the case of a positive indication by AMANDA-II, the IceCube facility will be capable of discriminating between the low and high crossover scenarios.

Cascade Limit

The panels of Fig. II.10 show also the *cascade limit* [94] from Ref. [82, 83], which applies to all scenarios where neutrinos originate from pion decays. Due to approximate isospin

[15] We have checked that for a change of $z_{\min}$ to zero and for $E_{\max}$ larger than the default 10^{12} GeV, the resulting cosmogenic neutrino fluxes do not change within the energy range shown in Fig. II.10. For smaller $E_{\max}$, the predicted fluxes get even smaller.

[16] The AMANDA/IceCube limits and sensitivies correspond to a 90% CL. At the 95% CL these upper limits will increase by 25% to 60% depending on the background [93].

symmetry the different pion flavors π^+, π^0, and π^- will be produced in a ratio $1:1:1$ with approximately the same energy. The charged pions decay via $\pi^- \to \mu^- + \bar{\nu}_\mu \to e^- + \bar{\nu}_e + \nu_\mu + \bar{\nu}_\mu$ and the charge conjugate process. In this decay each neutrino takes a quarter of the energy of the original pion. Instead, the neutral pion decays as $\pi^0 \to \gamma + \gamma$ into two high energy photons. These photons scatter off the interstellar photon background producing electron-positron pairs, which lose their energy rapidly due to synchrotron losses in the intergalactic magnetic field. This is also the fate of the electron produced by the decay of the charged pions with one quarter of their energy. The electrons and positrons from Bethe-Heitler pair production and pion decays initiate an electro-magnetic cascade and convert most of their energy into gamma radiation. The process of multiplication dies out when the center of mass energy of photon-photon scattering drops below the pair production threshold $2m_e \approx 1$ MeV. For CMB photons with mean energy of about 0.6 meV this occurs at energies of about 1 TeV. A more careful treatment shows that this process leads to a "pile-up" of gamma-rays in the energy range 10 MeV to 1 TeV [75].

The *cascade limit* is a consequence of the bolometric energy budget of this process. The synchrotron cascade will take half of the total energy of the pions, 1/3 from π^0 and 1/6 from $\pi^\pm$. Since the radiation should not exceed the gamma-radiation below 1 TeV we can derive a bound by

$$\int_{10\,\mathrm{MeV}}^{1\,\mathrm{TeV}} \mathrm{d}E_\gamma \, E_\gamma J_\gamma \gtrsim \int \mathrm{d}E_\nu \, E_\nu J_\nu \ . \tag{II.31}$$

A comparison with the EGRET measurement of the GeV-γ flux [82, 83] gives an upper bound (per flavor) of

$$J_\nu(E) \lesssim 4 \times 10^{-7} \left(\frac{E}{\mathrm{GeV}}\right)^{-2} \mathrm{GeV\,cm^{-2}\,s^{-1}\,sr^{-1}} \ . \tag{II.32}$$

IceCube Sensitivity

In the previous sections we have shown that if the nucleon-emitting sources are optically thin, then the diffuse flux of neutrinos produced by these sources provides a powerful tool in discriminating between the galactic and extragalactic CR origin. Should the entire scenario not be ruled out by AMANDA-II data, it is of interest to explore the potential of forthcoming neutrino telescopes to provide conclusive identification of the crossover energy. In anticipation of the next chapter covering the interactions of neutrinos we will estimate the rate of events expected at the IceCube detector from the low crossover model.

In deep ice/water/salt, neutrinos are detected by observation of the Cherenkov light emitted by charged particles produced in neutrino interactions. In the case of an incident high-energy muon neutrino, for instance, the neutrino interacts with a hydrogen or oxygen nucleus in the deep ocean water (or ice) and produces a muon traveling in

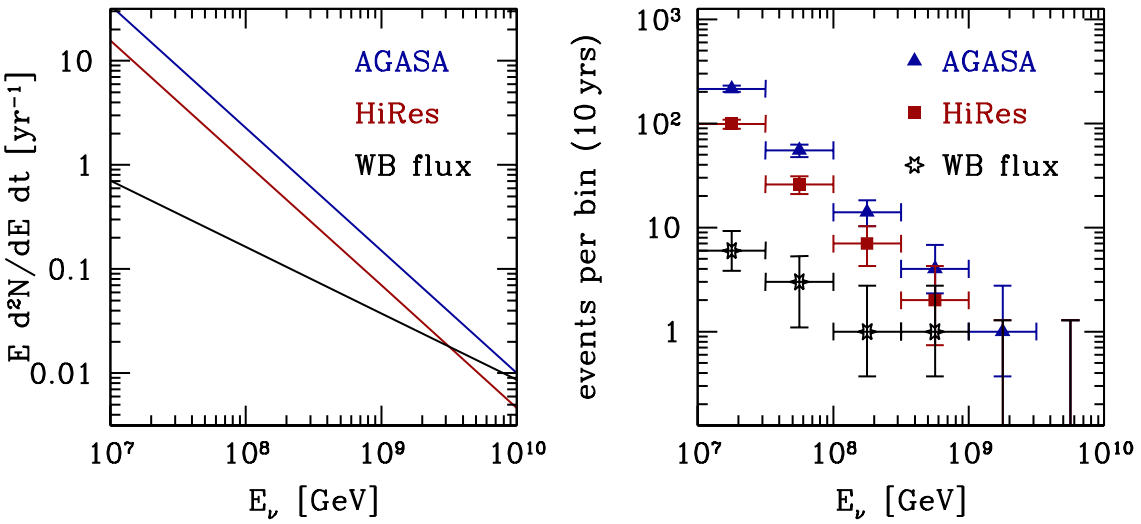

Figure II.11: **Left panel:** *Differential event rate at IceCube for the different neutrino flux predictions from AGASA (top), HiRes (middle) and WB (bottom) (Eq. II.27) obtained in Sec. 3.1.* **Right panel:** *Expected bin-by-bin event rates for 10 years of operation. The bin partition interval is taken as* $\Delta \log_{10} E = 0.5$.

nearly the same direction as the neutrino. The blue Cherenkov light emitted along the muon's kilometer-long trajectory is detected by strings of photomultiplier tubes deployed at depth shielded from radiation. The orientation of the Cherenkov cone reveals the neutrino direction. There may also be a visible hadronic shower if the neutrino is of sufficient energy.

The Antarctic Muon And Neutrino Detector Array (AMANDA) [95], using natural 1 mile deep Antarctic ice as a Cherenkov detector, has operated for more than 4 years in its final configuration of 680 optical modules on 19 strings. The detector is in steady operation collecting roughly four neutrinos per day using fast on-line analysis software. Its performance has been calibrated by reconstructing muons produced by atmospheric muon neutrinos [96].

Overall, AMANDA represents a proof of concept for the kilometer-scale neutrino observatory, IceCube [97], now under construction. IceCube will consist of 70 kilometer-length strings, each instrumented with 60 10-inch photomultipliers spaced by 17 m. The deepest module is 2.4 km below the surface. The strings are arranged at the apexes of equilateral triangles 125 m on a side. The instrumented detector volume is a cubic kilometer. A surface air shower detector, IceTop, consisting of 160 Auger-style [66] Cherenkov detectors deployed over 1 km^2 above IceCube, augments the deep-ice component by providing a tool for calibration, background rejection and air-shower physics. Construction of the detector started in the austral summer of 2004/2005. At the time of writing, 9 strings have been deployed in the polar ice so far. With a scheduled deployment of 13 to 14 strings per austral summer 50% (35 strings) of the final volume will be covered by 2008 and 100% of it by 2011.

In anticipation of the succeeding chapter we will estimate the prospects of the IceCube

detector to discriminate between the low and high crossover scenario. At the energies under consideration, there is no atmospheric muon or neutrino background in a km^3 detector. The differential event rate is given by

$$\frac{\mathrm{d}^2 N}{\mathrm{d}E\,\mathrm{d}t} \approx 2\pi \times n_{\mathrm{ice}} \times V_{\mathrm{eff}} \times \sigma_{\nu N}^{\mathrm{CC}} \times J_\nu \ , \tag{II.33}$$

where $n_{\mathrm{ice}} = \rho_{\mathrm{ice}}/m_p$ is the nucleon target density in ice, $V_{\mathrm{eff}} \approx 2$ km^3 is the effective volume and $\sigma_{\nu N}^{\mathrm{CC}} \approx 5.5\,\mathrm{pb} \times (E/\mathrm{GeV})^{0.363}$ is the charged current neutrino-nucleon cross section [98]. The effective volume used is conservative, since muon tracks can originate well outside the fiducial volume of the detector [99]. In addition, neutral current interactions of high energy neutrinos may also produce observable hadronic cascades in neutral current interactions, but with lower shower energy.

In Fig. II.11 we show the differential event rate at IceCube from optically thin sources. Also shown are the expected bin-by-bin event rates for 10 years of data collection, with a bin partition size $\Delta \log_{10} E = 0.5$. The vertical error bars are obtained on the basis of Poisson statistics with $\Delta \log_{10} N = 0.434\sqrt{N}/N$, for $N > 20$. For smaller statistics we use Poisson confidence intervals [93]. It is strongly indicated that within its lifetime IceCube will attain sufficient sensitivity to constrain the energy of transition between galactic and extragalactic dominance. RICE [100, 101, 102], PAO [66, 67], EUSO [103], ANITA [88], and OWL [104] also have the potential to measure the ultra-high energy neutrino flux. However, the energy thresholds, systematics, backgrounds, or time-scales to completion leave these experiments less promising than IceCube for a spectrum determination in the near future.

The 95% CL of the low crossover scenario presented in Fig. (II.10) indicates, that a different production mechanism of neutrinos with a larger pion energy ϵ_π relative to the neutron energy will be inconsistent with upper limits. In particular, if the primary proton spectrum $\propto E_i^{-\gamma}$, the dominance of inelastic pp collisions produces an isotropically neutral mix of pions that on decay give rise to a neutrino flux with spectrum $\propto E^{-\gamma}$ [105] The corresponding inelasticity of the process $p + p \rightarrow$ nucleons + pions, has been estimated as $\langle E_{\mathrm{pions}} \rangle / \langle E_{\mathrm{protons}} \rangle \approx 0.6$ [106]. With our notation this translates into $\epsilon_\pi \approx 2/3 \times 0.6/0.4 = 1$, assuming that 2/3 of the final state pions are charged. This would increase the normalization of the neutrino flux of Eq. (II.28) by a factor $\sim 0.28^{(1-\gamma)}$ which is ~ 7 in the case of the best fit value $\gamma = 2.55$. This sizeable augmentation of the neutrino flux based on optically thin sources with dominant pp scattering will result in the exclusion of the low crossover scenario.

Summary

The neutrino fluxes from optically thin proton sources associated with the "low crossover" scenario (Sec. II.2) extend the standard Waxman-Bahcall flux from a "high crossover" at energies below 10^9 GeV. At 10^7 GeV the neutrino flux from $p\gamma$ interactions in the source is marginally consistent with current experimental bounds from the AMANDA

Collaboration [86]. This result is robust w.r.t. variations of the data samples, calibration, and inclusion of preliminary data from the Pierre Auger Observatory. This complements the analysis of our Ref. [4]. The sensitivity of the AMANDA-II data, accumulated over five years of observation, should be sufficient to rule out the low crossover scenario, if no neutrino events are detected. In case of a positive indication, the IceCube detector may discriminate between a low and high crossover within 10 years of observation.

This section concludes our investigation of cosmic neutrino fluxes. We use these fluxes in the following chapter III for the discussion of neutrino-nucleon interactions. In section III.1 we start with a review of our current understanding of neutrino-nucleon scattering at ultra high energies and extend these ideas in sections III.2 and III.3 to well-motivated and exotic extensions of the SM.

III. Neutrino-Nucleon Scattering

1. Weak Interactions

The preceding discussion of cosmic neutrinos associated with CR production and propagation has implicitly assumed the knowledge of their interactions with matter. In this section we want to supplement the derivation of the neutrino's weak interaction, which is part of the Standard Model of particle physics. This will also provide the necessary techniques for the further discussion of neutrino interactions beyond the SM.

The Standard Model (SM) is a spontaneously broken Yang-Mills theory with a gauge group $\mathrm{SU(3)_c} \times \mathrm{SU(2)_L} \times \mathrm{U(1)_Y}$. The chiral representations[1] of quarks and leptons are arranged in three families $i = 1, 2, 3$. Each family i contains a gauge representation of left-handed quarks $Q_i = (3, 2)_{1/6}$ and leptons $L_i = (1, 2)_{-1/2}$ as well as right-handed up and down quarks, $u_i = (3, 1)_{2/3}$ and $d_i = (3, 1)_{-1/3}$, respectively, and the right-handed lepton $e_i = (1, 1)_{-1}$. The subgroup $\mathrm{SU(2)_L} \times \mathrm{U(1)_Y}$ is spontaneously broken to the electro-magnetic $\mathrm{U(1)_{em}}$ by the Higgs field $H = (1, 2)_{1/2}$ which has a non-zero vacuum expectation value v. In this process, three of the four components of the complex Higgs are "eaten" by the $W^\pm$ and Z^0 bosons, which receive masses $M_W^2 = \pi\alpha v^2 / \sin^2\theta_\mathrm{w}$ and $M_Z^2 = M_W^2 / \cos^2\theta_\mathrm{w}$, respectively.[2] The remaining Higgs component is left as a $\mathrm{U(1)_{em}}$ neutral real scalar. The $W^\pm$ and Z^0 bosons are superpositions of the gauge bosons A^a of $\mathrm{SU(2)_L}$ and B of $\mathrm{U(1)_Y}$ with a mixing $W^\pm = A^1/\sqrt{2} \mp iA^2/\sqrt{2}$ and $Z^0 = \cos\theta_\mathrm{w}\, A^3 - \sin\theta_\mathrm{w}\, B$. The measured values $M_W \approx 80.4$ GeV and $M_Z \approx 91.2$ GeV fix the weak mixing angle at $\sin^2\theta_\mathrm{w} \approx 0.23$ and the Higgs vacuum expectation value at $v \approx 246$ GeV.

The neutrino is part of the left-handed lepton representation L_i. In collisions with matter in the Earth's atmosphere or its interior the left-handed neutrino couples weakly via Z^0 and $W^\pm$ exchange to the constituents of a proton or neutron. For the calculation of this process a discussion of strong interactions between these constituents is necessary, which involves both, perturbative and non-perturbative aspects due to "hard" and "soft" processes, respectively, and due to the scale dependence of the coupling. In the following we discuss this behavior in more detail.

1.1. Parton Model

The renormalized couplings, masses and mixing matrices of a quantum field theory depend on the particular renormalization scale μ. This dependence is described by a set of

[1] We show the hypercharge Y as a subscript of the $\mathrm{SU(3)_c} \times \mathrm{SU(2)_L}$ gauge representation (A, B).
[2] $\alpha \approx 1/128$ at $Q^2 = M_W^2$

non-linear partial differential equations, so-called *renormalization group* (RG) equations. In a Yang-Mills theory like the SM the scale dependence of a gauge coupling g can be determined perturbatively as $\mu \mathrm{d}g/\mathrm{d}\mu = b\, g^3 + \mathcal{O}(g^5)$ where the coefficient b depends on the number of light representations of the gauge group. The dependence on the renormalization scale does not affect measurable quantities. However, in a perturbative expansion of the gauge coupling one typically comes across higher order corrections proportional to powers $(g^2 \ln(Q^2/\mu^2))^n$, where Q^2 is the momentum transfer between the particles. We can avoid a large contribution from these logarithmic factors and improve the convergence of the expansion, if we choose the value of the coupling $g(\mu)$ at $\mu^2 \approx Q^2$. In this way, the dependence on the renormalization scale translates into a *running* of the coupling with momentum transfer.

For the gauge coupling of *quantum chromodynamics* (QCD) one finds a negative $b = -3/(4\pi)^2$. As a result the coupling decreases with the scale μ, which is known as *asymptotic freedom* of this theory. Instead, at scales close to $\Lambda_{\mathrm{QCD}} \approx 200$–$300$ MeV the QCD coupling gets large. This behavior of the QCD coupling at small momentum transfers is the reason for the *confinement* of quarks and gluons within distance and time scales above $\Lambda_{\mathrm{QCD}}^{-1}$. In Nature the only manifestations of $\mathrm{SU}(3)_{\mathrm{c}}$ colored representations are composite gauge singlets such as mesons and baryons. These bound states consist of the *valence* quarks q_v, which determine the overall spin, isospin and flavor of the hadron and a *sea* of gluons and anti-quark-quark pairs, g and q_s, which results from QCD radiation and pair-creation.

Due to the strong coupling at small momentum transfer the interactions of nuclei cannot be described in a purely perturbative way. However, since the QCD interaction decreases with scale the constituents of a nucleon may be treated as loosely bound objects within sufficiently small distance and time scales ($\Lambda_{\mathrm{QCD}}^{-1}$). Hence, in a hard scattering process of a neutrino with a large momentum transfer to a nucleon the interactions between quarks and gluons may factorize from the subprocess (see Fig. III.1). Due to the renormalization scale dependence of the couplings this *factorization* will also depend on the absolute momentum transfer $Q^2 \equiv -q^2$.

A general lepton-nucleon scattering process is sketched in Fig. III.1. The nucleon N with mass M scatters off the lepton ℓ by a t-channel exchange of a boson. The final state consist of a lepton ℓ' and a hadronic state H with center of mass energy $(P+q)^2 = W^2$. This scattering process probes the *partons*, the constituents of the nucleon with a characteristic size M^{-1} at length scales of the order Q^{-1}. Typically, this probe will be *deep* and *inelastic*, corresponding to $Q \gg M$ and $W \gg M$, respectively. The sub-process between lepton and parton takes place on time scales which are short compared to those of QCD interactions and can be treated separately from the soft QCD interactions in the spirit of factorization. The intermediate colored states of this subprocess, the scattered parton and the remaining constituents of the nucleus, will then softly interact and hadronize into the final state H.

The kinematics of a lepton-nucleon scattering is conveniently described by the Lorentz scalars $x = -q^2/(2q \cdot P)$, also called *Bjorken-x*, and $y = (q \cdot P)/(k \cdot P)$ (see Fig. III.1 for

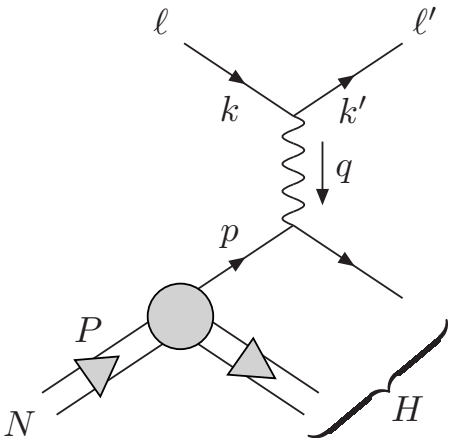

$$s \equiv (P+k)^2 \qquad t \equiv q^2 \equiv -Q^2$$

$$M^2 \equiv P^2 \qquad W^2 \equiv (P+q)^2$$

$$x \equiv \frac{Q^2}{2\,q\cdot P} \qquad y \equiv \frac{q\cdot P}{k\cdot P}$$

(Bjorken-x) (inelasticity)

$$Q \gg M \qquad W \gg M$$

(deep) (inelastic)

Figure III.1: *The kinematics of deep inelastic scattering.*

definitions). In the kinematic region of *deep inelastic scattering* (DIS) where $Q \gg M$ and $W \gg M$ we also have $Q^2 = -q^2 = 2q\cdot p + M^2 \approx 2q\cdot p$ and thus $x \approx (q\cdot p)/(q\cdot P)$. The scalars x and y have simple interpretations in particular reference frames. If we change to a reference frame where the nucleon is strongly boosted along the neutrino 3-momentum $\vec{k}$ the relative transversal momenta of the partons gets negligible. The parton momentum p in the boosted frame is approximately aligned with P and the scalar x expresses the momentum fraction carried by the parton. In the rest frame of the nucleus the quantity y may be expressed as $y = (E - E')/E$, where E and E' ate the lepton's energy before and after scattering, respectively, and y is equal to the relative energy loss of the lepton.

From the previous discussion we obtain the following procedure for the calculation of the total lepton-nucleon cross section $\sigma_{\ell N}$. The differential lepton-parton cross section $\mathrm{d}\sigma_{\ell i}/\mathrm{d}t$ for a parton of type i may be calculated using a perturbative expansion in the weak coupling. The relative contribution of a parton i with Bjorken-x in the nucleon N is described by *parton distribution functions* (PDFs) $f_i^N(x,\mu)$. The total inclusive lepton-nucleon cross section is then given as the sum over all possible sub-processes with a parton i and PDF $f_i^N(x,Q^2)$ and an integration over the relative parton momentum x and momentum transfer t:

$$\sigma_{\ell N}(s) = \sum_{\text{parton } i} \int \mathrm{d}x \int \mathrm{d}t\, f_i^N\left(x,Q^2\right) \frac{\mathrm{d}\sigma_{\ell i}}{\mathrm{d}t}(\hat{s},t) \qquad \text{with} \quad \hat{s} \equiv xs\ . \tag{III.1}$$

The parton distribution inside a nucleon will also depend on the factorization scale μ. The evolution with respect to μ can be calculated by a perturbative QCD expansion and results in the Dokshitzer-Gribov-Lipatov-Altarelli-Parisi (DGLAP) equations [108, 109, 110, 111]. In analogy to the running gauge couplings discussed earlier the solution of the (leading-order) DGLAP equations correspond to a re-summation of powers $(\alpha_s \ln(Q^2/\mu^2))^n$ which appear by QCD radiation in the initial state partons.

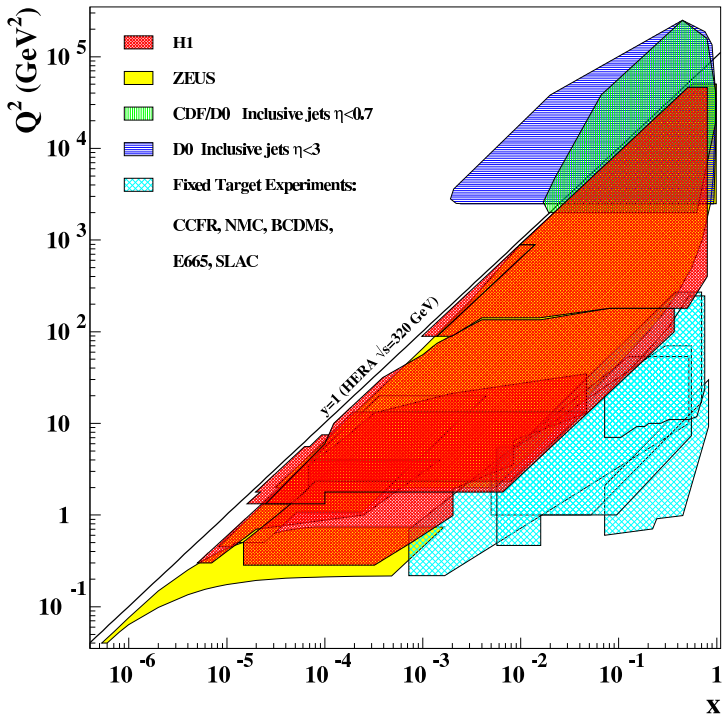

Figure III.2: *The kinematic plane (from [107]) investigated by various collider and fixed target experiments in terms of Bjorken-x and momentum transfer Q^2.*

However, these radiative processes will also generate powers $(\alpha_s \ln(1/x))^n$ and the applicability of the DGLAP formalism is limited to moderate values of Bjorken-x ($\ln(1/x)$ small) and large Q^2 (small α_s). If these logarithmic contributions from a small x get large, a formalism by Balitsky, Fakin, Kuraev, and Lipatov (BFKL) may be used to re-sum the $(\alpha_s \ln(1/x))^n$ terms [112, 113]. This approach applies for moderate values of Q^2, since contributions of $\alpha_s \ln(Q^2/\mu^2)$ have to be kept under control.

There are unified forms [114] and other improvements of the linear DGLAP and BFKL evolution for the problematic region of small Bjorken-x and large Q^2. The extrapolated solutions of the linear DGLAP and BFKL equations predict an unlimited rise of the gluon density at very small x. At some point non-linear effects like gluon recombination $g + g \rightarrow g$ should dominate the evolution and may screen or even saturate the gluon density. This idea is implemented in the Golec-Biernat Wüsthoff (GBW) model, which treats the deep inelastic scattering by interactions of color dipoles $q\bar{q}$ created in the sea of gluons [115, 116]. This ansatz has been carried out by the authors of Ref. [117] for the case of a unified DGLAP/BFKL evolution. Saturation effects at small x can also be accommodated by the formalism of *color glass condensate* (CGC) (e.g. [118]).

The evolution equations of PDFs do not predict the absolute normalization that has to be inferred from measurements. Fig. III.2 shows the regions in the kinematical x-Q^2-plane which have been covered in electron-proton (ZEUS and H1) and anti-proton-proton (CDF and D0) collisions as well as in fixed target experiments with neutrino (CCFR), electron (SLAC), and muon (BCDMS, E665, and NMC) beams (see e.g. [119]

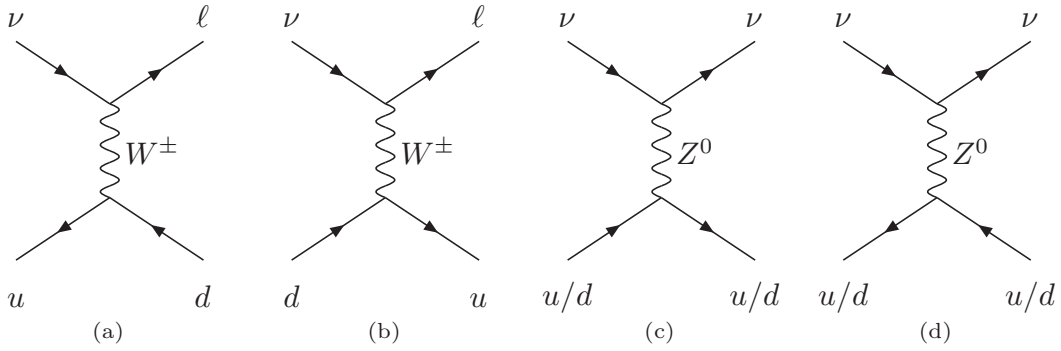

Figure III.3: *W (a/b) and Z (c/d) boson exchange between neutrinos and light quarks.*

and references therein). In the fit of the PDFs to the data one starts from an initial parameterization of $f(x, Q_0^2)$ at the reference scale Q_0 and evolves the PDFs to larger scales. The CTEQ6D [120] PDFs that we use in the following are determined by DGLAP evolution using next-to-leading order results from perturbative QCD with the DIS factorization scheme. The set of initial parameters is then optimized by a χ^2-fit to the data.

The CTEQ6D PDFs are given within the kinematic region $10^{-6} < x < 1$ and $1.3\,\mathrm{GeV} < Q < 10\,\mathrm{TeV}$ which fills out the largest part shown in Fig. III.1. However, we will see in the following that neutrino-nucleon scattering is dominated by Bjorken-x at roughly

$$x \approx \frac{M_{Z/W}^2}{2m_p E_\nu} \approx \frac{10^4\,\mathrm{GeV}}{E_\nu} \ , \tag{III.2}$$

due to the t-channel exchange of W and Z bosons. This is much smaller than 10^{-6} for neutrino energies above 10^{10} GeV. At very low x the sea-quark distribution will be driven by the gluons splitting into quark-antiquark pairs, $g \to q + \bar{q}$. At leading order, the gluon distribution evolves like

$$xg(x, Q^2) \sim A(Q^2)\, x^{-\lambda} \ , \tag{III.3}$$

where λ is in the range of 0.3 to 0.4 which depends only weakly on the scale Q^2 [121]. Hence, in our calculations we will extrapolate to smaller $x < x_0 = 10^{-6}$ by matching

$$xf(x, Q^2) = \left(\frac{x}{x_0}\right)^{-\lambda} x_0 f(x_0, Q^2) \ . \tag{III.4}$$

For simplicity, we determine the power index λ (for each parton) by a fit to the PDFs at $Q^2 = M_W^2$, the mass of the W boson.

The theoretical uncertainties of the neutrino-nucleon interaction resulting from different evolution schemes, *i.e.* a unified BFKL/DGLAP with and without nucleon screening effects and an evaluation with a color dipole scattering approach, has been estimated by

the authors of Ref. [117]. At $E_\nu = 10^{12}$ GeV, corresponding to $x \approx 10^{-8}$, the charged current cross section may diverge by a factor of 2 to 3. A (more speculative) evolution model using the formalism of CGC [122] may even decrease the gluon density at small Bjorken-x and reduce the neutrino-nucleon cross section by a factor ~ 20 compared to the un-screened case [123]. We will come back to this ambiguity w.r.t. the low-x behavior in the context of supersymmetric interactions.

1.2. Charged and Neutral Currents

The parton-level interactions of a neutrino with valence and sea quarks of a nuclei are shown in Fig. III.3 for the first family. The cross sections corresponding to these diagrams[3] are given by

$$\frac{\mathrm{d}\sigma^{(a)}}{\mathrm{d}t} = \frac{\pi\alpha^2}{2s_\mathrm{w}^4}\left[\frac{u}{s\,(t-M_W^2)}\right]^2 , \tag{III.5}$$

$$\frac{\mathrm{d}\sigma^{(b)}}{\mathrm{d}t} = \frac{\pi\alpha^2}{2s_\mathrm{w}^4}\left[\frac{1}{(t-M_W^2)}\right]^2 , \tag{III.6}$$

$$\frac{\mathrm{d}\sigma^{(c)}}{\mathrm{d}t} = \frac{\pi\alpha^2}{2s_\mathrm{w}^4}\frac{4}{c_\mathrm{w}^4}\left\{\left[\frac{u\,\mathcal{X}^i_{u_\mathrm{R}/d_\mathrm{R}}\mathcal{X}^i_\nu}{s\,(t-M_Z^2)}\right]^2 + \left[\frac{\mathcal{X}^i_{u_\mathrm{L}/d_\mathrm{L}}\mathcal{X}^i_\nu}{(t-M_Z^2)}\right]^2\right\} , \tag{III.7}$$

$$\frac{\mathrm{d}\sigma^{(d)}}{\mathrm{d}t} = \frac{\pi\alpha^2}{2s_\mathrm{w}^4}\frac{4}{c_\mathrm{w}^4}\left\{\left[\frac{u\,\mathcal{X}^i_{u_\mathrm{L}/d_\mathrm{L}}\mathcal{X}^i_\nu}{s\,(t-M_Z^2)}\right]^2 + \left[\frac{\mathcal{X}^i_{u_\mathrm{R}/d_\mathrm{R}}\mathcal{X}^i_\nu}{(t-M_Z^2)}\right]^2\right\} . \tag{III.8}$$

Summation over repeated indices is implied and we use the conventions and notations of Refs. [124, 125], in particular $\sin\theta_\mathrm{w} = s_\mathrm{w}$ and $\cos\theta_\mathrm{w} = c_\mathrm{w}$. In charged current interactions with an exchange of the $W^\pm$ boson only left-handed quarks and right-handed anti-quarks contribute corresponding to a coupling $\propto \sqrt{2}eT^3/s_\mathrm{w}$ depending on the weak isospin T^3.[4] In view of the supersymmetric interactions to be discussed in the next section we express the couplings to the Z boson in the basis of B and A^3 bosons $\propto e\mathcal{X}^i/(s_\mathrm{w}c_\mathrm{w})$. The "charge vector" $\mathcal{X}^i = Y\delta^{1i}s_\mathrm{w} + T^3\delta^{2i}c_\mathrm{w}$ depends on the hypercharge $Y = Q - T^3$ and the weak isospin T^3. Explicitly, we have,

$$\mathcal{X}^i_{u_\mathrm{L}}\mathcal{X}^i_\nu = \frac{1}{4}\left(1 - \frac{4}{3}s_\mathrm{w}^2\right) , \qquad \mathcal{X}^i_{d_\mathrm{L}}\mathcal{X}^i_\nu = \frac{1}{4}\left(-1 + \frac{2}{3}s_\mathrm{w}^2\right) ,$$
$$\mathcal{X}^i_{u_\mathrm{R}}\mathcal{X}^i_\nu = -\frac{1}{3}s_\mathrm{w}^2 , \qquad \mathcal{X}^i_{d_\mathrm{R}}\mathcal{X}^i_\nu = \frac{1}{6}s_\mathrm{w}^2 . \tag{III.9}$$

In the scattering processes of neutrinos with matter in the atmosphere or the Earth's interior one may substitute the protons and neutrons by *isoscalar nucleons* N, *i.e.* one

[3] The cross sections for the analogous processes with anti-neutrinos are the same.

[4] The SU(2) generators are taken to be $t^a = \frac{1}{2}\sigma^a$ with the Pauli matrices σ, in particular $t^3 = \mathrm{diag}\left(\frac{1}{2}, -\frac{1}{2}\right)$

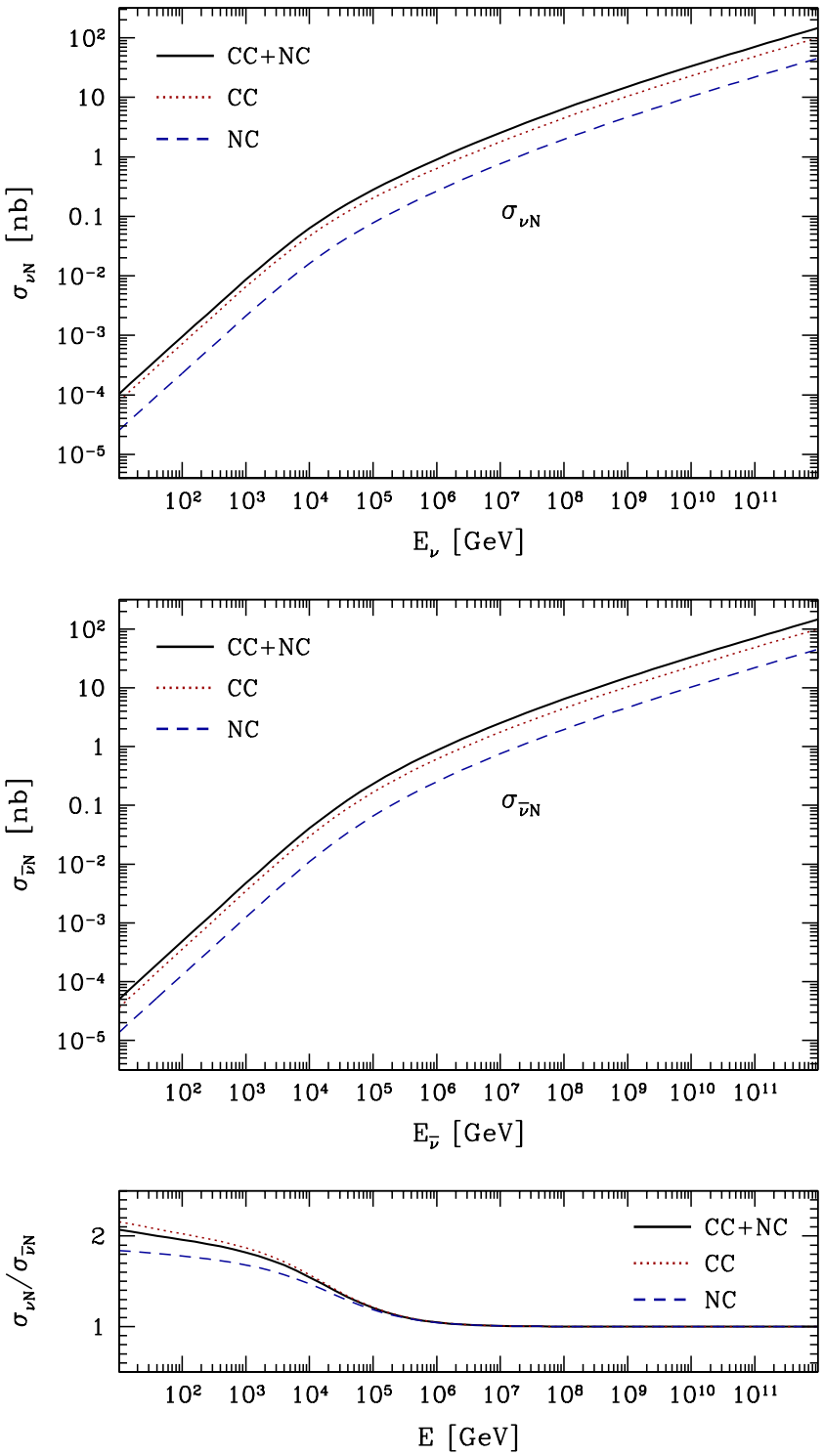

Figure III.4: *The charged (red dotted) and neutral (blue dashed) current cross section for neutrino-nucleon scattering from Z and W boson exchange.*

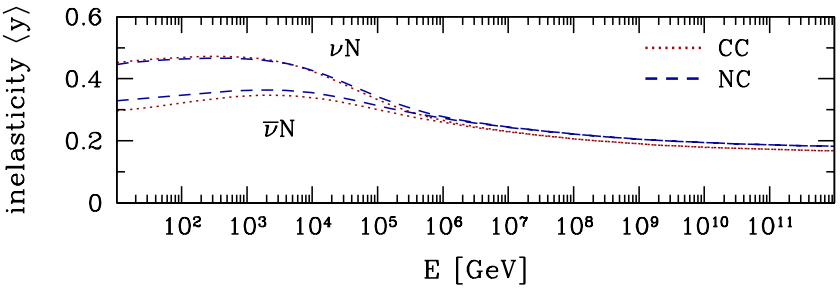

Figure III.5: *The mean inelasticity of charged (red dotted) and neutral (blue dashed) current cross section for neutrino-nucleon scattering from Z and W boson exchange.*

averages over weak isospin according to $\sigma_{\nu N} \approx (\sigma_{\nu p} + \sigma_{\nu n})/2$. We use this standard approximation in the following. Due to the approximate isospin symmetry between up and down quarks the PDFs of the neutron can be approximated by $f_u^n = f_d^p$ and $f_d^n = f_u^p$ and analogously for $\bar{u}$ and $\bar{d}$. The cross section at the nucleon level $\sigma_{\nu N}$ is then determined by Eq. (III.1) and shown in Fig. III.4.

The difference between the cross sections of νN and $\bar{\nu} N$ scattering is very small and shown in the lower panel of Fig. III.4. In the following section we will take an average cross section for our calculations. According to the authors of Ref. [98] the cross sections in the energy region $10^7\,\mathrm{GeV} < E_\nu < 10^{12}\,\mathrm{GeV}$ can be approximated within 10% accuracy by

$$\begin{aligned}
\sigma_{\nu N}^{\mathrm{CC}} &= 5.53\,\mathrm{pb}\left(\frac{E_\nu}{1\,\mathrm{GeV}}\right)^{0.363}, & \sigma_{\bar{\nu} N}^{\mathrm{CC}} &= 5.52\,\mathrm{pb}\left(\frac{E_\nu}{1\,\mathrm{GeV}}\right)^{0.363}, \\
\sigma_{\nu N}^{\mathrm{NC}} &= 2.31\,\mathrm{pb}\left(\frac{E_\nu}{1\,\mathrm{GeV}}\right)^{0.363}, & \sigma_{\bar{\nu} N}^{\mathrm{NC}} &= 2.29\,\mathrm{pb}\left(\frac{E_\nu}{1\,\mathrm{GeV}}\right)^{0.363}, \\
\sigma_{\nu N}^{\mathrm{tot}} &= 7.84\,\mathrm{pb}\left(\frac{E_\nu}{1\,\mathrm{GeV}}\right)^{0.363}, & \sigma_{\bar{\nu} N}^{\mathrm{tot}} &= 7.80\,\mathrm{pb}\left(\frac{E_\nu}{1\,\mathrm{GeV}}\right)^{0.363}. \qquad \text{(III.10)}
\end{aligned}$$

1.3. Neutrino Observation

Due to the feeble interaction of neutrinos with matter, neutrino observatories involve large-scale detection volumes with an efficient shielding from the background. Up to now, UHE cosmic neutrinos have been searched for in the Earth's atmosphere (AGASA [126]), in the Greenland (FORTE [127]) and Antarctic ice sheet (AMANDA [96, 128, 129, 84, 130], RICE [100, 101, 102], ANITA-lite [88]), in lake Baikal [131], in salt (SALSA [132]) or in the regolith of the moon (GLUE [133]). Up to now, all these experiments have only reported negative search results and quote upper limits on the diffuse flux of UHE neutrinos. In the following we give a brief overview of commonly used detection methods.

Optical Detection

Secondary charged particles produced in inelastic neutrino scattering may be observed by their emission of Cherenkov light in transparent media. We have already presented the

AMANDA detector and its follow-up IceCube as representatives of this detection technique. Other large scale Cherenkov telescopes, currently operating or under construction, are located in lake Baikal [131] and in the Mediterranean (Antares [134], NEMO [135], NESTOR [136]).

The mean inelasticity $\langle y \rangle$ in neutrino-nucleon interactions (see Fig. III.5) approaches about 20% for charged and neutral current interactions at large neutrino energies. The struck hadron carries 20% of the neutrino energy and initiates a *hadronic cascade* visible by its secondary charged particles, mostly muons and electrons. This process is not sensitive to neutrino flavor and its observation determines or limits the total neutrino flux.

The situation changes if we look for the scattered leptons. In neutral current interactions the neutrino travels on with about 80% of its initial energy and may undergo other inelastic collisions on rare occasions. In high energy charged current interactions the emerging lepton is visible by its Cherenkov light in the detector. However, the signature of the particular process will predominantly be determined by the secondary charged particles, created by bremsstrahlung, photonuclear interactions and e^+e^- pair production in matter, as well as the life-time of the lepton.

Electron and Tau Neutrinos

In the case of electron neutrinos the emerging electron will immediately initiate an *electro-magnetic cascade*, mainly due to strong bremsstrahlung and Bethe-Heitler pair production in matter.[5] The effective detection volume for these events almost coincides with the fiducial volume. Due to the topology of the elongated cascades, typically with a length of 5–10 m and a diameter of a few 10 cm, the incident angle of the electron neutrino can be determined with an accuracy of $\Delta\theta \sim 10°$–$30°$. On the other hand, the energy resolution of these events is comparatively good with $\Delta \log_{10}(E_\nu/\mathrm{GeV}) = 10\%$–$20\%$ since the detector operates as a calorimeter for the contained electro-magnetic and hadronic cascades.

The tau emerging in charged current interactions of tau neutrinos has a life-time of about 0.29 ns in its rest frame. After its production, the tau may propagate a distance of $\gamma_\tau \times 87\,\mu\mathrm{m} \sim E_\nu/10^6\,\mathrm{GeV} \times 39\,\mathrm{m}$ before it decays via $\tau^- \to e^- + \bar{\nu}_e + \nu_\tau$ and initiates an electro-magnetic cascade as in the case of the electrons. Hence, UHE neutrinos may produce *double bang* signals, consisting of almost coincident hadronic and electro-magnetic cascades separated by several meters. This particular feature allows for a discrimination of tau neutrinos from electron neutrinos. The topology of the event may also serve to improve the accuracy of the incident angle.

The rate of cascades produced by electron and tau neutrinos can be estimated as follows. The diffuse neutrino flux $J_{\nu_e+\nu_\tau}$ is exponentially attenuated along the line of

[5] At shower energies of the order of 10^9 GeV one has to account for the Landau-Pomeranchuk-Migdal (LPM) effect in dense media [137, 138]: Multiple scattering of electrons with nuclei suppresses the cross section for bremsstrahlung and pair production and increases the length of the electro-magnetic cascade.

sight $-\mathrm{d}z = n\,\mathrm{d}\ell$ by CC and NC interactions with matter in the atmosphere or the Earth's interior, denoted by the nucleon density $n = \rho/m_p$.[6] A neutrino traverses the integrated column depth z_{tot} before it reaches the detector with (effective) volume V_{eff} and nucleon density n_{ice}. The rate of cascades per unit of time t, solid angle Ω (with $\mathrm{d}\Omega = \sin\theta\,\mathrm{d}\theta\,\mathrm{d}\phi$), and neutrino energy E_ν is approximately (neglecting the smaller contributions from NC interactions)

$$\frac{\mathrm{d}^3 N_{\mathrm{cas}}}{\mathrm{d}t\,\mathrm{d}\Omega\,\mathrm{d}E_\nu} \approx n_{\mathrm{ice}} \times V_{\mathrm{eff}}(E_{\mathrm{sh}}) \times \sigma_{\nu N}^{\mathrm{CC}} \times J_{\nu_e+\nu_\tau} \times e^{-z_{\mathrm{tot}}\sigma^{\mathrm{tot}}} \ . \tag{III.11}$$

The effective detection volume V_{eff} depends on the energy converted into the shower, E_{sh}. At large energies the main contribution comes from directions above the horizon. In this case we can neglect the exponential attenuation of the initial neutrino flux and arrive at

$$\frac{\mathrm{d}^2 N_{\mathrm{cas}}}{\mathrm{d}t\,\mathrm{d}E_\nu} \approx 2\pi \times n_{\mathrm{ice}} \times V_{\mathrm{eff}}(E_{\mathrm{sh}}) \times \sigma_{\nu N}^{\mathrm{CC}} \times J_{\nu_e+\nu_\tau} \ . \tag{III.12}$$

For our order-of-magnitude estimation of neutrino-induced events from the low crossover scenario (Eq. (II.33)) we took $V_{\mathrm{eff}} = 2\,\mathrm{km}^3$ and substituted $J_{\nu_e+\nu_\tau}$ by the total neutrino flux J_ν. This, however, underestimates the muon events, to which we turn now.

Muon Neutrinos

In contrast, high energy muons from CC interactions of muon neutrinos will create *muon tracks* since their energy loss in matter is reduced by their larger mass ($m_\mu/m_e \approx 207$) and the life-time of 2.2 μs corresponds to distances of about $\gamma_\mu \times 660$ m. The secondary charged particles created along the muon track will be aligned with the muon due to their large Lorentz-boost and create a light cone along the track. The angular resolution for the incident neutrino is much better than in the case of cascades with $\Delta\theta = 0.3°$–$3°$. Most importantly, the effective detection volume for muon neutrinos is much larger than for other flavors since the muon can be created outside the fiducial volume. The price one has to pay in this case is the limitation in energy resolution of $\Delta \log_{10}(E_\mu/\mathrm{GeV}) = 25\%$–$50\%$ and the fact that no direct information on the neutrino energy can be extracted.

The flux of upward-going muons through the detector is estimated in the following way. The initial diffuse muon neutrino flux J_{ν_μ} is exponentially attenuated along the line of sight $-\mathrm{d}z = n\,\mathrm{d}\ell$ by CC and NC interactions in the Earth's interior with nucleon density $n = \rho_\oplus/m_p$ [139]. Here, ℓ is the distance to the detector center, which is 1.9 km below the horizon for the IceCube detector [140]. For a given nadir angle the maximal range, z_{max}, of a muon produced with an energy E_μ is limited by the integrated column depth of the Earth, $z_\oplus$, and the energy loss range in matter, which we are going to

[6] For the density of the atmosphere and the Earth's interior we use the parameterization of Ref. [139] and express the *column depth* in terms of its nucleon density per area. A column depth of 1 mb^{-1} corresponds to a column of water with depth ~ 17 m. A flux of particles with inelastic cross section of 1 mb is reduced to one e-fold after traversing this layer of water.

discuss in the next section. The flux of muons through the detector per unit of area A, time t, solid angle Ω, and neutrino energy E_ν is then approximately

$$\frac{\mathrm{d}^4 N_\mu}{\mathrm{d}t\,\mathrm{d}A\,\mathrm{d}\Omega\,\mathrm{d}E_\nu} \approx \int_{E_{\min}}^{E_{\max}} \mathrm{d}E_\mu \int_0^{z_{\max}} \mathrm{d}z\ \frac{\mathrm{d}\sigma_{\nu N}^{\mathrm{CC}}}{\mathrm{d}E_\mu} \times J_{\nu_\mu} \times \mathrm{e}^{-(z_\oplus - z)\sigma^{\mathrm{tot}}} \ . \tag{III.13}$$

The minimal and maximal muon energy, $E_{\min}$ and $E_{\max}$, is effectively limited by the detection efficiency and neutrino energy, respectively.

Air Shower Detection

Neutrino-nucleon interactions in the atmosphere may be identified by deeply penetrating showers in the quasi-horizontal directions. Cosmic particles (CR protons, cosmic neutrinos etc.) with a flux $J(E)$ interact at the point (ℓ, θ) in the atmosphere, where ℓ is the distance of this point to the detector center measured along the shower axis, and θ is the angle to the zenith at the point the shower axis hits the Earth's surface.[7] The number of *induced* showers ("N_{ind}") per unit of length ℓ along the shower axis, time t, area A perpendicular to the shower axis, particle energy E and solid angle Ω is

$$\frac{\mathrm{d}}{\mathrm{d}\ell}\left(\frac{\mathrm{d}^4 N_{\mathrm{ind}}}{\mathrm{d}t\,\mathrm{d}A\,\mathrm{d}\Omega\,\mathrm{d}E}\right) = n_{\mathrm{air}} \times \sigma^{\mathrm{tot}} \times J \times e^{-z\sigma^{\mathrm{tot}}} \ , \tag{III.14}$$

where $n = \rho_{\mathrm{air}}/m_p$ is the nucleon density of the atmosphere at altitude $h(\ell, \theta)$ [139]. Again, the energy deposited in the shower $E_{\mathrm{sh}} < E$ depends on the scattering process.

The number of *observed* showers ("N_{obs}") is determined by the trigger efficiency $\mathcal{P}(E_{\mathrm{sh}}, \theta)$ of the detector, and the effective range of the atmospheric depth contributing to visible showers. The latter, after carrying out the integral $n(\ell, \theta)\,\mathrm{d}\ell \equiv -\mathrm{d}z$, translates into a minimal and maximal atmospheric depth, $z_{\min}(\theta)$ and $z_{\max}(\theta)$, and

$$\frac{\mathrm{d}^4 N_{\mathrm{obs}}}{\mathrm{d}t\,\mathrm{d}A\,\mathrm{d}\Omega\,\mathrm{d}E} = \mathcal{P}(E_{\mathrm{sh}}, \theta) \times J \times \left(e^{-z_{\min}\sigma^{\mathrm{tot}}} - e^{-z_{\max}\sigma^{\mathrm{tot}}}\right) \ . \tag{III.15}$$

From this we can read off the experimental *exposure* $\mathcal{E}(E)$ [$\mathrm{s\,m^2\,sr}$] defined as:

$$N_{\mathrm{obs}} = \int \mathrm{d}\,E\,\mathcal{E}(E) J(E) \ . \tag{III.16}$$

The CR spectra of AGASA and HiRes shown in Fig. II.5 have been observed in the quasi-vertical direction with $\theta < 45°$ and $\theta < 60°$, respectively. The corresponding values of $z_{\min}$ and $z_{\max}$ are shown in Fig. III.6. In this angular range both detectors are sensitive to interactions in the outermost atmospheric layers and $z_{\min}(\theta)$ decreases to zero. The maximal atmospheric depth $z_{\max}(\theta)$ depends on the height of the detector sites and the

[7] In the following we will focus on showers with axis going through the detector. For detectors using the Fly's Eye technique this slightly underestimates the rate of induced event.

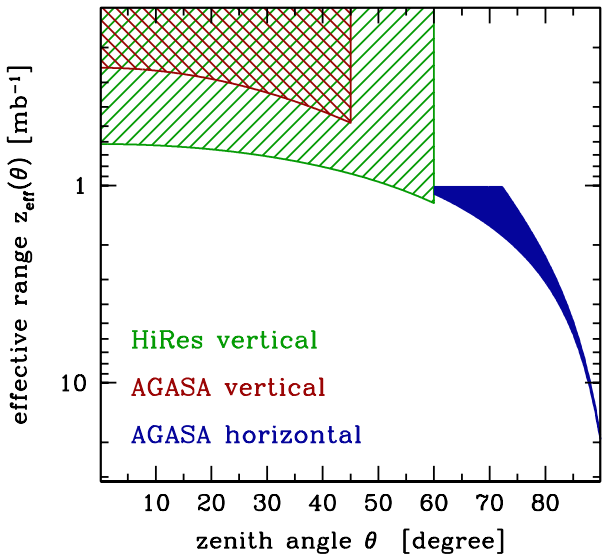

Figure III.6: *The range of atmospheric depths $z_{min} < z_{eff} < z_{max}$ used for the calculation of Eq. (III.15) for quasi-vertical showers at AGASA (red left-hatched) and HiRes (green right-hatched) and quasi-horizontal showers at AGASA (blue shaded). For the quasi-vertical showers we use $z_{min} = 0\,mb^{-1}$, corresponding to interactions in the outermost atmospheric layers.*

line of sight observed in the atmosphere. Also, for the case of AGASA we reduce the total atmospheric depth $z(\theta)$ by $500\,(g/m_p)\,cm^{-2}$ in order to exclude those interactions too close to the detector site in order to be triggered [141]. Note, that an average UHE shower develops to its maximum after traversing $800\,(g/m_p)\,cm^{-2}$ in the atmosphere.

The definition of $z_{\rm min}(\theta)$ and $z_{\rm max}(\theta)$ for quasi-horizontal directions ($\theta \gtrsim 60°$) at AGASA is described in Appendix A. The remaining window shown as the blue shaded region in Fig. III.6 has a small background from hadronic interactions since $z_{\rm min} \gtrsim 1\,{\rm mb}^{-1}$ and hence $z_{\rm hor}\,\sigma_{NN} \gg 1$. The non-observation of showers from this section of the atmosphere limits the total neutrino flux.

Radio Detection

electro-magnetic cascades induced by extremely high energy neutrino-nucleon interactions may coherently emit radio Cherenkov signals due to an anisotropic distribution of charge: Positrons annihilate with electrons in the media and additional electrons are swept into the shower by Compton scattering. This results in a local excess of negative charge in the form of a relativistically moving "pancake" with a thickness of about 1 cm and a diameter of 10 cm [142]. Cherenkov radiation from this charge excess may be emitted coherently for wavelengths larger than the shower dimension corresponding to strong radio emission scaling quadratically with the charge and hence the energy of the shower.

This *Askaryan* effect [143, 144] has been looked for in the Antarctic ice (RICE [100, 101, 102] and ANITA [88]), in salt (SALSA [132]) and the lunar regolith (GLUE [133] and FORTE [127]) to infer upper limits on the total neutrino flux [145]. For our investigation

of exotic neutrino nucleon interactions in section III.3 we will use the results from RICE which are described in Appendix A.

Acoustic Detection

The energy deployed by electro-magnetic and hadronic cascades in media is immediately converted into heat. The expanding medium generates an acoustic pulse with a width of a few ten microseconds orthogonal to the shower with a length of a few ten meters. Since the attenuation of acoustic waves in water is about a hundred times smaller than for optical waves, the acoustic signals of neutrino cascades may be observed in large reservoirs like lakes or oceans with a large spacing of detectors.

Currently, the neutrino observatories in the Mediterranean (Antares, NEMO, and NESTOR) and also the IceCube detector launch tests for a hybrid detection of UHE neutrinos supplementing the in-ice and in-water Cherenkov light detection with acoustic detection (for a nice overview see [145]). The energy threshold for these events is of the order of 10^9 GeV. For the experimental implementation the background noise in the relevant 1–100 kHz band – seasonal human activity, seasonal weather as well as marine activity for ocean sites – has to be studied carefully.

Summary

In this section we have introduced the necessary ingredients for the calculation of neutrino-nucleon interactions, *i.e.* the parton model of deep inelastic scattering, the parton distribution functions and their evolution. We have calculated the SM predictions for charged and neutral current interactions up to neutrino energies as large as 10^{12} GeV. Our calculation of the un-screened (anti-)neutrino-nucleon cross section and the mean inelasticity agrees well with calculations previously stated in the literature [139, 98], which have become standard in UHE neutrino physics. This give us an independent check for the consistency of our analysis. We have also discussed various neutrino detection methods based on SM interactions with nuclei in the Earth's atmosphere and interior.

Based on this knowledge we investigate the prospects of neutrino signals in physics beyond the SM in the succeeding sections. In the next section III.2 we introduce the supersymmetric analog of charged and neutral current interactions and discuss possible signals at Cherenkov telescopes. Section III.3 is devoted to the study of more exotic neutrino interactions which predict a much stronger interaction with matter than the SM.

2. Supersymmetric Interactions

Despite the convincing consistency of the SM in the confrontation with experimental results it is nevertheless believed to be a low energy limit of a more fundamental theory. The ultra-violet cutoff $\Lambda_{\rm UV}$ of the SM is certainly limited by the Planck scale $M_{\rm Pl} = (8\pi G_{\rm N})^{-1/2} = 2.4 \times 10^{18}$ GeV where a quantum theory of gravity might be necessary for the description of particle dynamics. However, there are reasons to believe that the break-down of the SM should occur even much below $M_{\rm Pl}$.

Most of the scepticism with respect to the SM is based on its lack of *naturalness*. In contrast to the masses of fermionic matter the mass of the scalar Higgs receives quantum corrections proportional to the square of the cutoff $\Lambda_{\rm UV}$. The mass of the Higgs should naturally be of the order of $v = 246$ GeV, the minimum of the Higgs potential and the scale of electroweak symmetry breaking. Hence, if the ultra-violet cutoff is of the order of the Planck scale the bare Higgs mass and quantum corrections have to cancel within more than 30 orders of magnitude. This *fine-tuned* cancellation seems unnatural, even if it is technically not a problem. Either the scale of new physics $\Lambda_{\rm UV}$ is much smaller than the Planck scale or we need a mechanism which assures this mysterious cancellation from a fundamental principle, *i.e.* a new symmetry principle extending the SM. In any case, an extension of the SM seems necessary.

Supersymmetry (SUSY) is currently the most popular extension of the SM (for reviews see e.g. [146, 147]). It is a fundamental symmetry between bosons and fermions with generators Q being a spinor under Lorentz transformation. Since the generators anti-commute, $\{Q, Q\} = \{Q^\dagger, Q^\dagger\} = 0$, SUSY is an exception to the *Coleman-Mandula* no-go theorem as a non-trivial extension of the space-time symmetries [148]. In particular, the generators obey $[P^\mu, Q] = [P^\mu, Q^\dagger] = 0$ and $\{Q, Q^\dagger\} \propto P^\mu$, with P^μ being the momentum generator of space-time translations. As a consequence, each SUSY representation is a mass eigenstate and comes with equal numbers of bosonic and fermionic degrees of freedom. This gives already an outline for the solution of the hierarchy problem. If a SUSY representation contains scalars and spinors, the quantum corrections to the mass have to vanish exactly since those of the former depend quadratically and those of the latter logarithmically on the cutoff. In exact SUSY the masses of the Higgs scalar and its SUSY partner, the *Higgsino*, are therefore protected from quadratic contributions of the cutoff.[8]

In the minimal SUSY extension of the SM (MSSM) each matter representation is contained in a *chiral multiplet* containing one Weyl fermion and a complex scalar, a so-called *sfermion*. Each gauge boson joins with a massless Weyl fermion, a so-called *gaugino*, forming a *vector multiplet*. The minimal extension of the Higgs sector requires two chiral multiplets in order to accomplish the necessary degrees of freedom to be "eaten up" by gauge bosons and gauginos.

[8] On the other hand, this does not explain at all, why the electroweak scale is that small compared to the Planck scale, the so-called *μ problem'*.

If SUSY is a symmetry of Nature it has to be broken in its vacuum state, since light sfermion like the *selectrons*, the SUSY partners of the electron, have not been observed. A spontaneous breaking can be achieved by a *Super-Higgs mechanism*, where auxiliary degrees of freedom of vector (*D-term*) or chiral (*F-term*) multiplets obtain a vacuum expectation value different from zero. However, there is some restriction to the (tree-level) mass spectrum after spontaneous symmetry breaking due to the fact that the super-trace of the squared mass matrices has to vanish. In particular, if we impose flavor and gauge symmetries the masses of the selectrons and the electron should obey $m^2_{\tilde{e}_1} + m^2_{\tilde{e}_2} = 2m^2_e$ and at least one selectron should be lighter or as heavy as the electron.

For this reason SUSY should be broken in a *hidden sector*, *i.e.* by additional supermultiplets which are not part of the MSSM. This SUSY breaking affects the *visible sector* containing the MSSM by *soft breaking terms*, *i.e.* mass terms and couplings with positive mass dimensions. This class of SUSY breaking terms guarantees that our original motivation for SUSY as a solution to the hierarchy problem is not spoiled. One can show that soft breaking terms give only quantum corrections to scalar squared masses proportional to m^2_{soft}. The process of *mediation* of these terms to the observable sector is model dependent. Popular soft SUSY breaking scenarios are gauge-mediated SUSY breaking (GMSB), where the mediation process is due to the SM gauge fields, or Planck-scale mediated SUSY breaking in supergravity-inspired scenarios [146].

In the following we will not be concerned about a specific SUSY breaking scenario for the mass spectra of the SUSY particles. Instead we will focus on the possibility, that the relevant SUSY masses are very close to the experimental lower limits. With these assumptions we will try to get an upper estimate of the effects, SUSY can play in neutrino-nucleon interactions. For completeness, we will also show the result in terms of a more realistic model where low energy SUSY masses are determined by GMSB.

2.1. Supersymmetry with a Long-lived Stau

In the MSSM one assumes an additional discrete symmetry between particles and SUSY particles called $\mathcal{R}$-parity, which has the effect of eliminating the possible baryon and lepton number violating interactions between the multiplets. In its simplest version each SM particle takes even parity $P_{\mathcal{R}} = +1$ and each SUSY particle $P_{\mathcal{R}} = -1$. If $\mathcal{R}$-parity is conserved the lightest SUSY particle (LSP) is stable. This makes it an excellent candidate for the dark matter. Most studies assume that this particle is a neutralino, a superposition of neutral higgsinos and gauginos, which interacts weakly and may therefore be observed in direct dark matter searches. However, if SUSY is extended to include gravity, there is an alternative LSP candidate, the gravitino $\widetilde{G}$. The next-to-lightest SUSY particle (NLSP) can only decay into final states containing the gravitino LSP. At tree level the direct decay into the gravitino is highly suppressed since, as the SUSY partner of the graviton, the gravitino takes part only in the gravitational

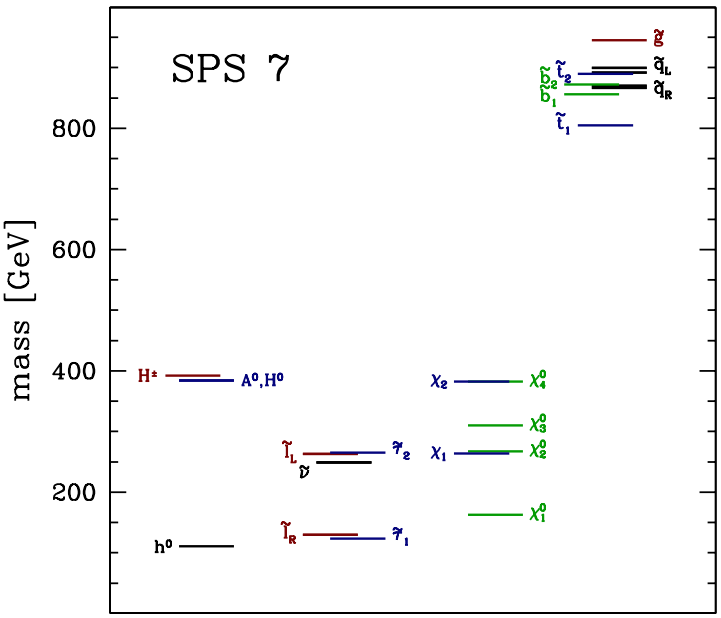

Figure III.7: *The SUSY mass spectrum of the benchmark point corresponding to SPS 7 [151]. The columns (1 to 4) show the masses of (1) the scalar Higgs sector, (2) the sfermions, (3) the charginos and neutralinos, and (4) the squarks and gluino. The SUSY particles of the third family are typically lighter than others due to the contributions of large Yukawa couplings in the renormalization group running (see text). It is also apparent that gauge interactions contribute to larger masses.*

interaction, which are suppressed by the Planck scale.[9]

Most scenarios for the generation of soft SUSY breaking terms assume universality with respect to flavor, either for the sake of simplicity or as a consequence of particular flavor-universal mediation processes like gravity mediation. The masses of the SUSY particles are scale-dependent corresponding to the renormalization group running. Starting from universal sfermion mass terms at the *input scale* far above the electroweak scale, the masses will spread in the infrared-running due to gauge ($\delta m^2 > 0$) and Yukawa interactions ($\delta m^2 < 0$).

A promising candidate for the lightest sfermion is the right-handed stau ($\widetilde{\tau}_\mathrm{R}$), the supersymmetric scalar partner of the right-handed tau: it has a large contribution from Yukawa interactions and only $\mathrm{U}(1)_\mathrm{em}$ interactions. More general, the lightest sfermion will be $\widetilde{\tau}_1$, a superposition of the gauge eigenstates $\widetilde{\tau}_\mathrm{L}$ and $\widetilde{\tau}_\mathrm{R}$. However, whether or not the stau is the NLSP depends on the particular assumptions about the soft mass terms and their value at the input scale. Figure III.7 shows the mass spectrum of SUSY particles and the Higgs sector corresponding to the benchmark point SPS 7 from [151]. If we assume a gravitino LSP the NLSP of the SPS 7 SUSY mass spectrum is the $\widetilde{\tau}_1$, which is mostly right-handed.

[9] The same is true in theories with an axino LSP, whose interactions are strongly suppressed by the large Peccei-Quinn scale, see e.g. [149]. The NLSP can also be very long-lived if its mass is very close to that of a neutralino LSP [150]. We do not study these alternatives in detail, but expect virtually the same results as in the case considered.

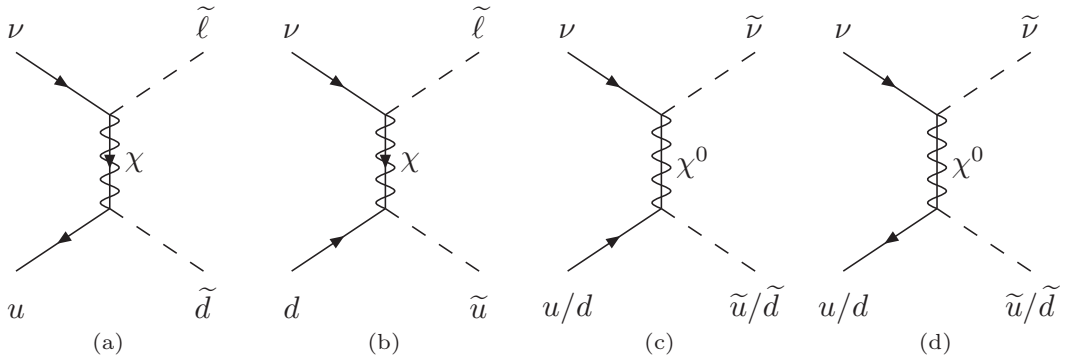

Figure III.8: *Chargino (a/b) and neutralino (c/d) exchange diagrams between neutrinos and light quarks .*

In the following we will assume that the NLSP is identical to the right-handed stau, denoted by "$\widetilde{\tau}$" in short. As a charged particle it can possibly be collected in collider experiments. The observation of the stau decays could then lead to an indirect discovery of the gravitino. This exciting possibility has attracted considerable interest recently [152, 153, 154, 155, 149]. Within this scenario, we discuss the possibility that stau NLSPs resulting from neutrino-nucleon interactions inside the Earth are sufficiently long-lived and might be detected in large ice or water Cherenkov neutrino telescopes as pointed out in Refs. [156, 157].

High energy muons are visible if they originate from up to a few tens of kilometers outside the detector. This defines the effective detection volume, which is limited by the energy loss of muons in matter. For a stau this effective detection volume increases dramatically due to the much smaller energy loss in matter [158]. This might compensate the suppression of the production cross section of SUSY particles compared to the one of the SM weak interactions. Moreover, interactions of cosmic neutrinos with nucleons inside the Earth will always produce pairs of staus, which appear as nearly parallel muon-like tracks in the detector due to their large boost-factor [156]. This is expected to be in contrast to the SM processes, which lead to muon pairs only in rare cases.

The rate of stau pairs has been estimated in Refs. [156, 159, 157, 160]. In our Ref. [5] we focus on the limited detector response for stau events using the detailed calculation of the stau energy loss in Ref. [158]. We calculate the NLSP event rates for a cubic-kilometer neutrino observatory such as IceCube [140], taking into account the dependence of the detection efficiencies on stau energy and spatial resolution. For the SUSY partner mass spectrum, we use, for illustration, the benchmark point corresponding to SPS 7 from [151] and a toy model where all SUSY partner masses are just above the experimental limits. Similarly, for the yet unknown high energy cosmic neutrino flux we adopt as a benchmark the Waxman-Bahcall flux [77] already discussed in section II.3 (Eq. II.27).

2.2. NLSP Production

In section III.1 we discussed the SM charged and neutral current interactions of neutrinos with matter in the Earth's interior and atmosphere. The leading order SUSY contribution consists of chargino χ or neutralino χ^0 exchange between neutrinos and quarks. This parton-level SUSY contributions are shown in Fig. III.8 for the case of the light u and d quarks. The reactions produce sleptons and squarks, which promptly decay into the lighter stau NLSP. The parton-level cross sections for these diagrams[10] are given by

$$\frac{\mathrm{d}\sigma^{(a)}}{\mathrm{d}t} = \frac{\pi\alpha^2}{2s_{\mathrm{w}}^4}\frac{1}{s^2}(tu - m_{\widetilde{\ell}_{\mathrm{L}}}^2 m_{\widetilde{q}}^2)\left[\frac{Z_-^{1i}Z_-^{1i}}{(t-m_{\chi_i}^2)}\right]^2 , \tag{III.17}$$

$$\frac{\mathrm{d}\sigma^{(b)}}{\mathrm{d}t} = \frac{\pi\alpha^2}{2s_{\mathrm{w}}^4}\frac{1}{s}\left[\frac{m_{\chi_i}Z_+^{1i}Z_-^{1i}}{(t-m_{\chi_i}^2)}\right]^2 , \tag{III.18}$$

$$\frac{\mathrm{d}\sigma^{(c)}}{\mathrm{d}t} = \frac{\pi\alpha^2}{2s_{\mathrm{w}}^4}\frac{4}{c_{\mathrm{w}}^4}\frac{1}{s^2}\left\{(tu - m_{\widetilde{\ell}_{\mathrm{L}}}^2 m_{\widetilde{q}}^2)\left[\frac{\mathcal{Y}^i_{u_{\mathrm{R}}/d_{\mathrm{R}}}\mathcal{Y}^i_\nu}{(t-m_{\chi_i^0}^2)}\right]^2 + s\left[\frac{m_{\chi_i^0}\mathcal{Y}^i_{u_{\mathrm{L}}/d_{\mathrm{L}}}\mathcal{Y}^i_\nu}{(t-m_{\chi_i^0}^2)}\right]^2\right\} , \tag{III.19}$$

$$\frac{\mathrm{d}\sigma^{(d)}}{\mathrm{d}t} = \frac{\pi\alpha^2}{2s_{\mathrm{w}}^4}\frac{4}{c_{\mathrm{w}}^4}\frac{1}{s^2}\left\{(tu - m_{\widetilde{\ell}_{\mathrm{L}}}^2 m_{\widetilde{q}}^2)\left[\frac{\mathcal{Y}^i_{u_{\mathrm{L}}/d_{\mathrm{L}}}\mathcal{Y}^i_\nu}{(t-m_{\chi_i^0}^2)}\right]^2 + s\left[\frac{m_{\chi_i^0}\mathcal{Y}^i_{u_{\mathrm{R}}/d_{\mathrm{R}}}\mathcal{Y}^i_\nu}{(t-m_{\chi_i^0}^2)}\right]^2\right\} . \tag{III.20}$$

Again, summation over repeated indices is implied and we use the conventions and notations of Refs. [124, 125]. The masses of the four neutralinos and two charginos are denoted by $m_{\chi_i^0}$ and m_{χ_i}, respectively. The mixing matrices are Z_N and $Z_\pm$. The neutralino couplings $\mathcal{Y}^i = YZ_N^{1j}s_{\mathrm{w}} + T^3Z_N^{2j}c_{\mathrm{w}}$ depend on the hypercharge $Y = Q - T^3$ and the weak isospin T^3:

$$\begin{aligned}
\mathcal{Y}^i_{u_{\mathrm{L}}} &= \frac{1}{6}Z_N^{1i}s_{\mathrm{w}} + \frac{1}{2}Z_N^{2i}c_{\mathrm{w}} , \quad \mathcal{Y}^i_{d_{\mathrm{L}}} = \frac{1}{6}Z_N^{1i}s_{\mathrm{w}} - \frac{1}{2}Z_N^{2i}c_{\mathrm{w}} , \quad \mathcal{Y}^i_{\nu} = -\frac{1}{2}Z_N^{1i}s_{\mathrm{w}} + \frac{1}{2}Z_N^{2i}c_{\mathrm{w}} , \\
\mathcal{Y}^i_{u_{\mathrm{R}}} &= \frac{2}{3}Z_N^{1i}s_{\mathrm{w}} , \qquad\qquad\qquad \mathcal{Y}^i_{d_{\mathrm{R}}} = -\frac{1}{3}Z_N^{1i}s_{\mathrm{w}} .
\end{aligned} \tag{III.21}$$

In the following we will focus on two SUSY mass spectra. One, denoted by "SPS 7" in the following, is given by the benchmark point corresponding to SPS 7 [151] for a gauge-mediated SUSY breaking (GMSB) scheme with a messenger mass of 80 TeV. The corresponding mass spectrum calculated by SoftSusy 2.0.4 [161] was already shown in Fig. III.7. The other spectrum, denoted by "min $\widetilde{m}$", consists of light charginos, neutralinos and sleptons at 100 GeV and squarks at 300 GeV. It is not motivated by any particular SUSY breaking scenario, but oriented at current experimental limits, in order to give an impression of what can be obtained in a very optimistic scenario.

In Eqs. (III.17)–(III.20), we have neglected family mixing and contributions proportional to Yukawa couplings. We have taken into account the exchange of the heavier

[10] The cross sections for the analogous processes with anti-neutrinos are the same.

neutralinos and charginos, since generically their contribution to the cross sections is large and can even dominate. It turns out that for the SPS 7 benchmark point, assuming equal neutralino masses is a rather good approximation that helps simplifying analytical calculations. Nevertheless, we use the exact expressions in the numerical calculations discussed in the following.

The resulting neutrino-nucleon cross sections are shown in Fig. III.9 and compared to the SM contribution from W and Z exchange. Here and in the following computations we have used the CTEQ6D parton distribution functions [120]. The contribution to the cross sections from charged currents is about twice as large as the one from neutral currents. As expected the mass spectrum "min $\widetilde{m}$" with the lowest threshold $E_{\nu,\mathrm{th}} = (m_{\widetilde{\ell}} + m_{\widetilde{q}})^2/(2m_p)$ reproduces the largest cross section which is still more than two orders of magnitude suppressed compared to the charged current SM contribution.[11]

2.3. NLSP Propagation

We assume that the squarks and sleptons produced in the interactions discussed in the previous section promptly decay into stau NLSPs. We have shown in the previous section that the branching ratio of these SUSY contribution compared to SM interactions is less than 1% for the most optimistic case of very light SUSY particle masses ("min $\widetilde{m}$"). For the observability at Cherenkov telescopes this deficit in production has to be balanced by a much larger effective target volume for this type of events. In particular, the energy loss length and decay length of the particle has to be sufficiently large.

Energy Loss

The mean energy loss per column depth z, measured in terms of nucleons per area, is approximately given by

$$-\left\langle \frac{\mathrm{d}E}{\mathrm{d}z} \right\rangle \approx \alpha + \beta E \ . \tag{III.22}$$

Here, α is determined by ionization effects and β accounts for bremsstrahlung, pair-production, and photohadronic processes. In general, these coefficients are weakly energy dependent. In the case of muons, it is sufficient to approximate their values by constants, $\alpha_\mu \approx 3.3 \times 10^{-3}$ GeV b and $\beta_\mu \approx 6.7 \times 10^{-6}$ b.

Above a *critical energy* E^{cr}, which we define in general as the solution to,

$$E^{\mathrm{cr}} = \frac{\alpha(E^{\mathrm{cr}})}{\beta(E^{\mathrm{cr}})} \ , \tag{III.23}$$

radiative energy losses dominate, which are proportional to the energy of the particle. Hence, Cherenkov detectors can make use of the energy loss (III.22) to determine the

[11] The branching ratio between muons and staus is larger by a factor of 3, since stau NLSPs might also be produced by electron and tau neutrinos.

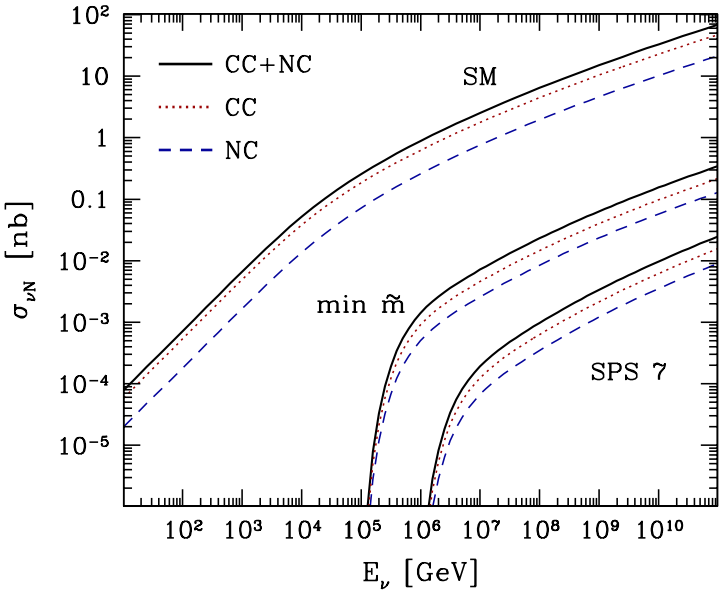

Figure III.9: *The charged (red dotted) and neutral (blue dashed) current cross section for neutrino-nucleon scattering compared to the chargino and neutralino exchange for the SPS 7 benchmark point and a scenario with light squark masses of 300 GeV.*

energy of a particle if $E \gg E^{\mathrm{cr}}$. The mean energy loss range of a particle with initial energy E and final energy $E_0 \ll E^{\mathrm{cr}}$ is then given by

$$\langle z \rangle \approx \frac{1}{\beta} \ln\left(\frac{\alpha + \beta E}{\alpha + \beta E_0}\right) \approx \frac{1}{\beta} \ln\left(1 + \frac{E}{E^{\mathrm{cr}}}\right) \ . \tag{III.24}$$

The mean energy loss range of a stau has been studied in great detail in Refs. [158, 157, 162]. The radiative term in Eq. (III.22) is suppressed, since $\beta_{\tilde{\tau}}$ approximately satisfies $\beta_{\tilde{\tau}}\, m_{\tilde{\tau}} \approx \beta_\mu\, m_\mu$, whereas ionization losses, contributing with the approximately constant α, have the same strength as for the muons. The typical range of a particle is given by the inverse coefficient $1/\beta$ (Eq. III.24). Hence the stau range $\langle z_{\tilde{\tau}} \rangle$, scaling linearly with the mass $m_{\tilde{\tau}}$, is about three orders of magnitude larger than the range of muons $\langle z_\mu \rangle$ with the same energy. In our calculations we have used an approximation for $\langle z_{\tilde{\tau}} \rangle$ from Ref. [158] for staus with energy $E_{\tilde{\tau}} > 4 \times 10^5\,\mathrm{GeV} \times (m_{\tilde{\tau}}/150\,\mathrm{GeV})$. Below this energy ionization losses dominate and were included in the calculation.

If the stau NLSP has a large admixture from $\widetilde{\tau}_{\mathrm{L}}$, the SUSY partner of the left-handed tau, charged and neutral current effects might be important [163]. A general analysis taking the stau NLSP as an arbitrary superposition of $\widetilde{\tau}_{\mathrm{L}}$ and $\widetilde{\tau}_{\mathrm{R}}$ showed that weak effects start to dominate the stau energy loss range above $10^7 - 10^8$ GeV [162]. We will come back to the point in the discussion of our results.

Decay

The lifetime of the stau NLSP can be very long, since its decay into the gravitino LSP can proceed only gravitationally. The corresponding decay length L for relativistic staus,

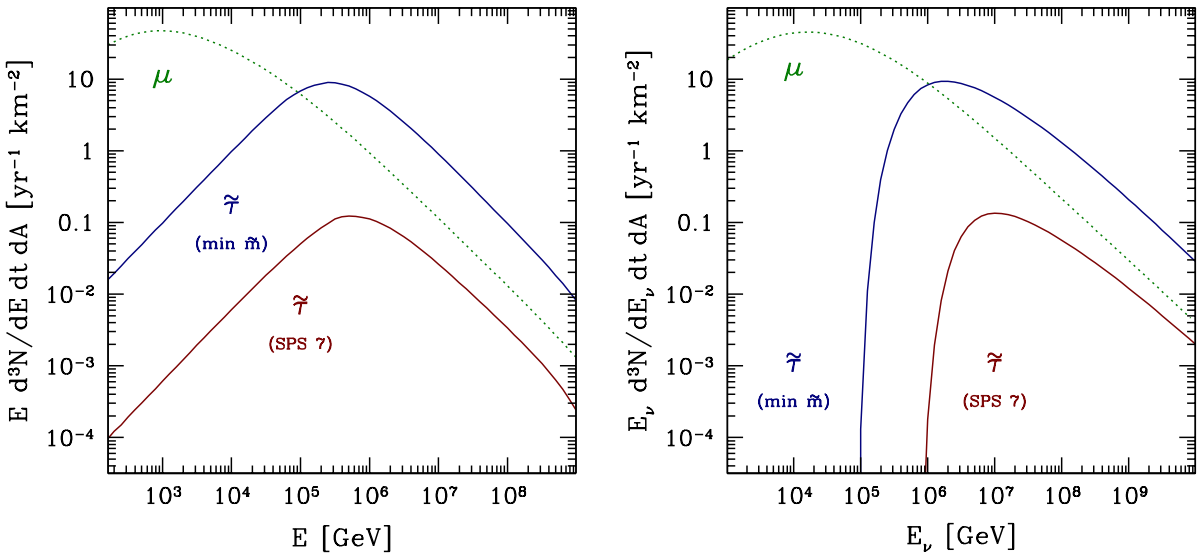

Figure III.10: *Expected fluxes of upward-going muons and staus assuming the Waxman-Bahcall neutrino flux [77]. The results are shown in terms of the energy at the detector E (left panel) and the neutrino energy E_ν (right panel). We have used a SUSY mass spectrum with light squarks of 300 GeV (blue upper solid) as well as the one from the benchmark point corresponding to SPS 7 (red lower solid). For comparison the flux of muons is shown as the green dotted line.*

in units of the Earth's diameter $2R_\oplus$, is (e.g. [147])

$$\left(\frac{L}{2R_\oplus}\right) \approx \left(\frac{m_{\tilde{\tau}}}{100\ \text{GeV}}\right)^{-6} \left(\frac{m_{3/2}}{400\ \text{keV}}\right)^{2} \left(\frac{E_{\tilde{\tau}}}{500\ \text{GeV}}\right) . \tag{III.25}$$

Hence, staus with a mass not much larger than 100 GeV will always reach the detector, if the gravitino is heavier than 400 keV.[12] In this case, the gravitino is a viable candidate for the dark matter [164]. Constraints from big bang nucleosynthesis and the cosmic microwave background yield an upper limit on the gravitino mass between 10 and 100 GeV [165, 166]. Masses in the lower part of the allowed region are typical for models with gauge-mediated SUSY breaking, while masses of some tens of GeV can occur in gravity and gaugino mediation (for a review, cf. e.g. [167]).

2.4. Detection Rate at Neutrino Telescopes

Cosmic neutrinos are exposed to SM charged and neutral current interactions in the Earth matter before they might undergo a SUSY process at some distance ℓ from the observer. We take these interactions into account by an exponential attenuation of the initial diffuse neutrino flux J_ν along the line of sight $-\mathrm{d}z = n(\vec{x})\mathrm{d}\ell$ using the Earth's nucleon density $n = \rho_\oplus/m_p$ summarized in Ref. [139]. The integrated column depth of

[12] Actually, we expect that our results remain unchanged even if the gravitino is lighter by an order of magnitude, since the dominant contribution to the event rate is due to staus with energies considerably larger than 500 GeV.

the Earth, $z_\oplus$, depends on the nadir angle θ and the depth of the detector center below the horizon, which we fix at 1.9 km corresponding to the IceCube detector [140]. For the (yet unknown) high energy cosmic neutrino flux we will adopt as a benchmark the Waxman-Bahcall flux of neutrinos from optically thin sources (Eq. II.27 with $\epsilon_\pi = 1$ and $\xi_z = 3$): $E_\nu^2\, J_{\rm WB}(E_\nu) \approx 6 \times 10^{-8}\,{\rm GeV\,cm^{-2}\,s^{-1}\,sr^{-1}}$ (all flavor).

We assume that the emerging sleptons and squarks will promptly decay into the $\widetilde{\tau}$ NLSP with an average energy of $\langle E_{\widetilde{\tau}}\rangle_{\widetilde{l}}/E_{\widetilde{l}} = 0.5$ (1.0) and $\langle E_{\widetilde{\tau}}\rangle_{\widetilde{q}}/E_{\widetilde{q}} = 0.3$ (0.5) for the "SPS 7" ("min $\widetilde{m}$") mass scenario, respectively. This determines the average energy loss ranges $\langle z_{\widetilde{\tau}}\rangle_{\widetilde{l}}$ and $\langle z_{\widetilde{\tau}}\rangle_{\widetilde{q}}$. For a given nadir angle the maximal range $z_{\rm max}$ of an observable stau is then the lesser of $z_\oplus$ and $\langle z_{\widetilde{\tau}}\rangle_{\widetilde{l}}$ or $\langle z_{\widetilde{\tau}}\rangle_{\widetilde{q}}$, depending on the history of the stau. The flux of staus through the detector from the decay of the emerging $\widetilde{p}$, either slepton or squark, is then given by

$$\frac{{\rm d}^4 N_{\widetilde{\tau}\leftarrow\widetilde{p}}}{{\rm d}t\,{\rm d}A\,{\rm d}\Omega\,{\rm d}E_\nu} \;\approx\; \sum_{\text{parton j}} \int_{E_{\rm min}}^{E_{\rm max}} {\rm d}E_{\widetilde{p}} \int_0^{z_{\rm max}} {\rm d}z \int_{x_{\rm min}}^1 {\rm d}x\; f_j(x,Q^2) \times \frac{{\rm d}^2\sigma^{\rm SUSY}}{{\rm d}x\,{\rm d}E_{\widetilde{p}}} \times J_\nu(E_\nu) \times {\rm e}^{-(z_\oplus - z)\sigma^{\rm SM}} \;. \tag{III.26}$$

The total flux of staus and muons through the IceCube detector is shown in Fig. III.10. The left panel shows the flux in terms of muon and stau energy at the detector and in the right panel the flux is expressed in terms of the initial neutrino energy. Most of the staus will originate from neutrinos with an energy below 10^8 GeV (10^9 GeV) in the "min $\widetilde{m}$" ("SPS 7") mass scenario. In analogy to the considerations that led to Eq. (III.2) we can estimate the values of Bjorken-x which are probed at these neutrino energies by the exchange of charginos with a mass ~ 100 GeV (~ 300 GeV) as

$$x \approx \frac{m_\chi^2}{2 m_p E_\nu} \gtrsim 10^{-5} \;. \tag{III.27}$$

Similar values are probed for neutralino exchange. This is within the kinematic region of the CTEQ6D PDFs [120], which are used in the calculation, and we expect that the corresponding uncertainties are negligible in our calculations.

The peak contribution of the stau flux comes from stau energies in the range 10^5–10^6 GeV. At these energies the weak contributions to the energy loss of the left-handed SUSY partners are still sub-dominant compared to electro-magnetic losses [162]. Therefore, our results should also apply to the general case of a stau NLSP being an arbitrary superposition of the gauge eigenstates $\widetilde{\tau}_{\rm L}$ and $\widetilde{\tau}_{\rm R}$.

Surprisingly, the stau flux in the mass scenario "min $\widetilde{m}$" is larger than the muon flux for energies larger than 10^5 GeV. However, we will argue in the following that this will not produce a visible excess of stau tracks in the detector.

Energy Calibration

The analysis of particle tracks observed in neutrino telescopes is calibrated for muons. Their energy E_μ can be reconstructed by the energy loss ΔE per column depth Δz

Table III.1: *The expected number of muon and stau events for a one year observation at IceCube, assuming the Waxman-Bahcall neutrino flux per flavor,* $E_\nu^2 F(E_\nu) \approx 2 \times 10^{-8}$ *GeVcm*$^{-2}\,s^{-1}\,sr^{-1}$ *[77]. The "detected" energy* E_d *is equivalent to* E_μ *for the muons, but equals* $m_\mu/m_{\widetilde{\tau}} \times E_{\widetilde{\tau}}$ *in the case of the staus (see text). The effective areas of IceCube have been calculated by Monte-Carlo simulations and are given in Ref. [97].*

Rate of $\widetilde{\tau}$ and μ events $[\,\mathrm{yr}^{-1}\,]$					
E_d [GeV]	$(10, 10^2)$	$(10^2, 10^3)$	$(10^3, 10^4)$	$(10^4, 10^5)$	$(10^5, 10^6)$
A_eff^μ [km^2]	0.1	0.6	0.8	1.0	1.2
N_μ	3	60	100	80	20
$N_{\widetilde{\tau}}$ (min $\widetilde{m}$)	< 0.7	< 10	< 5	< 0.9	< 0.1
$N_{\widetilde{\tau}}$ (SPS 7)	< 0.006	< 0.1	< 0.1	< 0.02	< 0.003

and Eq. (III.22). This is appropriate for muons with energies above the critical energy $E_\mu^\mathrm{cr} = \alpha_\mu/\beta_\mu \approx 500$ GeV. A high-energy stau with energy $E_{\widetilde{\tau}}$ will deposit a much smaller energy fraction in the detector compared to a muon with the same energy, due to the reduced radiative energy loss.

This has two effects. Firstly, the critical energy of a stau $E_{\widetilde{\tau}}^\mathrm{cr} = \alpha_{\widetilde{\tau}}/\beta_{\widetilde{\tau}} \approx (m_{\widetilde{\tau}}/m_\mu) E_\mu^\mathrm{cr}$ is much higher compared to that of the muons. Secondly, due to the calibration of the detector, high-energy staus will be detected as muons with reduced energy $(m_\mu/m_{\widetilde{\tau}})E_{\widetilde{\tau}}$ as long as the stau energy is larger than the critical energy. We define the *detected energy* E_d as

$$E_\mathrm{d} \equiv \frac{m_\mu}{m_{\widetilde{\tau}}} E_{\widetilde{\tau}} \,. \tag{III.28}$$

Note that this consistently identifies the boost factor of the particle as $\gamma = E_{\widetilde{\tau}}/m_{\widetilde{\tau}} = E_\mathrm{d}/m_\mu$ and also the Cherenkov angle as $\cos\theta_C \propto (1 - 1/\gamma^2)^{-1/2}$.

One-Stau Events

The calculation of the total rate of events requires the knowledge of the detection efficiency of the corresponding particle depending on its energy and direction. This is usually combined with the cross sectional area of the detector as an effective area A_eff. The IceCube Collaboration has determined the effective area $A_\mathrm{eff}^\mu(\cos\theta, E_\mu)$ for upward-going muons by Monte-Carlo simulations in Ref. [97]. The angle-averaged values are shown in Tab. III.1 together with the expected rates of muon events for the WB flux. The expected rates from our calculation are in good agreement with those quoted in Ref. [97], if one takes into account the different normalizations of the initial neutrino fluxes.

Despite the fact that the staus are produced in pairs, they may also appear as single staus in the detector. This may happen if the stau tracks are too close or one particle of the pair misses the detector. These are indistinguishable from one-muon events, at

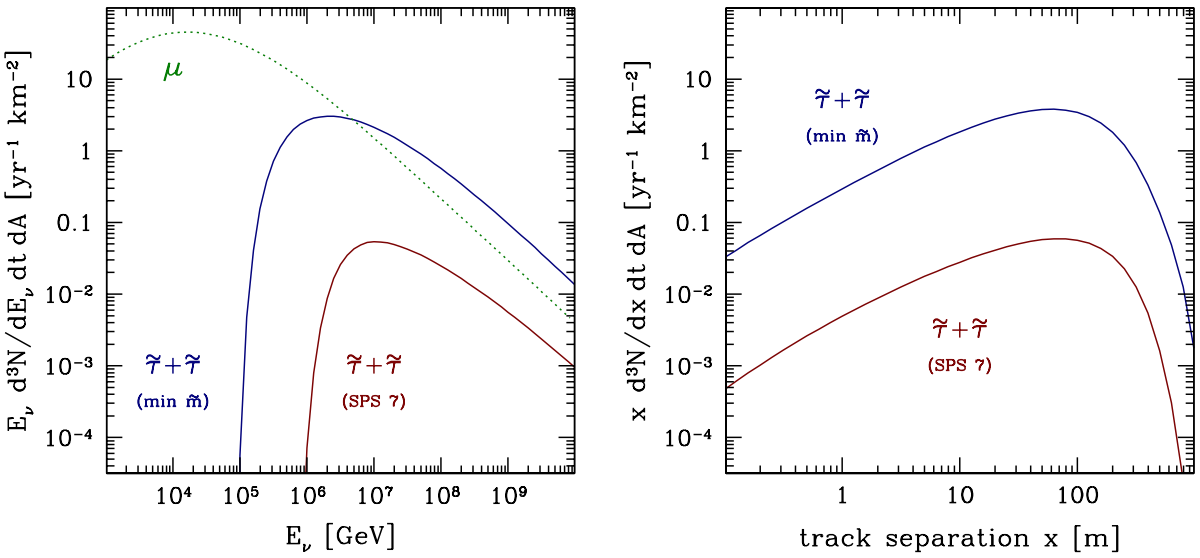

Figure III.11: *Expected flux of stau pairs assuming the Waxman-Bahcall neutrino flux [77]. The results are shown in terms of the neutrino energy E_ν (right panel). Again, we have used a SUSY mass spectrum with light squarks of 300 GeV (blue upper solid) as well as the one from the benchmark point corresponding to SPS 7 (red lower solid) and compare this with the flux of single muons shown as the green dotted line. The right panel shows the distribution of stau separation in the detector.*

least for high energies. A very conservative upper bound on the rate of one-stau events is given by the total rate of staus computed from Eq. (III.26) and a detection efficiency $A^{\widetilde{\tau}}_{\rm eff}(E_{\widetilde{\tau}}) \approx A^{\mu}_{\rm eff}(E_{\rm d})$. This upper bound is also shown in Tab. III.1 for the two different SUSY mass spectra. It shows that in the fiducial energy region one-stau events are subdominant compared to the flux of muons, even for the most optimistic case of very light squarks with masses around 300 GeV. This seems to be generic, independent of the initial high-energy cosmic neutrino flux, as we have checked.

Staus in the energy region $E^{\rm cr}_{\mu} < E \ll E^{\rm cr}_{\widetilde{\tau}}$, which lose their energy predominantly via ionization, could produce an excess of through-going *minimally ionizing* tracks in the detector. We have checked that even in the case of the "min $\widetilde{m}$" mass scenario the contribution of these events is not significant compared to the muons. In addition, the flux of upward-going muons in this energy region will further increase by the flux of atmospheric neutrinos coming from directions below the horizon, which otherwise do not effect the analysis of stau events [97]. Hence, the total rate of one-particle events can be used for reconstructing the neutrino flux without taking into account the contributions from NLSPs. This decouples the analysis of the neutrino flux from the search for parallel-stau events, to which we turn now.

Parallel-Stau Events

The detection efficiency of stau pairs, *i.e.* coincident parallel tracks, depends on the energies and directions of the staus, as in the case of single events, but also on their separation. The left panel of Fig. III.11 shows the flux of stau pairs for the two SUSY scenarios. For the calculation we make use of Eq. (III.26) where now the maximal range

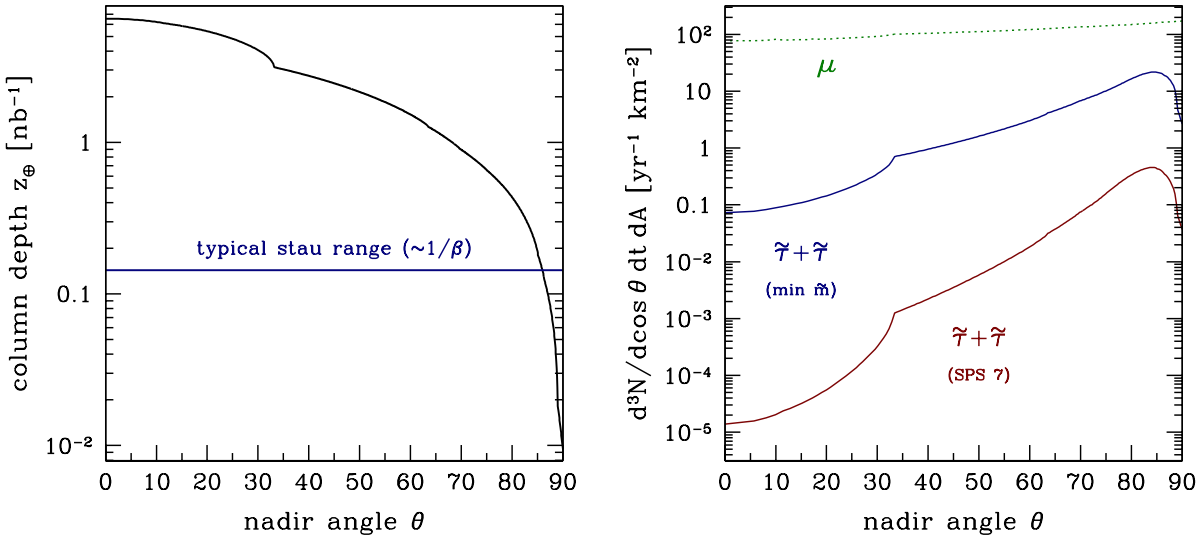

Figure III.12: *The left panel shows the integrated column depth of the Earth, $z_\oplus$, with respect to the IceCube detector with detector center at 1.9 km below the surface. Also shown as a line is the typical stau range which intersects $z_\oplus$ at about 5 degrees below horizon. This results in a reduction above $\theta \approx 85°$ in the angular distribution of stau pairs shown in the right panel for the two SUSY mass scenarios. As a comparison we also show the flux of single muons.*

$z_{\max}$ of a pair is determined by the lesser of $z_\oplus$, $\langle z_{\tilde{\tau}} \rangle_{\tilde{l}}$ and $\langle z_{\tilde{\tau}} \rangle_{\tilde{q}}$. A comparison of the right panel of Fig. III.10 shows that most of the staus will reach the vicinity of the detector as pairs.

However, not all of the stau pairs might be seen as separable tracks in a Cherenkov telescope if they emerge from interactions too close to or also too far from the detector. As an estimate we use the opening angle δ between the slepton and squark in DIS to calculate the separation of stau tracks in the detector by $x = 2\,\Delta\ell\,\tan(\delta/2)$, where $\Delta\ell$ is the distance of the interaction to the detector center. The right panel of Fig. III.11 shows the distribution of stau tracks according to the distance of the tracks in the detector. The peak contribution is at about 100 m and is strongly suppressed for separations larger than 1 km. The rate of events per effective detector area is shown in Tab. III.2 for a minimal separation $x_{\min}$ of 0 m, 10 m, 50 m, and 100 m, respectively.

The detector resolution of stau pairs should also depend on the arrival direction of the staus. The distribution of stau pairs according to the nadir angle θ is shown in Fig. III.12. It reflects the exponential attenuation of the flux of neutrinos depending on the integrated column depth of the Earth ($z_\oplus$) in the line of sight, which is shown in the left panel of the same figure. The steepening of the differential rate below 33° is an effect of the dense inner core of the Earth. Most of the stau pairs arrive from about 85° with respect to nadir. This corresponds to the suppression at larger nadir angles due to the small column depth of the Earth, $z_\oplus$, compared to the typical energy loss range of the staus, which is also plotted in the left panel of Fig. III.12.

On completion the IceCube detector will consist of 70 strings separated by 125 m [140], where each string carries 60 optical modules separated by about 17 m. Since most of the

stau pairs will arrive from about 5° below the horizon an effective detector resolution of $x_{\min} = 50$ m with respect to their separation seems possible. For the Waxman-Bahcall neutrino flux this corresponds to about 7 pair events per century for the benchmark point corresponding to SPS 7 and about 5 events per year for our toy model with light sparticle masses (see Tab. III.2). These numbers should be taken as an order of magnitude estimate of the event rates. A full-fledged Monte-Carlo study that accounts for a variation of the detection efficiency with stau energy, nadir angle and track separation is beyond the scope of our study.

Currently, the IceCube Collaboration quotes an upper limit at 90% confidence level of $E_\nu^2 F(E_\nu) \lesssim 3 \times 10^{-7}\ \mathrm{GeV\,cm^{-2}\,s^{-1}\,sr^{-1}}$ (per flavor, AMANDA-B10 [168]) for the diffuse flux of cosmic neutrinos (see also Fig. II.10). This is approximately one order of magnitude above the Waxman-Bahcall flux taken for our calculation. We have seen in section II.3 that neutrino fluxes in the low crossover scenario are close to current neutrino bounds at energies of about 10^7 GeV. Hence, it is possible that the predicted event rates will increase by a factor 10, giving up to 50 pair events per year for the optimistic SUSY mass spectrum.

Stau Capture

If the stau reaches the detector as a minimally ionizing particle it is possible that it is stopped in the detector. On decay via $\widetilde{\tau} \to \tau + \widetilde{G}$ the emerging tau might initiate a cascade whose position coincides with the end-point of a previous stau track. However, the energy of the tau is limited by the mass of the stau and a tau cascade with energy of $\mathcal{O}(100)$ GeV should be close to the detection threshold of the IceCube detector [169].

But even in the optimistic case of a full detection efficiency these events will occur on a very rare basis. The event rate $\dot{N}$ may be estimated as

$$\begin{aligned}\dot{N} &\approx \Delta z_{\mathrm{IceCube}} \times \left[\left| \frac{\mathrm{d}E_{\widetilde{\tau}}}{\mathrm{d}z} \right| \times \frac{\mathrm{d}^2 N_{\widetilde{\tau}}}{\mathrm{d}t\,\mathrm{d}E_{\widetilde{\tau}}} \right]_{E_{\widetilde{\tau}}=m_{\widetilde{\tau}}} \\ &\approx \Delta z_{\mathrm{IceCube}} \times \frac{\alpha}{m_{\widetilde{\tau}}} \times \left[E_{\widetilde{\tau}} \frac{\mathrm{d}^2 N_{\widetilde{\tau}}}{\mathrm{d}t\,\mathrm{d}E_{\widetilde{\tau}}} \right]_{E_{\widetilde{\tau}}=m_{\widetilde{\tau}}} . \end{aligned} \tag{III.29}$$

If we compare this with the left panel of Fig. III.10 and use $\Delta z_{\mathrm{IceCube}} \approx 1\,\mathrm{km} \times n_{\mathrm{ice}}$, we should expect that the rate is less than one event per century in the case of the optimistic scenario "min $\widetilde{m}$". A proper treatment of the detector efficiency should further reduce this.

Background

One source of the background consists of parallel muon pair events from random coincidences. This is bounded from above by the number of muons arriving within a (generous) time-window of 1 μs. Even this is several orders of magnitude below the stau pair event rate,

$$\frac{N_{\mu+\mu}(E)}{N_\mu(E)} \lesssim \frac{1}{2} \min\left(1\,;1\ \mu\mathrm{s} \cdot \frac{\mathrm{d}N_\mu}{\mathrm{d}t} \right) \sim \mathcal{O}(10^{-12}) . \tag{III.30}$$

Table III.2: *Rates of upward-going stau pairs for two different SUSY mass scenarios and different detection thresholds of the track separation x.*

Rate of $\widetilde{\tau}$ pairs $[\,\mathrm{yr}^{-1}\,\mathrm{km}^{-2}\,]$				
$x_{\min}$ [m]	0	10	50	100
$N_{\widetilde{\tau}+\widetilde{\tau}}$ (min $\widetilde{m}$)	12	9	5	2
$N_{\widetilde{\tau}+\widetilde{\tau}}$ (SPS 7)	0.19	0.14	0.07	0.03

Double muon events from processes like $\nu_\mu + N \to \mu^- + X \to \mu^- + \mu^+ + \nu_\mu + X'$ are expected to be more likely. The authors of Ref. [157] have estimated the double muon events arising from the production and decay of charmed hadrons. The event rates might be comparable to stau pairs. However, as a background the production of these muon pairs should be close to the detector due to the limited stau range. Correspondingly, their separation is not large and their background is simply cut by the limited detector resolution for parallel tracks [157]. Hence, the SM background of well-separated parallel muon-like tracks is expected to be very small.

2.5. Complementarity with Collider Experiments

The observation of long-lived charged sleptons at neutrino telescopes requires SUSY partner masses close to experimental bounds as it is assumed in the mass scenario "min $\widetilde{m}$". Even in this optimistic case the rate of single stau events has to compete with a much larger flux of muons produced by the same flux of neutrinos. This is the result of the reduced energy loss of staus in the detector and the corresponding mis-identification as low energy muons.

Long-lived charged sleptons in the "min $\widetilde{m}$" mass scenario should immediately be visible in the CMS and ATLAS detectors at the LHC, which is scheduled to start its operation in 2007/2008. The IceCube detector will reach its final size of about one cubic-kilometer in 2011.[13] By that time, the spectrum of light and long-lived charged sleptons should already be fixed by the LHC.

In the case of $\mathcal{R}$-parity conservation and a light and long-lived stau NLSP the detection of muon-like parallel tracks by the IceCube detector at a rate of a few per year is possible. With the complementary knowledge of low-lying slepton masses from the LHC and the detection of cosmic neutrino fluxes in the energy region of around 10^6–10^7 GeV this signal might be used for a lower bound on the NLSP life-time. This might indirectly establish a (model dependent) lower bound of the LSP mass.

[13] However, the telescope is already operating during its construction and 35 of its 70 strings carrying the optical modules will already be deployed in the polar ice by 2008.

The capture of long-lived stau NLSPs by active kilo-ton stoppers at the LHC and next-generation colliders like the ILC has been proposed by several authors [152, 153, 154, 155, 149]. The detection of stau tracks and the succeeding decay into a tau and the LSP may fix the life-time of the NLSP as well as the mass of the LSP and its spin. This measurement may also distinguish between a gravitino (spin 3/2) and an axino (spin 1/2) LSP.

At Cherenkov telescopes the trapping of staus from cosmic neutrino fluxes and the observation of their decay is not feasible. These events should take place at a rate of order one per century. Atmospheric neutrino fluxes which dominate at energies below 10^5–10^6 GeV may not contribute to the production of staus since their center of mass energies in the scattering off nucleons do not exceed the SUSY production threshold.

Nevertheless, the observation of well-separated muon-like tracks at neutrino telescopes seems to be a very clear signal for new physics with a low background from SM processes. It should not be difficult to disentangle these events from the observation of upward-going muons. With complementary information from collider experiments this might establish a cost-efficient way to estimate the life-time of the NLSP. In addition, the production via neutrino-nucleon interactions instead of proton-proton collisions may provide an independent check on systematics.

Summary

Supersymmetric (SUSY) contributions to neutrino-nucleon interactions have a very small branching ratio since SUSY particles share the same couplings with their particles, but with higher mass thresholds (Sec. III.2.2). We have followed the idea posed by the authors of Ref. [156, 157] that long-lived charged sleptons may possess a much larger effective target volume at Cherenkov observatories as a result of their reduced energy loss in matter (Sec. III.2.3). This may (over-)compensate for the small branching ratio, but does not necessarily discriminate against the muon background (Sec. III.2.4).

The situation changes in $\mathcal{R}$-parity conserving SUSY where SUSY particles are always produced in pairs. The lightest SUSY particle (LSP) is stable in this case and the next-to-lightest SUSY particle (NLSP) may be the long-lived charged particle. The NLSP pairs may appear as well-separated muon-like tracks in the detector with a small background from SM processes. For standard neutrino fluxes and optimistic SUSY partner masses close to experimental lower limits we have shown that a few events per year are a realistic estimate taking into account the limited detector resolution w.r.t. the track separation. Special signals produced by NLSP capture and decay are too rare for an observation at neutrino telescopes on realistic time scales.

This section reviews and extends the analysis of Ref. [5] (see also Ref. [6]). The author of this thesis has contributed in all the steps of the investigation, in particular in the numerical derivation of event distributions and in the estimation of detection efficiencies.

In the next section III.3 we will investigate the possibility that exotic neutrino-nucleon interactions produce even stronger cross sections then the SM predictions. We will see

that this may bypass the Greisen-Zatsepin-Kuzmin cutoff in the spectrum, which has not been observed unambiguously by experiments.

3. Exotic Interactions

The appearance of EHE CRs ($E > 10^{11}$ GeV) is a mystery. We have already seen in section II.1.1 that if nuclei are accelerated in cosmic sources they should be limited in energy corresponding to the size and magnetic field of the accelerating environment (Hillas criterion) [14]. Additional constraints arise from energy losses during the acceleration of the nuclei, that has to be balanced by the acceleration rate [35]. In particular, the synchrotron loss length decreases with the third power of the magnetic field (at constant gyro-radius), which rules out a large class of small candidate acceleration sites. The very few sources that seem to be capable of accelerating protons up to 10^{12} GeV include radio galaxy lobes, relativistically moving sources like jets of active galactic nuclei or gamma-ray bursts, or one-shot accelerators like neutron stars and magnetars [14, 35].

Alternative explanations utilize the fragmentation spectra of annihilating topological defects or decaying superheavy dark matter particles. The corresponding power spectra are typically hard [18] with power index $\gamma \lesssim 2$ and may be in conflict with the observed powerlaw range $2.7 \lesssim \gamma \lesssim 3.3$. However, propagation effects may alter the slope as we have seen in section II.1.2. A severe problem of these scenarios are the large GeV gamma ray fluxes which should appear from electro-magnetic cascades of leptons and photons which are initiated by $\pi^- \to \mu^- + \bar{\nu}_\mu \to e^- + \bar{\nu}_e + \nu_e + \bar{\nu}_\mu$ or $\pi^0 \to \gamma + \gamma$. In addition, from a dark matter halo surrounding our Milky Way we should expect to observe an anisotropic distribution of their annihilation fragments due to our off-center position.

Even in the presence of EHE sources we are still facing the limitations from CR propagation. Every source distribution that significantly extends to propagation distances larger than a few 10 Mpc should be reflected by the appearance of the Greisen-Zatsepin-Kuzmin cutoff in the corresponding CR spectrum: The propagated fluxes summed over different cosmological epoches with varying source intensities should exhibit a drop at about 5×10^{10} GeV due to meson photoproduction in the CMB. Hence, the GZK-problem can be read in two directions: either there are too many events above E_{GZK} or too few below.

There are various proposals for a solution to the GZK-problem, which focus on (i) a CR production in our local environment, (ii) modification of CR interactions, or (iii) alternative particle with exotic interactions. Let us briefly discuss possible realizations of these ideas.

Local CR Production

Dark matter halos may increase the production of CRs in the vicinity of our Milky Way. The production is expected to be anisotropic due to our relative distance to the galactic center. This anisotropy should be stronger in the case of dark matter annihilation, its rate depending quadratically on the halo density and not linearly as in the case of decay. Such a large-scale anisotropy of UHE CR is not confirmed by experiments. However, the statistics of EHE CRs is very low and it is possible that these top-down scenarios start to dominate beyond the GZK cutoff. The Pierre Auger Observatory located in the

southern hemisphere is well suited to observe a possible excess in the direction of the galactic center, if this type of top-down scenarios apply.

It has also been proposed that high energy neutrinos scattering off the cosmic neutrino background (CνB) with a temperature of about 1.9 K could produce UHE nuclei [79]. These neutrinos should originate from top-down scenario since the energy fraction carried off in hadronic decays and reactions is small and would necessitate large injection energies. In particular, the resonant production of hadrons via $\nu + \nu_{1.9\,\mathrm{K}} \to Z^0 \to$ hadrons with a resonance energy at $M_Z^2/2m_\nu$ could significantly contribute to CRs if neutrino fluxes are large enough and if the CνB neutrinos cluster in our galaxy. However, it seems that the neutrino mass is too small [41] in order to form a halo of the size of our galaxy [170] or the size of galaxy clusters [171]. In addition, the *Z-burst scenario* requires large neutrino fluxes (from pion decays) and these are typically connected to unacceptably high fluxes of GeV-photons (from the corresponding electro-magnetic cascades).

Modification of CR Interactions

Lorentz invariance may be weakly broken at large energies in a quantum theory of gravity or string theory [172]. This can be formulated in terms of a particle type dependent maximal velocity c_a with an energy-momentum relation $E_a^2 = \vec{p}_a^{\,2} c_a^2 + m_a^2 c_a^4$ [173]. This effect might modify the threshold of pion photoproduction and electron-positron pair production. In particular, resonant pion production via the $\Delta(1232)$ resonance at the energy E_Δ, given in Eq. (II.5), is kinematically excluded if $(c_\Delta^2 - c_p^2) E_\Delta \gtrsim E_\gamma$. Moreover, a deviation from Lorentz invariance of $c_p^2 - c_\pi^2 \sim 5 \times 10^{-24} \, (E_\gamma / T_{CMB})^2$ is sufficient to completely switch off non-resonant pion photo-production [173]. This turns out to be small compared to experimental bounds [174, 175, 176]. Electron-positron pair production might independently be modified, which could hold up the successful interpretation of the "ankle" as the electron-positron pair production "dip" on the CMB.

Alternative Primaries with Exotic Interactions

The GZK-problem might also be avoided if we assume that a different primary initiates EHE events. Within the SM a particularly attractive candidate is the neutrino, which is only subject to red-shift losses and mass oscillations during propagation. However, besides considerations involving the different topology of neutrino-induced events, the corresponding fluxes and SM interactions are not expected to be large enough to account for the abundance of EHE CRs. Berezinsky and Zatsepin proposed that cosmogenic neutrinos [89, 177] produced in the decay of the GZK photo-pions could explain events exceeding the cutoff if we assume a rapid rise of the neutrino-nucleon interaction with a nucleonic shower characteristic. This flux of cosmogenic neutrinos naturally reaches the flux-level of protons just below the cutoff and might extend the CR spectra continuously.

In this section we will elaborate on this idea of exotic neutrino-nucleon interactions as super-GZK events. We will first start with a theoretical motivation of these scenarios giving examples of the underlying background of exotic physics. In section III.3.3 we will

proceed to confront this exotic behavior with neutrino and CR data, which will establish minimal criteria for the crossover between weakly and strongly interacting neutrinos.

3.1. Exotic Neutrino-Nucleon Interactions

The SUSY interactions that we have encountered in the last section had a small branching ratio compared to the SM contribution. This is due to the fact that particles and their SUSY partners share the same gauge couplings. The interactions involving SUSY particles are then suppressed by their heavier masses (cf. Fig. III.9). For the observation at neutrino telescopes we had to assume that SUSY interactions contribute with long-lived SUSY particles, that may reach the Cherenkov detector from a large effective detection volume.

In this section we will go one step further and consider the hypothetic case that neutrino interactions are enhanced beyond SM predictions and reach values which are comparable to hadronic interactions. The realization of such a behavior has been proposed abundantly in scenarios beyond the (perturbative) SM: e.g. arising through leptoquarks [178, 179, 180], compositeness [181, 182, 183], electroweak sphalerons [184, 185, 186, 187, 188, 189, 190, 26, 191], string excitations in theories with a low string and unification scale [192, 193, 194, 195, 196], Kaluza-Klein modes from compactified extra-dimensions [197, 198, 199, 200, 201, 202], or black hole/p-brane production in models with (wrapped) extra-dimensions [203, 204, 205, 206, 207], respectively (for a recent review, see Ref. [208]). We will briefly discuss some of these ideas in the following.

Leptoquarks

Leptoquarks are massive bosonic states with tree-level coupling to leptons and quarks, which may appear in technicolor models or grand unified theories. These new states S can appear as s-channel resonances in neutrino-nucleon scattering. For long-lived scalar leptoquarks we can estimate the neutrino-nucleon cross section above the production threshold by the narrow-width approximation according to the substitution

$$\frac{1}{(\hat{s}-M_S^2)^2+(\Gamma_S M_S)^2} \;\rightarrow\; \frac{\pi}{\Gamma_S M_S}\delta(\hat{s}-M_S^2) \qquad \text{with} \qquad \Gamma_S = \frac{M_S}{16\pi}\lambda^2 \;.$$

Here, λ^2 is an effective coupling that receives contributions from all possible final states. The integration over Bjorken-x singles out the parton density at $x \approx M_S^2/s$ and the neutrino-nucleon cross section (up to factors of $\mathcal{O}(1)$) is given as [178, 179, 180]

$$\sigma_{\nu N} \sim \frac{\pi\lambda^2}{4M_S^2} \sum_{\text{parton}} \Big[x f(x,Q^2) \Big]_{\hat{s}\approx Q^2 \approx M_S^2} \;. \tag{III.31}$$

We have already argued in section II.1.1 that for small Bjorken-x the sea-quark distribution is driven by gluon splitting and should follow $x f(x,Q^2) \sim x^{-\lambda}$ with $\lambda \sim 0.3$–0.4. According to Eq. (III.31) the cross section should follow the same power $\sim s^\lambda$ at large

energies. However, for $\lambda = \mathcal{O}(1)$ and $M_S > 100$ GeV this cross section cannot significantly increase beyond the SM prediction and its application for strongly interacting neutrinos requires either fine-tuning or a multiplicity of resonances as we will see in the following.

Composite Neutrinos

Since the QCD interactions are confined it is possible that neutrinos are not fundamental particles, but composite states, composed of light colored states, the *preons*. Above the compositeness scale Λ_c the preons will reveal their QCD colour and interact strongly with the quarks and gluons. The t-channel exchange of gluons with $Q > \Lambda_c$ will contribute with a differential cross section

$$\frac{\mathrm{d}^2\sigma}{\mathrm{d}x\mathrm{d}y} \sim 2\pi\alpha_s^2 \frac{s}{t^2}(1 + (1+y)^2) \sum_{\text{parton}} x f(x, Q^2) \ , \tag{III.32}$$

where it is assumed that the preon contribution of the neutrino momentum is of $\mathcal{O}(1)$. It was shown in Ref. [209] that for a compositeness scale $\Lambda_c > 100$ GeV the total neutrino-nucleon cross section derived from Eq. (III.32) is not sufficient to reach nucleonic values below the GZK cutoff. Hence, similar to the previous case of leptoquarks, this simple version of composite neutrinos may not contribute significantly to super-GZK events.

Electroweak sphalerons

In quantum flavor dynamics (QFD) there exist processes which cannot be described by a perturbative expansion of the weak gauge coupling α_w. These interactions correspond to tunneling processes in Minkowski space-time between topologically inequivalent vacua, which are described by *instanton* solutions. The potential barrier of the vacua is given by the mass of the *sphaleron* which is approximately given as $m_\mathrm{sph} \approx \pi M_W/\alpha_\mathrm{w} \approx 10$ TeV. The instanton process corresponds to axial anomalies which violate the otherwise conserved $B+L$, the sum of baryon (B) and lepton (L) number. This provides an attractive possibility to describe the apparent baryon and lepton asymmetry of the Universe by an sphaleron-induced mechanism in its high temperature phase $T \gg m_\mathrm{sph}$ [210, 211]. The estimation of these non-perturbative aspects in UHE neutrino-nucleon interaction is difficult (for a review see Refs. [212, 213, 214]). However, some calculations predict a steep increase of the cross section at the GZK cutoff [189, 191]. In a later section we will compare this result with the outcome of our statistical analysis.

Kaluza-Klein Excitations

It is possible that there exist hidden extra dimensions in Nature, that have not been so far visible in experiments. Such an embedding of our 4-dimensional space-time into a higher dimensional framework could be possible, if the extra-dimensions are compact and produce a mass gap corresponding to discrete extra-dimensional components of the momentum, so-called *Kaluza-Klein* (KK) excitations.[14] In this case, the SM particles could

[14] Alternatively, the extra-dimension could be infinite if the SM matter is localized on 4-dimensional world sheets [215, 216].

posses a tower of KK modes, where the zero modes are given by the low scale SM masses and the mass separation by the inverse radius R of the extra-dimensions.[15] In particular, if the graviton, the Higgs and/or the weak gauge bosons extend to the extra-dimensions, the neutrino-parton cross section would receive additional contributions from low-lying mass excitations $m_{\vec{n}}^2 = \vec{n}^{\,2}/R^2 < \hat{s}$. If we consider tree-level exchange of KK modes the integration over accessible states typically predicts a power-law enhancement of the cross section $\sim (\hat{s}R^2)^{m/2}$, where m is the number of extra dimensions with (universal) size $L = 2\pi R$. However, it was argued [200] that an exponential suppression of couplings for high-level modes, as it is appears for KK gravitons, may alter this behavior significantly. In this case, the cross section is too small for a significant contribution of neutrinos in vertical showers.

Black Holes

In scenarios with n flat and compact extra-dimensions the 4-dimensional (reduced) Planck mass $M_{\rm Pl} = 2.4 \times 10^{18}$ GeV is an effective scale, related to the fundamental scale M_* in $4+n$ dimensions by the extra-dimensional volume V_n as $8\pi M_{\rm Pl}^2 = M_*^{2+n} V_n$. If the extra-dimensions are much larger than the Planckian size M_*^{-1}, the fundamental scale M_* might be as low as the TeV scale and UHE neutrinos may produce black holes in their scattering off nucleons [203, 204]. The Schwarzschild radius r_s for a point-mass M in $4+n$ dimensions is given as

$$\pi r_s^2(M) = \left[\frac{1}{\pi} V_n \frac{M}{M_{\rm Pl}^2} \left(\frac{1}{2+n}\right) \Gamma\left(\frac{3+n}{2}\right)\right]^{\frac{2}{1+n}} . \tag{III.33}$$

According to Thorne's hoop conjecture [217] a black hole will develop in neutrino-parton scattering if the impact parameter is smaller than r_s for $M = \sqrt{\hat{s}}$. Up to form factors of $\mathcal{O}(1)$ the universal neutrino-parton cross section is given by the projective disk πr_s^2 of the black hole and the inelastic neutrino-nucleon cross section may be approximated as

$$\sigma_{\nu N} \sim \sum_{\rm parton} \int {\rm d}x \, f_{\rm p}(x, Q^2) \, \pi r_s^2(\sqrt{\hat{s}}) \ , \tag{III.34}$$

with $Q = \min(\sqrt{\hat{s}}, 10\,{\rm TeV})$ according to Ref. [207].

p-Branes

A p-brane can be viewed as a generalization of a black hole in $4+n$ dimensional space-time, that "wraps" p extra-dimensions. For the case of neutrino scattering we consider p-branes that extends to r of m small dimensions with (Planckian) length $L \sim L_* = M_*^{-1}$ and to $(p-r)$ of $(n-m)$ dimensions with larger length L'. The "radius" of the the p-brane, analogously to the Schwarzschild radius, is given by

$$\pi r_p^2(M) = \left[\frac{1}{\pi} \frac{V_n}{V_p} \frac{M}{M_{\rm Pl}^2} \sqrt{\frac{1+p}{(2+n)(2+n-p)}} \, \Gamma\left(\frac{3+n-p}{2}\right)\right]^{\frac{2}{1+n-p}} , \tag{III.35}$$

[15] For simplicity, we consider universal extra dimensions with a length $L = 2\pi R$.

where $V_p = L'^{p-r}L^r$ is the volume wrapped by the p-brane and $V_n = L'^{n-m}L^m$ the volume of the extra-dimensions. For TeV-scale gravity with $M_* \ll M_{\rm Pl}$, p-brane production is negligible relative to black hole (0-brane) production unless $p = r$, *i.e.* the p-brane wraps only Planck size dimensions [207]. In this case, the full neutrino-parton cross section is given by the sum over all possible p-brane contributions with $r = p \leq m$. At the end of this section we will provide one example of this type of interaction that might provide a contribution of neutrinos in CRs.

String Excitations

In string theories with low string or unifaction scale M_* additional s-channel resonances of leptoquarks might open up due to string excitations [195, 196]. In strongly coupled string theories the level density of the first few excited string states may depend exponentially on the resonance level as $\propto \exp(1.24N)$ [192, 193, 194]. One can estimate the behavior in the limit $\hat{s} \to \infty$ by duality between resonances in the s-channel with Regge exchanges in the t-channel: The parton-level cross section should approach a constant, since $\sigma_{\nu \rm p} \propto \hat{s}^{\,\alpha(0)-1} \approx$ const, where $\alpha(0) \approx 1$ is the Regge-intercept of the Z boson trajectory. A mathematically convenient choice that interpolates between the effect of an exponentially increasing density of the first few resonances and the asymptotic behavior is given by

$$\sigma_{\nu \rm p} \sim \Theta(\hat{s} - M_*^2)\, \frac{16\pi}{M_*^2}\, \frac{C \exp(1.24 N_0)}{1 + \frac{\hat{s}}{M_*^2} \exp\left(1.24\left(N_0 - \frac{\hat{s}}{M_*^2}\right)\right)}\,, \tag{III.36}$$

with $N_0 = \hat{s}_0/M_*^2$ such that $\sigma_{\nu \rm p}(\hat{s}_0) = \frac{1}{2}\sigma_{\nu \rm p}(\hat{s} \to \infty)$. The constant C is a normalization factor, naturally of $\mathcal{O}(1)$. Later, we will discuss one realization of this type of cross section.

3.2. Neutrinos as Super-GZK Events

In section II.3 we discussed two contributions to the flux of neutrinos at very high energies, cosmogenic neutrinos and neutrinos from optically thin sources. As an illustration Fig. III.13 shows an overlay of the proton and neutrino fluxes at the 95% CL of the low crossover scenario. Note that even in the case of close-by proton sources within 50 Mpc the GZK suppression at $E_{\rm GZK} = 5 \times 10^{10}$ GeV is visible in the spectrum. In the absence of close-by sources, the flux of cosmogenic and extragalactic neutrinos dominates over the proton flux, since the neutrino production is tied to the mechanism reducing the protons. This is our main motivation to consider exotic neutrino interactions as a solution to the GZK-problem.

In this section we want to investigate to which extent these neutrino fluxes may contribute in CRs as super-GZK events. Quantitatively, this requires an enhancement of the inelastic neutrino-nucleon cross section $\sigma_{\nu N}^{\rm in}$ by at least five orders of magnitude compared to the SM prediction, $\sigma_{\nu N}^{\rm SM}(E_{\rm GZK}) \sim 100$ nb (Eqs. III.10), before the size of

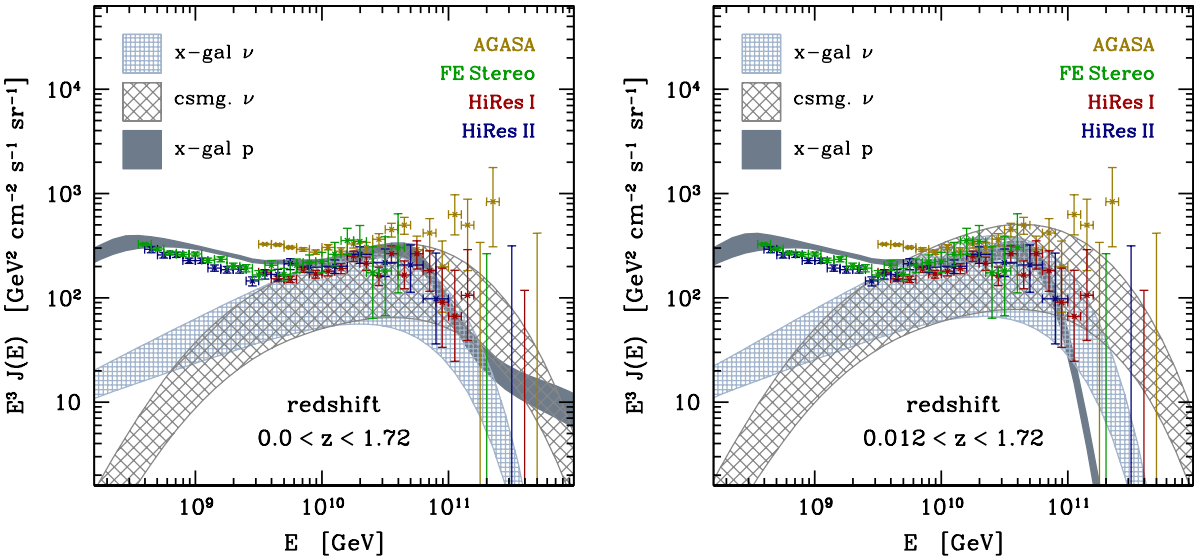

Figure III.13: *The fluxes of protons, cosmogenic neutrinos, and extragalactic neutrinos of the low crossover scenario (Sec. II.3) at 95% CL. The fluxes are normalized to an average value of the CR data weighted with their relative exposures. The left and right panel show the fit to the redshift range* $0 < z < 1.72$ *and* $0.012 < z < 1.72$*, respectively, corresponding to an inclusion or exclusion of close-by sources within* 50 *Mpc.*

the cross section gets similar to the inverse atmospheric column depth near the zenith, $z_{\rm atm}^{-1} \sim 10$ mb.

However, the inelastic neutrino-nucleon cross section is in general constrained by the search results on normal weakly-interacting UHE neutrinos. In strongly-interacting neutrino scenarios, this requires the neutrino-nucleon inelastic cross section to pass very rapidly through the intermediate energy range, where its anomalously large cross section induces an unacceptably large number of neutrino events in conflict with observations (Sec. III.1.3).

Cosmic ray experiments may also discriminate between different CR primaries by an analysis of the shower characteristics. The super-GZK events observed so far are consistent with a light nucleus primary [24, 218]. The experimental resolution is, however, limited by the systematic uncertainties of the scattering process and shower development of UHE CRs. For consistency, the showers induced by strongly interacting neutrinos should therefore be similar – within experimental resolution – to showers of light nuclei.

In summary, a consistent scenario using exotic neutrino interactions for events beyond the GZK cutoff requires (i) a strong interaction $\sigma_{\nu N}^{\rm in} \gtrsim 10$ mb above the GZK cutoff, (ii) a rapid transition through the energy region where an anomalously large $\sigma_{\nu N}^{\rm in}$ would induce unacceptably many events in neutrino observatories, and (iii) conformity with event signatures of nuclei for $\sigma_{\nu N}^{\rm in} \gtrsim 10$ mb.

In the following we will focus on the first two of these three requirement in order to derive necessary conditions on the total neutrino-nucleon cross section for scenarios with neutrinos as super-GZK events. For generality, we will assume that the characteristics

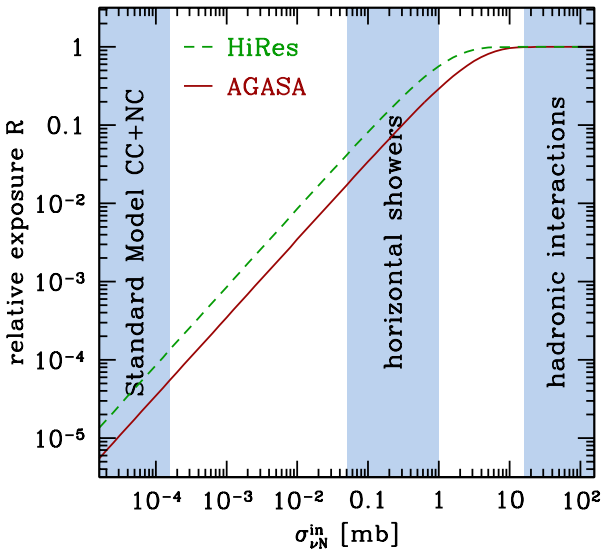

Figure III.14: *Relative exposure $\mathcal{R}$ (Eq. (III.37)) to strongly-interacting neutrinos as a function of the neutrino-nucleon inelastic cross section $\sigma^{\text{in}}_{\nu N}$, of AGASA (solid) and HiRes (dashed), respectively. The left and right bands show typical contributions from SM charged current interaction [98, 219] and typical values of hadronic interactions, respectively. The middle band marks the region of $\sigma^{\text{in}}_{\nu N}$ which strongly contribute to horizontal showers.*

of neutrino-induced showers are indistinguishable from those induced by protons.

3.3. Quantitative Analysis

In analogy with our investigation of the low crossover scenario (Sec. II.2), we will use CR data above 5×10^8 GeV to normalize the flux of cosmic protons and neutrinos from a source distribution depending on the injection index γ and evolution index n. In contrast to our previous analysis we will now account for EHE CRs up to 10^{12} GeV and assume that protons and neutrinos with exotic interactions constitute the corresponding primaries.

Also, we exclude close-by sources ($r < 50$ Mpc or $z < 0.012$) following the treatment of our Ref. [9]. This excludes the hypothetic contribution of extragalactic proton sources in our local Virgo supercluster. Whereas the analysis of the "low crossover" scenario (section II.2), using CR data below 10^{11} GeV, does not depend on this lower cut in redshift, this will have a strong influence on the outcome of the statistical analysis with exotic neutrino interactions. This is already obvious from the comparison of the fluxes in Fig. III.13.

For the statistical evaluation of this hypothesis we define $\mathcal{R}(\sigma^{\text{in}}_{\nu N})$ as the relative experimental exposure to strongly interacting neutrinos compared to the exposure $\mathcal{E}(E)$ to protons. The number of detected events is then given by

$$N_{\text{obs}} = \int \mathrm{d}\, E\, \mathcal{E}(E) \left(J_p(E) + \mathcal{R}(\sigma^{\text{in}}_{\nu N}(E))\, J_\nu(E) \right) \ . \tag{III.37}$$

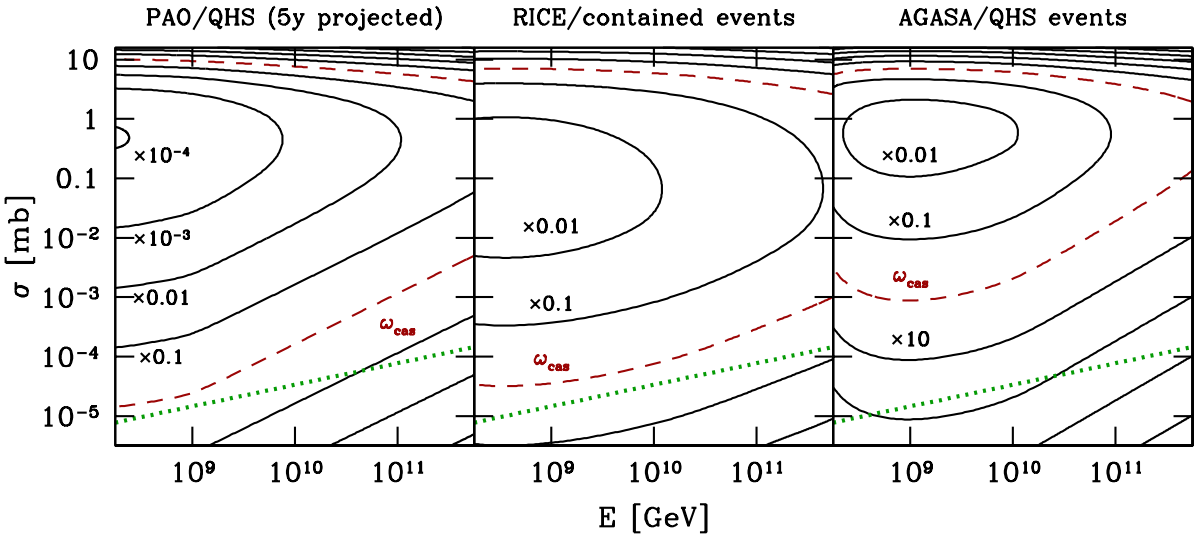

Figure III.15: *The sensitivity in terms of the the maximal average flux J^{max} per bin $\log_{10}\Delta E/E = \pm 0.05$, with average cross section per bin σ consistent to the 95% C.L. with the experimental results on QHS events at AGASA (left), contained events at RICE (center) and QHS events at PAO (right). The flux is shown as $E^2 J^{max}$ relative to the energy density $\omega_{cas} = 8.5 \times 10^{-7}\,GeV\,cm^{-2}\,s^{-1}\,sr^{-1}$ (dashed), corresponding to the cascade limit of Ref. [220]. The contours show the increase of the sensitivity by one order of magnitude (compare Appendix A). The dotted line is the extrapolation of SM charged and neutral current cross sections.*

The relative exposure $\mathcal{R}(\sigma^{\rm in}_{\nu N}(E))$ is estimated by the search criterion on the zenith angle θ and the (observed) atmospheric depth (cf. Sec. 1.3, Eq. (III.16), and Fig. III.6) adopted by each experiment. HiRes ($\theta \leq 60°$) thus has a larger relative exposure than AGASA ($\theta \leq 45°$), as Fig. III.14 shows. In both experiments neutrinos start to contribute significantly to quasi-vertical showers for $\sigma^{\rm in}_{\nu N} \gtrsim 10$ mb.

On the other hand, in the intermediate range $\sigma^{\rm SM}_{\nu N} \lesssim \sigma^{\rm in}_{\nu N} \lesssim 1$ mb, neutrinos may penetrate deeply in the atmosphere from quasi-horizontal directions or in the upper surface of the ice. For a given neutrino flux, the non-observation of such events can be turned into a model-independent upper bound on the neutrino-nucleon inelastic cross section. As already stated, this also constrains models which predict an anomalous enhancement of $\sigma^{\rm in}_{\nu N}$ at EHE [221]. In the following we will focus on the search results on quasi-horizontal showers (QHS) at AGASA [126] and contained events at RICE [102]. Fig. III.15 shows the sensitivity of these experiments in terms of the maximal average flux ($J^{\rm max}_{\nu}$) per bin and mean inelastic cross section ($\sigma^{\rm in}_{\nu N}$) consistent with the experimental results. Here, we also show the prospects of a 5-year observation at the Pierre Auger Observatory [222, 221]. For the calculation of events we always assume a maximal detection efficiency. Details are provided in Appendix A.

We have already introduced various theoretical ideas for an enhancement of the neutrino-nucleon cross section $\sigma_{\nu N}$ referring to physics beyond the (perturbative) SM. Based on our previous considerations we will use a flexible parameterization of a strong neutrino-nucleon inelastic cross section ($\sigma^{\rm new}_{\nu N}$) focusing on three characteristic parame-

ters: (i) the energy scale $E_{\rm th}$ of the new underlying physics, (ii) the amplification $\mathcal{A}$ compared to the SM predictions, and (iii) the width $\mathcal{B}$ of the transition between weak and strong interaction. A mathematically convenient parameterization is given by

$$\log_{10}\left(\frac{\sigma_{\nu N}^{\rm new}}{\mathcal{A}\,\sigma_{\nu N}^{\rm SM}}\right) = \frac{1}{2}\left[1+\tanh\left(\log_{\mathcal{B}}\frac{E_\nu}{E_{\rm th}}\right)\right] \ . \tag{III.38}$$

An example of this parameterization is shown in upper left panel of Fig. III.16.

Goodness-of-Fit Test

Our statistical analysis of the strongly interacting neutrino scenario follows the procedure outlined in section II.2 (see also Ref. [26, 9]). In this case the probability P is made up by Poisson distributions of vertical events (AGASA, Fly's Eye Stereo, Hires, and PAO), QHSs at AGASA and contained events at RICE (see Appendix A). The expectation value is now determined by the hypothesis $\mathcal{H}(\gamma, n, \sigma_{\nu N}^{\rm in})$, *i.e.* by the particular model for the inelastic neutrino-nucleon cross section $\sigma_{\nu N}^{\rm in}$ together with the source luminosity given by an injection index γ and an evolution index n.

The absolute value of the predicted flux is a priori unknown due to our lack of knowledge of the CR source luminosity. We normalize the events induced by protons and neutrinos to the data between 5×10^8 GeV and 10^{12} GeV individually for each experiment. The resulting ambiguity in the normalization of the proton and neutrino fluxes has to be removed for a prediction of horizontal events at AGASA and contained events at RICE. In this case, we normalize the fluxes to an average data set interpolating between AGASA, Fly's Eye, HiRes, and PAO according to the exposure of the individual bins.

The results of our goodness-of-fit test for the inelastic cross section (III.38) are shown in Figs. III.17–III.19. The range and resolution of the fitted parameters are shown in Table III.3. Each panel of the figures shows the goodness-of-fit w.r.t. two parameters as confidence levels (CLs). The remaining parameters of the set $\{\gamma, n, \mathcal{A}, \mathcal{B}, E_{\rm th}\}$ are marginalized over by a χ^2 minimization using simulated annealing as in Ref. [223]. The left panels of Figs. III.17–III.19 show the parameterization of the cross section. For comparison with our previous results (Sec. II.2) of the low crossover scenario we also show the source luminosity in the right panels. It is apparent that the results vary w.r.t. the underlying neutrino fluxes, cosmogenic neutrinos ("Cν") and extragalactic neutrinos ("Xν"), the CR data, with or without preliminary PAO data or energy calibration ("CAL"), and the inclusion of close-by sources ("Z0").

Comparing the boundaries of the parameters in Table III.3 with the contours in Figs. III.17–III.19 it seems that the results are correlated to our choice of the maximal amplification $\mathcal{A}$ and the minimal width $\mathcal{B}$. For our statistical analysis we kept the relative width $\mathcal{B}$ always larger than $10^{0.1}$ in order to account for the relative width of the bins. The relative exposure of strongly interacting neutrinos shown in Fig. III.14 indicates that the contribution of neutrinos to the vertical spectrum saturates under an

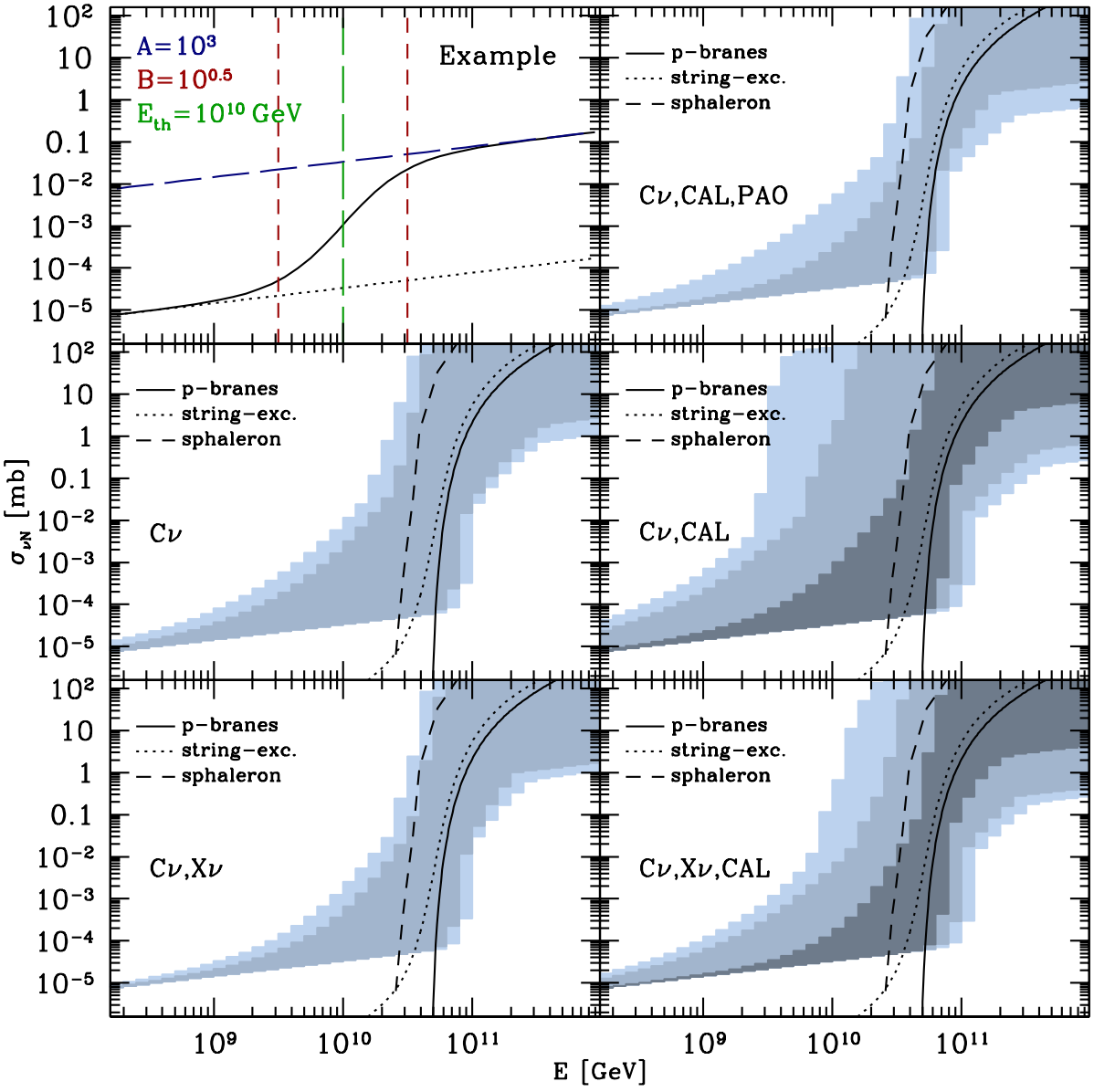

Figure III.16: *The goodness-of-fit results of the neutrino-nucleon cross section parameterized by $\mathcal{A}$, $\mathcal{B}$ and E_{th} as in Eq. (III.38). The upper left panel gives an example. The color-code is the same as in Figs. III.17, III.18 and III.19. The variations of the fit involve a re-calibration of the data ("CAL"), cosmogenic ("Cν") and extragalactic ("Xν") neutrino fluxes and the additional inclusion of the preliminary PAO data. The lines are theoretical predictions of an enhancement of the neutrino-nucleon cross-section by electroweak sphalerons [191] (short-dashed), p-branes [207] (long-dashed) and string excitations [194] (dotted).*

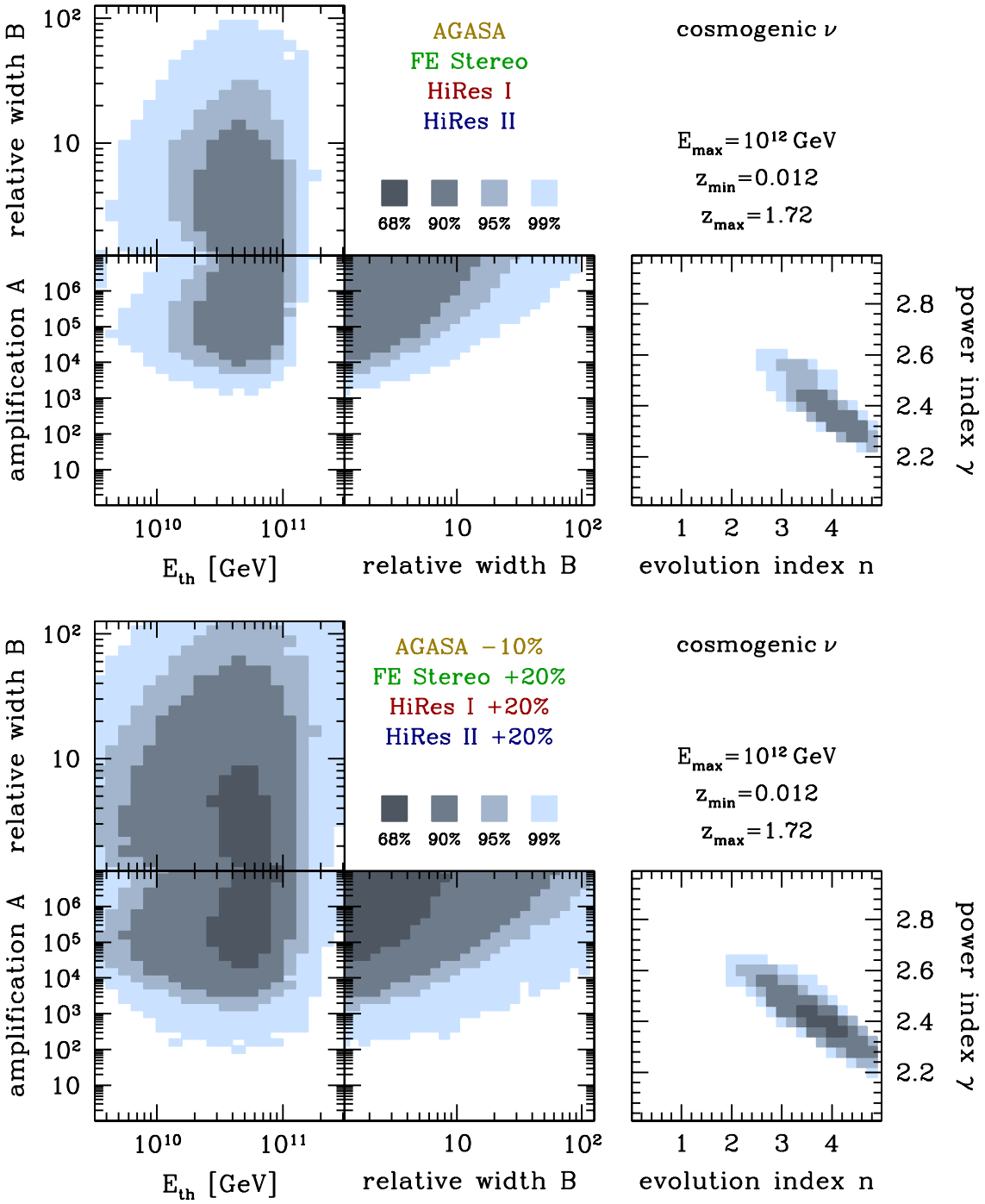

Figure III.17: *The result of a goodness-of-fit test in terms of the 68%, 90%, 95% and 99% confidence level in parameter space. We marginalize w.r.t. the other parameters. The left group of plots show the neutrino-nucleon cross section according to the parameters of Eq. (III.38). The right hand side shows the parameters of the source luminosity.*
Upper panel: *The results using AGASA, Fly's Eye and HiRes-I/II data for cosmogenic neutrinos (Sec. II.3).*
Lower panel: *As above, but with an energy re-calibration according to the results of Ref. [29].*

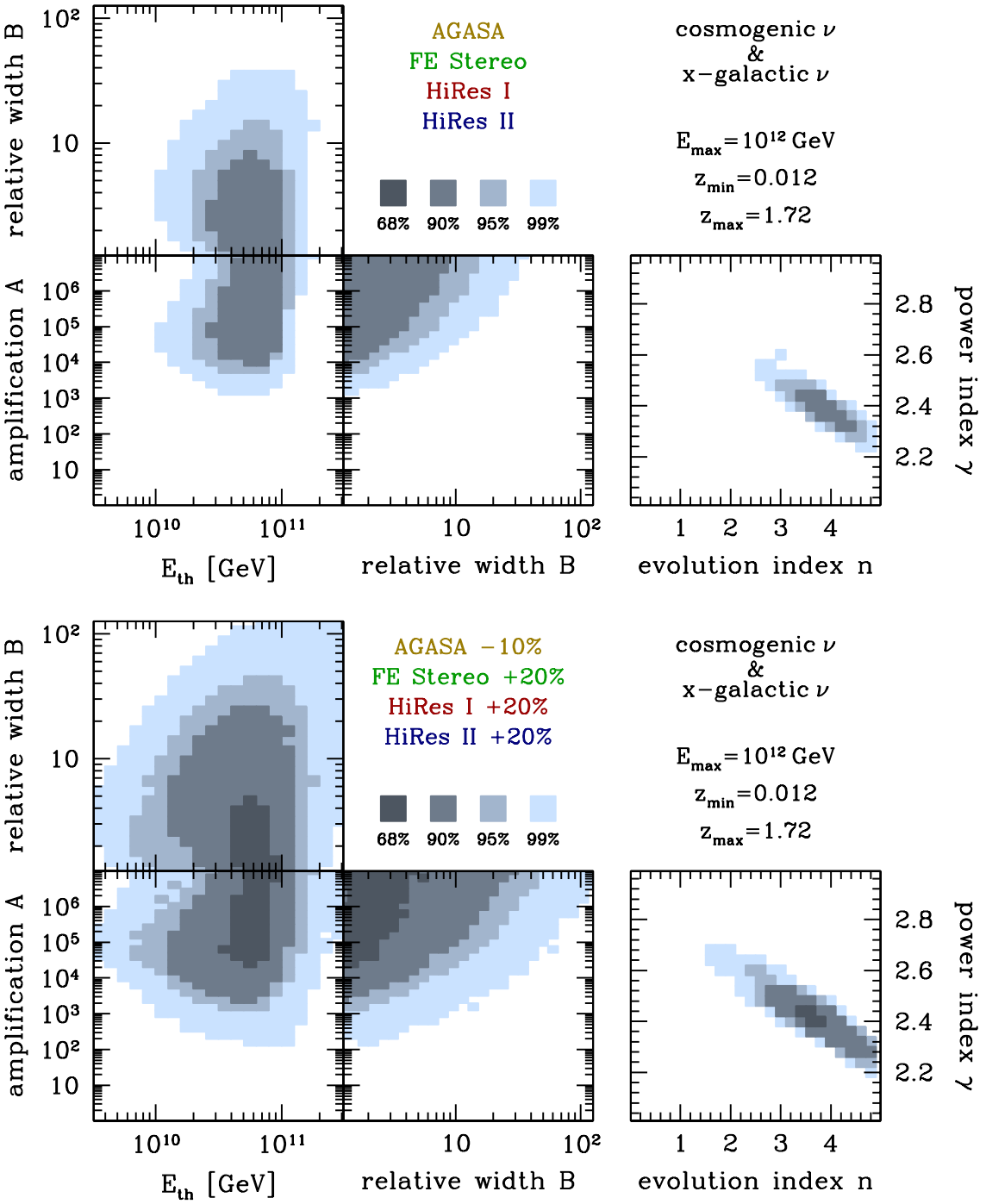

Figure III.18: *The result of a goodness-of-fit test in terms of the 68%, 90%, 95% and 99% confidence level in parameter space. We marginalize w.r.t. the other parameters. The left group of plots shows the neutrino-nucleon cross section according to the parameters of Eq. (III.38). The right hand side shows the parameters of the source luminosity.*
Upper panel: *The results using AGASA, Fly's Eye and HiRes-I/II data for cosmogenic neutrinos and neutrinos from optically thin sources (Sec. II.3).*
Lower panel: *As above, but with an energy re-calibration according to the results of Ref. [29].*

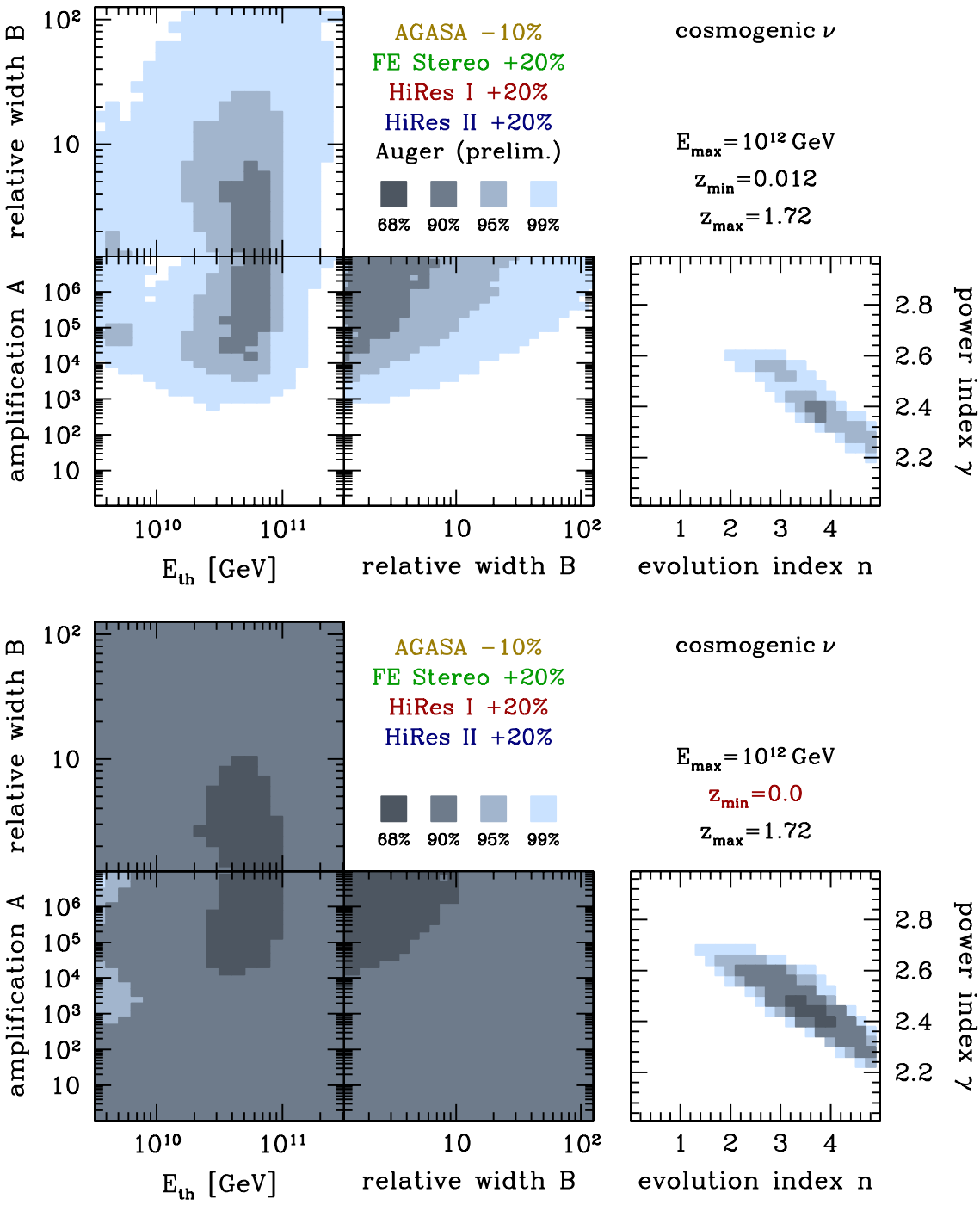

Figure III.19: *The result of a goodness-of-fit test in terms of the 68%, 90%, 95% and 99% confidence level in parameter space. We marginalize w.r.t. the other parameters. The left group of plots shows the neutrino-nucleon cross section according to the parameters of Eq. (III.38). The right hand side shows the parameters of the source luminosity.*
Upper panel: *The results using AGASA, Fly's Eye, HiRes-I/II data with an energy re-calibration according to the results of Ref. [29] together with the preliminary PAO data for cosmogenic neutrinos (Sec. II.3).*
Lower panel: *The results using AGASA, Fly's Eye, HiRes-I/II data with an energy re-calibration according to the results of Ref. [29] for cosmogenic neutrinos and close-by proton sources ($z_{min} = 0$).*

Table III.3: *Resolution and range of the fitted parameters.*

	γ	n	$\log_{10}\mathcal{A}$	$\log_{10}\mathcal{B}$	$\log_{10}\frac{E_{\rm th}}{\rm GeV}$
step size	0.01	0.05	0.2	0.08	0.1
min	2.00	0.00	0.0	0.1	9.45
max	2.99	4.95	7.0	2.1	11.45

amplification of the inelastic cross section by more than seven orders of magnitude. This motivates us to limit the amplification below $\mathcal{A} \leq 10^7$ in our analysis.

Discussion

Compared to our previous results [9] the re-calibrated spectrum (lower panels of Fig III.17 and III.18) is in much better statistical agreement with the combined flux of protons and neutrinos from exotic interactions. This is mainly due to the fact that the calibration method "optimizes" the CR data to extragalactic proton spectra below the GZK cutoff. However, within this particular model the re-calibrated data still favors an additional contribution from strongly interacting cosmogenic neutrinos.

The inclusion of neutrinos from extragalactic sources (Fig. III.18) slightly weakens the goodness-of-fit result compared to scenarios where only cosmogenic neutrinos may contribute (Fig. III.17). We have separated the analysis of these fluxes, since cosmogenic neutrinos are "guaranteed" in models with extragalactic protons whereas neutrinos from CR production involves additional assumptions on the acceleration mechanism.

The overall goodness of the fit worsens if we also include the preliminary PAO data shown in the upper panel of Fig. III.19. However, we already argued in section II.2 that the results based on this preliminary data should be regarded as an estimate of its tendency. The high resolution results of the Pierre Auger Observatory will certainly help to clarify our picture of UHE CRs in the future. In particular, PAO is a hybrid detector combining the experimental techniques of AGASA and HiRes and its energy calibration will be much more reliable.

For comparison, we show also the results from the inclusion of close-by sources shown in the lower panel of Fig. III.19. At the 90% CL the data is consistent with a proton spectrum without a contribution from strongly interacting neutrinos corresponding to $\mathcal{A} = 1$. However, the fit can still be improved below the 68% CL if strongly interacting neutrinos contribute with an amplification of the SM interaction by $\mathcal{A} \approx 10^4$.

In summary, in the absence of close-by sources exotic interactions of cosmic neutrinos might extend the CR spectrum beyond the GZK cutoff. At the 95% CL the corresponding neutrino-nucleon cross section should exhibit a steep increase by an amplification factor of $\mathcal{A} \gtrsim 10^3$. For $\mathcal{A} < 10^5$ the transition should be very rapid ($\mathcal{B} \lesssim 30$) at about 5×10^{11} GeV.

For the 68%, 90% and 95% allowed range of the parameters shown in Figs. III.17–III.19 we plot the range of the corresponding cross section in Fig. III.16, which can be used as a *benchmark* test for scenarios proposing strongly interacting neutrinos as a solution to the GZK puzzle. As an illustration, we have considered three models of a rapidly increasing neutrino-nucleon cross section based on electroweak sphalerons [191], p-branes [207] ($m = 6$, $L/L_* = 0.005$, and $M_D = 300$ TeV) and string excitations [194] ($M_* = 70$ TeV and $N_0 = C = 16$). We have also checked [9], that the direct fit of γ and n with these particular cross sections is in very good agreement with the goodness-of-fit test of the parameterization shown in Fig. III.16 (compare Eq. (III.38).

Dispersion Relations

Finally, we should also mention that a neutrino-nucleon cross section much larger than the SM predictions at some high energy scale will also have an impact on the elastic scattering amplitude at much lower energies. Regardless of a particular model, high energy cross sections have to fulfill criteria regarding the analyticity and unitarity of the S-matrix. As was emphasized in [224] the total cross sections at high energies are constrained by low energy elastic amplitudes due to dispersion relations.

One can relate the elastic scattering amplitude[16] $\Re\mathrm{e}\, A$ to the principal value of an integral involving the total (anti-)neutrino-nucleon cross section $\sigma^{\mathrm{tot}} = \sigma^{\mathrm{SM}} + \sigma^{\mathrm{new}}$ as

$$\Re\mathrm{e}\, A(E_\nu) - \Re\mathrm{e}\, A(0) = \frac{E_\nu}{4\pi}\, \mathcal{P} \int\limits_0^\infty \mathrm{d}E' \left(\frac{\sigma^{\mathrm{tot}}_{\nu N}(2m_p E')}{E'(E' - E_\nu)} + \frac{\sigma^{\mathrm{tot}}_{\bar{\nu} N}(2m_p E')}{E'(E' + E_\nu)} \right) . \tag{III.39}$$

We assume that our high energy cross section obeys the Pomeranchuk theorem, i.e. $\sigma^{\mathrm{new}}_{\nu N} - \sigma^{\mathrm{new}}_{\bar{\nu} N} \to 0$ for $E_\nu \to \infty$. The elastic amplitude at $E_\nu \approx 0$ is dominated by Z-boson exchange of the order of $G_F/2\sqrt{2}$. For $E_\nu \ll E_- \ll E_{\mathrm{th}} - \Delta E$ we can use Eq. (III.39) to estimate the relative contribution of new physics at low energies by

$$\frac{\Re\mathrm{e}\, A_{\mathrm{new}}(E_\nu)}{\Re\mathrm{e}\, A_{\mathrm{SM}}(E_\nu)} \approx \frac{\sqrt{2} E_\nu}{0.637 \pi G_{\mathrm{F}}} \int\limits_{E_-}^\infty \mathrm{d}E' \frac{\sigma^{\mathrm{SM}}}{E'} \frac{\mathrm{d}}{\mathrm{d}E'} \left(\frac{\sigma^{\mathrm{tot}}}{\sigma^{\mathrm{SM}}} \right) . \tag{III.40}$$

For the 99% CL the maximal relative contribution might reach $\mathcal{O}(20\%)$ at $E_\nu = 100$ GeV (see Ref. [9]). However, it seems to be challenging to measure the elastic neutrino-nucleon scattering amplitude with this experimental accuracy.

Summary

The excess of events beyond the Greisen-Zatsepin-Kuzmin (GZK) cutoff claimed by some cosmic ray (CR) experiments is a mystery (Sec. II.1.4). We have already discussed in sections II.1.1 and II.1.2 that these events require a close-by production in powerful CR

[16] We do not consider helicity of the nucleons in the following.

sources. There have been a plethora of explanations how this might be circumvented by a local enhancement of CR production, modifications of CR propagation as well as different and even exotic primaries and interactions.

We have followed the idea of Ref. [89] that exotic neutrino interactions might be the source of super-GZK events [9, 10, 11, 12]. In particular, cosmogenic neutrinos produced by extragalactic protons may reach the right flux-level for a continuation of the CR spectrum beyond the GZK cutoff. This requires a strong enhancement of inelastic neutrino-nucleon scattering. Since neutrino observatories provide upper limits on the neutrino flux the transition to the strong interaction has to be very rapid.

This requirement has motivated our statistical analysis of Ref. [9]. Our approach combines CR data and neutrino upper limits in a single goodness-of-fit test of the scenario. The author of this thesis was involved in the formulation and performance of the statistical analysis. In addition to our publication [9] we have provided in this thesis the results of variations w.r.t. data samples, neutrino fluxes, energy re-calibrations and close-by sources.

Our findings are the following. In the absence of close-by sources exotic interactions of cosmic neutrinos might extend the CR spectrum beyond the GZK cutoff. At the 95% CL the corresponding neutrino-nucleon cross section should exhibit a steep increase with an amplification factor of $\mathcal{A} \gtrsim 10^3$. For $\mathcal{A} < 10^5$ the transition should be very rapid ($\mathcal{B} \lesssim 30$) at about 5×10^{11} GeV. This behavior is realized in cross sections based on electroweak sphalerons, p-branes, and string excitations and may be used as a benchmark test of generic scenarios with strong neutrino-nucleon interactions.

IV. Conclusions and Outlook

Low Crossover Model

The "2nd knee" in the spectrum of cosmic rays (CRs) at about 5×10^8 GeV might be signal of a low transition between galactic components and extragalactic protons. Such a low crossover finds support in the chemical composition analysis of HiRes data [24], and reproduces the steepening at the "2nd knee" and the flattening at the "ankle" via e^+e^- production on the cosmic microwave background [25, 28, 225]. The low crossover energy is well below the threshold energy for resonant $p\gamma_{\rm CMB}$ absorption, and so samples sources even at large redshift. Thus, it is important to take source evolution into consideration.

We have reviewed our statistical analysis of Ref. [4] using combined data samples of Akeno [73] & AGASA [57] and Fly's Eye [69, 54] & HiRes [58]. The fit of the propagated proton fluxes to the data between 5×10^8 GeV and 10^{11} GeV reveals the statistically allowed regions for the redshift evolution (index n), injection spectrum (index γ), and power density of the extragalactic sources. In addition to our previous study [4], we have discussed variations of the fit w.r.t. normalization and energy calibration of the data. In this case, the best fit values of γ and n vary by $\pm 5\%$ and $\pm 10\%$, respectively. The preliminary data set of the Pierre Auger Collaboration weakens the goodness of the fit, but is consistent with the model predictions at the 99% confidence level. A power index γ smaller than 2.3 is excluded at the 95% confidence level. The best fit values range between $\gamma = 2.4$–2.6 and $n = 3.2$–3.7 depending on data samples and energy calibration.

Based on this analysis we have estimated the extragalactic diffuse neutrino flux emitted from optically thin sources. The neutrino flux obtained using the Waxman-Bahcall [77] consideration for energetics at the source mirrors the steep spectrum predicted in the low crossover model. In addition to Ref. [4] we provide the range of the neutrino flux at the 95% confidence level of the goodness-of-fit tests. Comparison of the resulting flux with existing AMANDA-II bounds (1 year) [85] reveals the following: (1) If neutrinos are generated by pp interactions at the source, the resulting flux is within the excluded region. (2) For dominance of $p\gamma$ interactions, the best fit to the data yields a neutrino flux which is marginally consistent with the AMANDA-II upper limit.

A complete analysis of the AMANDA-II data (5 years) or one year of observation at Auger will provide sufficient sensitivity to rule out the model. The neutrino flux from the source in this scenario dominates the cosmogenic flux below 10^9 GeV. Thus, should data from AMANDA not rule out the model, we show that IceCube can measure the characteristic power law of the neutrino spectrum, and thus provide a window on the source dynamics.

Supersymmetric Interactions

High energy cosmic neutrinos collide with matter in the Earth at center of mass energies beyond the capability of any earth-bound experiment. The attempt to measure the CR fluxes in various observatories is therefore tightly connected to extrapolations of the SM interactions of these particles to very high energies. Besides, one can look for deviations from the SM predictions for the strength of the interactions or even for new particles.

Supersymmetry (SUSY) is currently one of the most popular extensions of the SM and predicts a super-partner for each particle. We have reviewed the analysis of Refs. [5, 6], where we examine the question whether neutrino telescopes could play a significant role in the discovery and study of SUSY extensions of the SM with a gravitino LSP ("lightest SUSY particle") and a long-lived stau NLSP ("next-to-lightest SUSY particle"). In these models, neutrino-nucleon interactions can produce pairs of staus which show up as quasi-parallel tracks in the detector [156, 157].

We have argued that events with a single stau in the detector are virtually indistinguishable from muon events at high energies. However, the reduced energy loss of staus in matter, which increases the effective volume, reduces also the detection efficiency in the telescope. As a result, single stau events play only a subdominant role compared to muon events. Consequently, the reconstruction of the initial high-energy neutrino flux from the total rate of muon-like events can proceed assuming SM interactions alone. Alternative signals of single staus may arise from their capture and subsequent decay into a tau and a gravitino within a neutrino telescope: An excess of time-correlated tau cascades coincident with the end-point of a muon-like track may have only a small background from SM processes. However, we have shown that for the most optimistic case this signals may occur once per century which is clearly above realistic observation times.

The typical spatial resolution of ice or water Cherenkov telescopes is of the order of a few 10 meters. We have shown that about 40% of the stau pairs through the detector produce quasi-parallel tracks which are well-separated by more than 50 m. This is in contrast to contributions of SM "di-muon" events which have typically a smaller separation due to their close-by production [157, 160]. Hence, the appearance of well-separated quasi-parallel tracks in neutrino telescopes is evidence for a contribution of physics beyond the SM. If the SUSY particle masses are close to the current experimental limits and if the cosmic neutrino flux is also close to current experimental bound, we expect up to 50 pair events per year in a cubic kilometer detector such as IceCube, with negligible background. Less favorable event rates are obtained for SUSY mass spectra of commonly used scenarios for SUSY breaking, mainly because the squarks are significantly heavier.

Long-lived charged sleptons with masses close to 100 GeV should immediately be visible at the LHC, which starts its operation in 2007. If the mass of the stau NLSP is known, neutrino telescopes may derive (model-dependent) upper bounds on the mass of a gravitino LSP: For a gravitino mass larger than about 400 keV, as we have assumed,

the stau decay length is larger than the Earth's diameter. Thus, the spectrum is independent of the gravitino mass. For lighter gravitinos, the rate of stau pairs will drop, starting at the low-energy end of the spectrum. Therefore, it might be possible to obtain information about the gravitino mass, if the spectrum is measured very accurately and if the superpartner masses are known. However, with the small number of pair events we find, this appears doubtful.

Exotic Interactions

The spectrum of extragalactic cosmic rays (CRs) is expected to follow the Greisen-Zatsepin-Kuzmin (GZK) cutoff [7, 8] at about 5×10^{10} GeV which results from energy losses of charged nuclei in the cosmic microwave background. So far the confrontation of this feature with CR data is inconclusive. In the absence of close-by sources a power law continuation of the spectrum might signal the contribution of new physics in the production, propagation or observation of CRs.

The GZK suppression of extragalactic proton fluxes is intrinsically tied to the appearance of cosmogenic neutrinos. These neutrino fluxes may reach the right flux level for a continuation of the CR spectrum beyond the GZK cutoff [89]. However, this requires a very strong enhancement of inelastic neutrino-nucleon scattering. Moreover, for consistency with the (non-)observation of UHE neutrino fluxes, the transition to the strong interaction has to be very rapid.

These requirements have motivated our statistical analysis, which combines current CR data and neutrino upper limits in a single goodness-of-fit test of the low crossover scenario [9] (see also Refs. [10, 11, 12]). We have used a flexible parameterization of the inelastic neutrino-nucleon cross section, which focuses on (1) the energy scale $E_{\rm th}$ of new underlying physics, (2) the amplification $\mathcal{A}$ compared to the SM predictions, and (3) the width $\mathcal{B}$ of the transition between weak and strong interaction.

We have shown that current data on the highest energy CRs from AGASA [57], Fly's Eye [69, 54], HiRes [58] and the Pierre Auger Observatory [66, 67] (preliminary data) may be interpreted as a combined flux of extragalactic protons and strongly interacting cosmic neutrinos in the low crossover scenario. This is statistically consistent with the (non-)observation of quasi-horizontal showers at AGASA [126] and contained events at RICE [101]. We have estimated the neutrino events generously, assuming a full conversion of the neutrino energy into the shower energy and a maximal detection efficiency of these events.

In extension to our analysis of Ref. [9] we have also presented the results of a fit to the AGASA and HiRes data, shifted according to the "dip"-calibration from extragalactic proton spectra [29]. With these modifications the overall goodness of the fit improves and a contribution of neutrinos is still favored by the data. If we also include close-by sources, the data fits without neutrinos at the 90% confidence level. We have shown that the inclusion of neutrinos from optically thin sources changes the goodness of the

fit insignificantly. In contrast, the preliminary data of the Pierre Auger Observatory weakens the results of the goodness-of-fit test.

In summary, at the 95% confidence level the corresponding neutrino-nucleon cross section should exhibit a steep increase by an amplification factor of $\mathcal{A} \gtrsim 10^3$. For $\mathcal{A} < 10^5$ the transition should be very rapid ($\mathcal{B} \lesssim 30$) at about 5×10^{11} GeV. The range of the cross section shown in Fig. III.16 may be used as a benchmark for scenarios of strongly interacting neutrinos.

The Pierre Auger Observatory will play a crucial role on models of strongly interacting neutrinos. Beside the spectrum of vertical showers with much higher statistics than AGASA and HiRes, the search of quasi-horizontal showers will soon have a stronger sensitivity to weakly interacting neutrinos as Fig. III.15 indicates. Within our approach it will be easy to implement any future data, notably from Auger, which might finally reach large sensitivity on strongly interacting neutrino scenarios. Here, also possible correlations with distant astrophysical sources can give a hint on neutrino primaries [226, 227].

A. Neutrino Event Rates

Quasi-Horizontal Showers at AGASA

The AGASA Collaboration has observed one quasi-horizontal ($\theta > 60°$) shower (QHS) during an operation time of 1710.5 days with an expected background of $1.72^{+0.14+0.65}_{-0.07-0.41}$ (MC statistics and systematics) [126]. The search criteria for quasi-horizontal events set the following constraints on the shower maximum $z_{\max}$: $z(\theta) - z_{\max}(\theta) < 500\,(\mathrm{g}/m_p)\,\mathrm{cm}^{-2}$ and $z_{\max} \geq 2500\,(\mathrm{g}/m_p)\,\mathrm{cm}^{-2}$. On average the shower develops its maximum after traversing $800\,(\mathrm{g}/m_p)\,\mathrm{cm}^{-2}$ in the atmosphere. Hence the observed atmospheric depth varies between $z_-(\theta) = \max(1700\,(\mathrm{g}/m_p)\,\mathrm{cm}^{-2}, z(\theta) - 1300\,(\mathrm{g}/m_p)\,\mathrm{cm}^{-2})$ and $z_+(\theta) = z(\theta)$ (cf. Fig. III.6). The number of observed QHS events can then be calculated by Eq. (III.15). As the effective detector area for hadronic showers we took $A = 56.1\ \mathrm{km}^2$. The horizontal detection efficiency $\mathcal{P}_{\mathrm{hor}}(E)$ for QHSs is reported to be 100% above 10^{10} GeV and approximately zero below 10^8 GeV. In between we use a power-law approximation $\propto (\log_{10}(E/\mathrm{GeV}) - 8)^n$, which is fitted [228] to reproduce the upper bound of 3.52 events (95% CL) for the observation of one QHS from charged current interactions reported by the AGASA Collaboration. The left panel of Fig. III.15 shows the sensitivity of AGASA for QHSs in terms of the maximal neutrino flux $E_\nu^2\, J_\nu^{\max}(E_\nu)$ per flavor and per energy range $\log_{10} \triangle E/E = \pm 0.05$ consistent to the 95% CL with the observation.

Contained Events at RICE

The Radio Ice Cherenkov Experiment (RICE) at the South Pole has searched for electromagnetic and hadronic showers based on the principle of "radio coherence". During an observation time of 20500 hours no candidate of an neutrino-induced event has been observed [102]. For strongly interacting neutrinos with cross section $\sigma_{\nu\mathrm{N}}$ we approximate the expected number of events as:

$$\frac{\mathrm{d}^3 N}{\mathrm{d}t\,\mathrm{d}\Omega\,\mathrm{d}E} = n_{\mathrm{ice}} \int\limits_{V_{\mathrm{eff}}(E)} \mathrm{d}\vec{r}\, J_\nu\, \sigma_{\nu N}\, e^{-z(\vec{r},\theta)\sigma_{\nu\mathrm{N}}}\ . \tag{A.1}$$

We approximate the ice target as a cylinder with $V_{\mathrm{eff}}(E) = h\pi r^2(E)$ and a fixed height $h = 1\,\mathrm{km}$. From this we can approximate the distance $d(\vec{r},\theta)$ a quasi-horizontal neutrino has to traverse in ice before it interacts with a nucleon inside the detector. Hence, the depth $z(\theta)$ is composed of the atmospheric depth $z_{\mathrm{atm}}(\theta)$ and the depth in ice $d(\vec{r},\theta) n_{\mathrm{ice}}$. The sensitivity of RICE to the neutrino flux is shown as the center plot in Fig. III.15.

The time-averaged effective detection volume $V_{\rm eff}(E)$ has been determined with Monte-Carlo simulations in Ref. [102] (Fig. 20 in terms of $2\pi \times V_{\rm eff} \times$ lifetime). For the calculation of neutrino events from exotic interactions (Sec. III.3) we assume a maximal efficiency for the event detection and a full conversion of the neutrino energy into a hadronic shower. The experimental exposure time used in Ref. [102] (20500 hours) is larger compared to the previous analysis in Ref. [100] (3500 hours) by about a factor 6. However, the time-averaged effective volume for hadronic showers used in Ref. [102] is reduced compared to the estimates in Ref. [100] by more than a factor 6.[1] Correspondingly, the RICE bound applied in our new fit is slightly weaker then in Ref. [9].

Quasi-Horizontal Showers at PAO

The Pierre Auger Observatory (PAO), which is actually comprised of two sub-observatories, is the next large-scale neutrino detector in operation. The southern site is currently operational and growing to its final size of about 3000 km^2 with 1600 water Cherenkov detectors separated by about 1.5 km and 24 fluorescence detectors. By the time of writing there are more than 1000 water Cherenkov tanks deployed and 18 of the 24 fluorescence detectors are operating.

The rate of neutrino-induced events at the ground arrays of PAO can be calculated using Eq. (III.15). The effective aperture has been parameterized in Ref. [221] through a comparison with the geometric acceptance published in Ref. [222]. In short, to estimate the sensitivity for PAO, the following selection criteria were adopted: *i)* $75^\circ \leq \theta \leq 90^\circ$ for the zenith angle, *ii)* $z_{\rm max} \geq 2500\,({\rm g}/m_p)\,{\rm cm}^{-2}$ for the shower maximum, which corresponds to requiring $z_-(\theta) = 1700\,({\rm g}/m_p)\,{\rm cm}^{-2}$ in this work. The altitude of the PAO Southern site (1200 m above sea level) was also taken into account in $z_+(\theta) = z(\theta)$. For hadronic showers with axis falling in the array, the effective area can then be parameterized as $A_\perp(\theta, E)\,P(E)$, with $A_\perp(\theta, E) \approx \cos\theta \times 1.475$ km$^2\,(E/{\rm eV})^{0.151}$, and $P(E) = 1$ for $E \geq 10^{8.6}$ GeV, while $P(E) = 0.654\ \log_{10}(E/{\rm eV}) - 10.9$ below this energy. The effective aperture for all showers (i.e. including showers with axis not going through the array) is roughly 1.8 to 2.5 times larger, as shown in Ref. [222].

A first model-independent investigation of the sensitivity of PAO to anomalous neutrino interactions was performed in Ref. [221]. Assuming one year of operation with no event observed above the expected hadronic SM background (95% CL corresponding to 3.09 events), we estimate the prospects for PAO to strengthen the existing constraints imposed by AGASA and RICE. The 1-year projected sensitivity is shown in Fig. III.15 (right panel).

[1] In Ref. [9] we use the non-LPM result shown as a dotted curve in Fig. 10 as an approximation for $V_{\rm eff}(E)$. For energies larger than 10^{11} GeV we approximate the volume as 100 km^3.

Bibliography

[1] Super-Kamiokande, J. Hosaka *et al.*, Phys. Rev. **D74**, 032002 (2006), hep-ex/0604011.

[2] J. N. Bahcall, A. M. Serenelli, and S. Basu, Astrophys. J. **621**, L85 (2005), astro-ph/0412440.

[3] SNO, B. Aharmim *et al.*, Phys. Rev. **C72**, 055502 (2005), nucl-ex/0502021.

[4] M. Ahlers *et al.*, Phys. Rev. **D72**, 023001 (2005), astro-ph/0503229.

[5] M. Ahlers, J. Kersten, and A. Ringwald, JCAP **0607**, 005 (2006), hep-ph/0604188.

[6] M. Ahlers, Submitted to J. Phys. Conf. Ser. (2006) , astro-ph/0610775.

[7] K. Greisen, Phys. Rev. Lett. **16**, 748 (1966).

[8] G. T. Zatsepin and V. A. Kuzmin, JETP Lett. **4**, 78 (1966).

[9] M. Ahlers, A. Ringwald, and H. Tu, Astropart. Phys. **24**, 438 (2006), astro-ph/0506698.

[10] M. Ahlers, A. Ringwald, and H. Tu, PoS **JHW2005**, 014 (2006), astro-ph/0512439.

[11] M. Ahlers, Prog. Part. Nucl. Phys. **57**, 353 (2006), astro-ph/0511483.

[12] M. Ahlers, astro-ph/0611890, To appear in the proceedings of "Exotic Physics with Neutrino Telecopes", Uppsala, Sweden, September 20-22, 2006.

[13] Particle Data Group, S. Eidelman *et al.*, Phys. Lett. **B592**, 1 (2004).

[14] A. M. Hillas, Ann. Rev. Astron. Astrophys. **22**, 425 (1984).

[15] T. K. Gaisser, *Cosmic rays and particle physics* , Cambridge, UK: Univ. Pr. (1990) 279 p.

[16] V. L. Ginzburg, V. A. Dogiel, V. S. Berezinsky, S. V. Bulanov, and V. S. Ptuskin, *Astrophysics of cosmic rays* , Amsterdam, Netherlands: North-Holland (1990) 534 p.

[17] L. O. Drury, Contemp. Phys. **35**, 231 (1994).

[18] P. Bhattacharjee and G. Sigl, Phys. Rept. **327**, 109 (2000), astro-ph/9811011.

[19] KASCADE-Grande, A. Haungs *et al.*, J. Phys. Conf. Ser. **47**, 238 (2006), astro-ph/0508286.

[20] EAS-TOP, M. Aglietta *et al.*, Astropart. Phys. **21**, 583 (2004).

[21] J. R. Hörandel, N. N. Kalmykov, and A. V. Timokhin, J. Phys. Conf. Ser. **47**, 132 (2006), astro-ph/0508015.

[22] KASCADE-Grande, G. Navarra *et al.*, Nucl. Instrum. Meth. **A518**, 207 (2004).

[23] IceCube, T. Stanev and R. Ulrich, Nucl. Phys. Proc. Suppl. **145**, 327 (2005), astro-ph/0501046.

[24] HiRes, D. R. Bergman, Nucl. Phys. Proc. Suppl. **136**, 40 (2004), astro-ph/0407244.

[25] V. Berezinsky, A. Z. Gazizov, and S. I. Grigorieva, Phys. Rev. **D74**, 043005 (2006), hep-ph/0204357.

[26] Z. Fodor, S. D. Katz, A. Ringwald, and H. Tu, Phys. Lett. **B561**, 191 (2003), hep-ph/0303080.

[27] V. Berezinsky, A. Gazizov, and S. Grigorieva, Nucl. Phys. Proc. Suppl. **136**, 147 (2004), astro-ph/0410650.

[28] V. Berezinsky, A. Z. Gazizov, and S. I. Grigorieva, Phys. Lett. **B612**, 147 (2005), astro-ph/0502550.

[29] R. Aloisio *et al.*, Astropart. Phys. **27**, 76 (2007), astro-ph/0608219.

[30] A. Achterberg, Y. A. Gallant, J. G. Kirk, and A. W. Guthmann, Mon. Not. Roy. Astron. Soc. **328**, 393 (2001), astro-ph/0107530.

[31] D. Allard, E. Parizot, and A. V. Olinto, Astropart. Phys. **27**, 61 (2007), astro-ph/0512345.

[32] AGASA, M. Takeda *et al.*, Astrophys. J. **522**, 225 (1999), astro-ph/9902239.

[33] HiRes, R. U. Abbasi *et al.*, Astrophys. J. **610**, L73 (2004), astro-ph/0404137.

[34] M. Nagano and A. A. Watson, Rev. Mod. Phys. **72**, 689 (2000).

[35] R. J. Protheroe, Astropart. Phys. **21**, 415 (2004), astro-ph/0401523.

[36] A. M. Hillas, J. Phys. **G31**, R95 (2005).

[37] D. F. Torres and L. A. Anchordoqui, Rept. Prog. Phys. **67**, 1663 (2004), astro-ph/0402371.

[38] A. Vilenkin, Phys. Rept. **121**, 263 (1985).

[39] I. Tkachev, S. Khlebnikov, L. Kofman, and A. D. Linde, Phys. Lett. **B440**, 262 (1998), hep-ph/9805209.

[40] V. A. Kuzmin and I. I. Tkachev, Phys. Rept. **320**, 199 (1999), hep-ph/9903542.

[41] D. N. Spergel *et al.*, Submitted to Astrophys. J. (2006) , astro-ph/0603449.

[42] D. V. Semikoz and G. Sigl, JCAP **0404**, 003 (2004), hep-ph/0309328.

[43] Z. Fodor and S. D. Katz, Phys. Rev. **D63**, 023002 (2001), hep-ph/0007158.

[44] W. L. Freedman *et al.*, Astrophys. J. **553**, 47 (2001), astro-ph/0012376.

[45] A. Mucke, R. Engel, J. P. Rachen, R. J. Protheroe, and T. Stanev, Comput. Phys. Commun. **124**, 290 (2000), astro-ph/9903478.

[46] J. Miralda-Escude and E. Waxman, Astrophys. J. **462**, L59 (1996), astro-ph/9601012.

[47] KASCADE, T. Antoni *et al.*, Astrophys. J. **604**, 687 (2004), astro-ph/0312375.

[48] KASCADE, T. Antoni *et al.*, Astrophys. J. **608**, 865 (2004), astro-ph/0402656.

[49] P. P. Kronberg, Rept. Prog. Phys. **57**, 325 (1994).

[50] R. Aloisio and V. Berezinsky, Astrophys. J. **612**, 900 (2004), astro-ph/0403095.

[51] AGASA, M. Takeda *et al.*, Astropart. Phys. **19**, 447 (2003), astro-ph/0209422.

[52] M. Ave, J. Knapp, J. Lloyd-Evans, M. Marchesini, and A. A. Watson, Astropart. Phys. **19**, 47 (2003), astro-ph/0112253.

[53] A. V. Glushkov and M. I. Pravdin, J. Exp. Theor. Phys. **101**, 88 (2005).

[54] HiRes, D. J. Bird *et al.*, Astrophys. J. **424**, 491 (1994).

[55] HiRes, R. U. Abbasi *et al.*, Phys. Lett. **B619**, 271 (2005), astro-ph/0501317.

[56] R. U. Abbasi *et al.*, Astropart. Phys. **23**, 157 (2005).

[57] M. Takeda *et al.*, Phys. Rev. Lett. **81**, 1163 (1998), astro-ph/9807193.

[58] HiRes, T. Abu-Zayyad *et al.*, Astropart. Phys. **23**, 157 (2005), astro-ph/0208301.

[59] D. De Marco, P. Blasi, and A. V. Olinto, Astropart. Phys. **20**, 53 (2003), astro-ph/0301497.

[60] Shinozaki (AGASA Collaboration), talk presented at GZK40, Moscow 2006.

[61] AGASA, N. Hayashida *et al.*, Phys. Rev. Lett. **77**, 1000 (1996).

[62] AGASA, M. Takeda *et al.*, Prepared for the 27th International Cosmic Ray Conference (ICRC 2001), Hamburg, Germany, 7-15 Aug 2001.

[63] AGASA, M. Teshima *et al.*, Prepared for the 28th International Cosmic Ray Conferences (ICRC 2003), Tsukuba, Japan, 31 Jul - 7 Aug 2003.

[64] AGASA, N. Hayashida *et al.*, astro-ph/9906056, Prepared for the 26th International Cosmic Ray Conference (ICRC 99), Salt Lake City, Utah, 17-25 Aug 1999.

[65] HiRes, R. Abbasi *et al.*, Astropart. Phys. **21**, 111 (2004), astro-ph/0309457.

[66] Pierre Auger, J. Abraham *et al.*, Nucl. Instrum. Meth. **A523**, 50 (2004).

[67] Pierre Auger, K.-H. Kampert, Submitted to Int.J.Mod.Phys.**E** (2006) , astro-ph/0608136.

[68] Pierre Auger, M. Aglietta *et al.*, (2006), astro-ph/0607382.

[69] HiRes, D. J. Bird *et al.*, Phys. Rev. Lett. **71**, 3401 (1993).

[70] Z. Fodor, S. D. Katz, A. Ringwald, and H. Tu, JCAP **0311**, 015 (2003), hep-ph/0309171.

[71] E. Waxman, Astrophys. J. **452**, L1 (1995), astro-ph/9508037.

[72] M. Nagano *et al.*, J. Phys. **G10**, 1295 (1984).

[73] M. Nagano *et al.*, J. Phys. **G18**, 423 (1992).

[74] L. Anchordoqui, private communication.

[75] K. Mannheim, R. J. Protheroe, and J. P. Rachen, Phys. Rev. **D63**, 023003 (2001), astro-ph/9812398.

[76] L. A. Anchordoqui, H. Goldberg, F. Halzen, and T. J. Weiler, Phys. Lett. **B600**, 202 (2004), astro-ph/0404387.

[77] E. Waxman and J. N. Bahcall, Phys. Rev. **D59**, 023002 (1999), hep-ph/9807282.

[78] F. W. Stecker, Phys. Rev. Lett. **21**, 1016 (1968).

[79] T. J. Weiler, Phys. Rev. Lett. **49**, 234 (1982).

[80] B. Eberle, A. Ringwald, L. Song, and T. J. Weiler, Phys. Rev. **D70**, 023007 (2004), hep-ph/0401203.

[81] A. Ringwald and L. Schrempp, JCAP **0610**, 012 (2006), astro-ph/0606316.

[82] A. W. Strong, I. V. Moskalenko, and O. Reimer, astro-ph/0306345, Prepared for the 28th International Cosmic Ray Conferences (ICRC 2003), Tsukuba, Japan, 31 Jul - 7 Aug 2003.

[83] U. Keshet, E. Waxman, and A. Loeb, JCAP **0404**, 006 (2004), astro-ph/0306442.

[84] AMANDA, M. Ackermann *et al.*, Astropart. Phys. **22**, 339 (2005).

[85] IceCube, L. Gerhardt, Prepared for the 29th International Cosmic Ray Conference (ICRC 2005), Pune, India, 3-11 Aug 2005.

[86] IceCube, M. Ribordy *et al.*, Phys. Atom. Nucl. **69**, 1899 (2006), astro-ph/0509322.

[87] X. Bertou, P. Billoir, O. Deligny, C. Lachaud, and A. Letessier-Selvon, Astropart. Phys. **17**, 183 (2002), astro-ph/0104452.

[88] ANITA, S. W. Barwick *et al.*, Phys. Rev. Lett. **96**, 171101 (2006), astro-ph/0512265.

[89] V. S. Beresinsky and G. T. Zatsepin, Phys. Lett. **B28**, 423 (1969).

[90] D. De Marco, T. Stanev, and F. W. Stecker, Phys. Rev. **D73**, 043003 (2006), astro-ph/0512479.

[91] D. Allard *et al.*, JCAP **0609**, 005 (2006), astro-ph/0605327.

[92] R. Engel, D. Seckel, and T. Stanev, Phys. Rev. **D64**, 093010 (2001), astro-ph/0101216.

[93] G. J. Feldman and R. D. Cousins, Phys. Rev. **D57**, 3873 (1998), physics/9711021.

[94] V. S. Berezinsky and A. Y. Smirnov, Phys. Lett. **B48**, 269 (1974).

[95] AMANDA, E. Andres *et al.*, Astropart. Phys. **13**, 1 (2000), astro-ph/9906203.

[96] E. Andres *et al.*, Nature **410**, 441 (2001).

[97] IceCube, J. Ahrens *et al.*, Astropart. Phys. **20**, 507 (2004), astro-ph/0305196.

[98] R. Gandhi, C. Quigg, M. H. Reno, and I. Sarcevic, Phys. Rev. **D58**, 093009 (1998), hep-ph/9807264.

[99] F. Halzen and D. Hooper, Rept. Prog. Phys. **65**, 1025 (2002), astro-ph/0204527.

[100] RICE, I. Kravchenko *et al.*, Astropart. Phys. **20**, 195 (2003), astro-ph/0206371.

[101] RICE, I. Kravchenko, astro-ph/0306408, Presented at 28th International Cosmic Ray Conferences (ICRC 2003), Tsukuba, Japan, 31 Jul - 7 Aug 2003.

[102] RICE, I. Kravchenko *et al.*, Phys. Rev. **D73**, 082002 (2006), astro-ph/0601148.

[103] EUSO, G. D'Ali Staiti, Nucl. Phys. Proc. Suppl. **136**, 415 (2004).

[104] OWL, F. W. Stecker *et al.*, Nucl. Phys. Proc. Suppl. **136C**, 433 (2004), astro-ph/0408162.

[105] L. Anchordoqui, H. Goldberg, and C. Nunez, Phys. Rev. **D71**, 065014 (2005), hep-ph/0408284.

[106] J. Alvarez-Muniz, R. Engel, T. K. Gaisser, J. A. Ortiz, and T. Stanev, Phys. Rev. **D66**, 033011 (2002), astro-ph/0205302.

[107] Provided by `http://www-zeus.desy.de/`.

[108] V. N. Gribov and L. N. Lipatov, Sov. J. Nucl. Phys. **15**, 438 (1972).

[109] L. N. Lipatov, Sov. J. Nucl. Phys. **20**, 94 (1975).

[110] G. Altarelli and G. Parisi, Nucl. Phys. **B126**, 298 (1977).

[111] Y. L. Dokshitzer, Sov. Phys. JETP **46**, 641 (1977).

[112] E. A. Kuraev, L. N. Lipatov, and V. S. Fadin, Sov. Phys. JETP **45**, 199 (1977).

[113] I. I. Balitsky and L. N. Lipatov, Sov. J. Nucl. Phys. **28**, 822 (1978).

[114] J. Kwiecinski, A. D. Martin, and A. M. Stasto, Phys. Rev. **D56**, 3991 (1997), hep-ph/9703445.

[115] K. Golec-Biernat and M. Wüsthoff, Phys. Rev. **D59**, 014017 (1999), hep-ph/9807513.

[116] K. Golec-Biernat and M. Wüsthoff, Phys. Rev. **D60**, 114023 (1999), hep-ph/9903358.

[117] K. Kutak and J. Kwiecinski, Eur. Phys. J. **C29**, 521 (2003), hep-ph/0303209.

[118] E. Iancu and R. Venugopalan, (2003), hep-ph/0303204, To be published in QGP3, Eds. R.C. Hwa and X.N.Wang, World Scientific.

[119] A. D. Martin, R. G. Roberts, W. J. Stirling, and R. S. Thorne, Eur. Phys. J. **C4**, 463 (1998), hep-ph/9803445.

[120] J. Pumplin *et al.*, JHEP **07**, 012 (2002), hep-ph/0201195.

[121] R. K. Ellis, Z. Kunszt, and E. M. Levin, Nucl. Phys. **B420**, 517 (1994).

[122] E. M. Henley and J. Jalilian-Marian, Phys. Rev. **D73**, 094004 (2006), hep-ph/0512220.

[123] L. A. Anchordoqui, A. M. Cooper-Sarkar, D. Hooper, and S. Sarkar, Phys. Rev. **D74**, 043008 (2006), hep-ph/0605086.

[124] J. Rosiek, Phys. Rev. **D41**, 3464 (1990), Erratum hep-ph/9511250.

[125] A. Denner, H. Eck, O. Hahn, and J. Kublbeck, Nucl. Phys. **B387**, 467 (1992).

[126] AGASA, S. Yoshida *et al.*, (2001), Prepared for the 27th International Cosmic Ray Conference (ICRC 2001), Hamburg, Germany, 7-15 Aug 2001.

[127] A. R. Jacobson, S. O. Knox, R. Franz, and D. C. Enemark, Radio Sci. **34**, 337 (1999).

[128] AMANDA, J. Ahrens *et al.*, Phys. Rev. **D66**, 012005 (2002), astro-ph/0205109.

[129] M. Ackermann *et al.*, Astropart. Phys. **22**, 127 (2004).

[130] IceCube, A. Achterberg *et al.*, (2005), astro-ph/0509330, Prepared for the 29th International Cosmic Ray Conference (ICRC 2005), Pune, India, 3-11 Aug 2005.

[131] Baikal, V. Aynutdinov *et al.*, Astropart. Phys. **25**, 140 (2006), astro-ph/0508675.

[132] P. Gorham *et al.*, Nucl. Instrum. Meth. **A490**, 476 (2002), hep-ex/0108027.

[133] P. W. Gorham *et al.*, Phys. Rev. Lett. **93**, 041101 (2004), astro-ph/0310232.

[134] ANTARES, J. A. Aguilar *et al.*, Astropart. Phys. **26**, 314 (2006), astro-ph/0606229.

[135] NEMO, P. Piattelli, Nucl. Phys. Proc. Suppl. **143**, 359 (2005).

[136] NESTOR, G. Aggouras *et al.*, Astropart. Phys. **23**, 377 (2005).

[137] L. D. Landau and I. Pomeranchuk, Dokl. Akad. Nauk Ser. Fiz. **92**, 735 (1953).

[138] A. B. Migdal, Phys. Rev. **103**, 1811 (1956).

[139] R. Gandhi, C. Quigg, M. H. Reno, and I. Sarcevic, Astropart. Phys. **5**, 81 (1996), hep-ph/9512364.

[140] IceCube, J. Ahrens *et al.*, Nucl. Phys. Proc. Suppl. **118**, 388 (2003), astro-ph/0209556.

[141] D. A. Morris and A. Ringwald, Astropart. Phys. **2**, 43 (1994), hep-ph/9308269.

[142] A. B. McDonald, C. Spiering, S. Schonert, E. T. Kearns, and T. Kajita, Rev. Sci. Instrum. **75**, 293 (2004), astro-ph/0311343.

[143] G. A. Askaryan, JETP **14**, 441 (1962).

[144] G. A. Askaryan, JETP **21**, 658 (1965).

[145] D. Saltzberg, Phys. Scripta **T121**, 119 (2005), astro-ph/0501364.

[146] S. P. Martin, In "Kane, G. L. (ed.): Perspectives on Supersymmetry" 1-98 (1997), hep-ph/9709356.

[147] G. F. Giudice and R. Rattazzi, Phys. Rept. **322**, 419 (1999), hep-ph/9801271.

[148] S. R. Coleman and J. Mandula, Phys. Rev. **159**, 1251 (1967).

[149] A. Brandenburg, L. Covi, K. Hamaguchi, L. Roszkowski, and F. D. Steffen, Phys. Lett. **B617**, 99 (2005), hep-ph/0501287.

[150] T. Jittoh, J. Sato, T. Shimomura, and M. Yamanaka, Phys. Rev. **D73**, 055009 (2006), hep-ph/0512197.

[151] B. C. Allanach *et al.*, Eur. Phys. J. **C25**, 113 (2002), hep-ph/0202233.

[152] W. Buchmüller, K. Hamaguchi, M. Ratz, and T. Yanagida, Phys. Lett. **B588**, 90 (2004), hep-ph/0402179.

[153] K. Hamaguchi, Y. Kuno, T. Nakaya, and M. M. Nojiri, Phys. Rev. **D70**, 115007 (2004), hep-ph/0409248.

[154] J. L. Feng and B. T. Smith, Phys. Rev. **D71**, 015004 (2005), hep-ph/0409278.

[155] K. Hamaguchi and A. Ibarra, JHEP **02**, 028 (2005), hep-ph/0412229.

[156] I. Albuquerque, G. Burdman, and Z. Chacko, Phys. Rev. Lett. **92**, 221802 (2004), hep-ph/0312197.

[157] I. F. M. Albuquerque, G. Burdman, and Z. Chacko, (2006), hep-ph/0605120.

[158] M. H. Reno, I. Sarcevic, and S. Su, Astropart. Phys. **24**, 107 (2005), hep-ph/0503030.

[159] X.-J. Bi, J.-X. Wang, C. Zhang, and X.-m. Zhang, Phys. Rev. **D70**, 123512 (2004), hep-ph/0404263.

[160] I. F. M. Albuquerque, (2006), hep-ph/0612090, To appear in the proceedings of "Exotic Physics with Neutrino Telecopes", Uppsala, Sweden, September 20-22, 2006.

[161] B. C. Allanach, Comput. Phys. Commun. **143**, 305 (2002), hep-ph/0104145.

[162] Y. Huang, M. H. Reno, I. Sarcevic, and J. Uscinski, Phys. Rev. **D74**, 115009 (2006), hep-ph/0607216.

[163] J. Beacom, private communication.

[164] H. Pagels and J. R. Primack, Phys. Rev. Lett. **48**, 223 (1982).

[165] D. G. Cerdeño, K.-Y. Choi, K. Jedamzik, L. Roszkowski, and R. Ruiz de Austri, JCAP **0606**, 005 (2006), hep-ph/0509275.

[166] F. D. Steffen, JCAP **0609**, 001 (2006), hep-ph/0605306.

[167] D. J. H. Chung *et al.*, Phys. Rept. **407**, 1 (2005), hep-ph/0312378.

[168] IceCube, M. Ackermann *et al.*, Nucl. Phys. Proc. Suppl. **145**, 319 (2005).

[169] C. Spiering (IceCube Collaboration), private communication.

[170] S. Tremaine and J. E. Gunn, Phys. Rev. Lett. **42**, 407 (1979).

[171] Q. Shafi and F. W. Stecker, Phys. Rev. Lett. **53**, 1292 (1984).

[172] H. Sato and T. Tati, Prog. Theor. Phys. **47**, 1788 (1972).

[173] S. R. Coleman and S. L. Glashow, Phys. Rev. **D59**, 116008 (1999), hep-ph/9812418.

[174] F. W. Stecker and S. L. Glashow, Astropart. Phys. **16**, 97 (2001), astro-ph/0102226.

[175] T. A. Jacobson, S. Liberati, D. Mattingly, and F. W. Stecker, Phys. Rev. Lett. **93**, 021101 (2004), astro-ph/0309681.

[176] T. Jacobson, S. Liberati, and D. Mattingly, Annals Phys. **321**, 150 (2006), astro-ph/0505267.

[177] F. W. Stecker, Astrophys. J. **228**, 919 (1979).

[178] W. Buchmüller, R. Rückl, and D. Wyler, Phys. Lett. **B191**, 442 (1987).

[179] M. A. Doncheski and R. W. Robinett, Phys. Rev. **D56**, 7412 (1997), hep-ph/9707328.

[180] L. A. Anchordoqui, C. A. Garcia Canal, H. Goldberg, D. G. Dumm, and F. Halzen, Submitted to Nucl. Instrum. Meth. **A** (2006) , hep-ph/0609214.

[181] G. Domokos and S. Nussinov, Phys. Lett. **B187**, 372 (1987).

[182] J. Bordes, H.-M. Chan, J. Faridani, J. Pfaudler, and S. T. Tsou, (1997), hep-ph/9705463.

[183] J. Bordes, H.-M. Chan, J. Faridani, J. Pfaudler, and S. T. Tsou, Astropart. Phys. **8**, 135 (1998), astro-ph/9707031.

[184] H. Aoyama and H. Goldberg, Phys. Lett. **B188**, 506 (1987).

[185] A. Ringwald, Nucl. Phys. **B330**, 1 (1990).

[186] O. Espinosa, Nucl. Phys. **B343**, 310 (1990).

[187] V. V. Khoze and A. Ringwald, Phys. Lett. **B259**, 106 (1991).

[188] A. Ringwald, Phys. Lett. **B555**, 227 (2003), hep-ph/0212099.

[189] F. Bezrukov, D. Levkov, C. Rebbi, V. A. Rubakov, and P. Tinyakov, Phys. Lett. **B574**, 75 (2003), hep-ph/0305300.

[190] A. Ringwald, JHEP **10**, 008 (2003), hep-ph/0307034.

[191] T. Han and D. Hooper, Phys. Lett. **B582**, 21 (2004), hep-ph/0307120.

[192] G. Domokos, S. Kovesi-Domokos, and P. T. Mikulski, Nucl. Phys. Proc. Suppl. **B91**, 3 (2001), hep-ph/0006328.

[193] G. Domokos, S. Kovesi-Domokos, W. S. Burgett, and J. Wrinkle, JHEP **07**, 017 (2001), hep-ph/0011156.

[194] W. S. Burgett, G. Domokos, and S. Kovesi-Domokos, Nucl. Phys. Proc. Suppl. **136**, 327 (2004), hep-ph/0409029.

[195] F. Cornet, J. I. Illana, and M. Masip, Phys. Rev. Lett. **86**, 4235 (2001), hep-ph/0102065.

[196] R. Emparan, M. Masip, and R. Rattazzi, Phys. Rev. **D65**, 064023 (2002), hep-ph/0109287.

[197] G. Domokos and S. Kovesi-Domokos, Phys. Rev. Lett. **82**, 1366 (1999), hep-ph/9812260.

[198] S. Nussinov and R. Shrock, Phys. Rev. **D59**, 105002 (1999), hep-ph/9811323.

[199] P. Jain, D. W. McKay, S. Panda, and J. P. Ralston, Phys. Lett. **B484**, 267 (2000), hep-ph/0001031.

[200] M. Kachelriess and M. Plümacher, Phys. Rev. **D62**, 103006 (2000), astro-ph/0005309.

[201] L. Anchordoqui *et al.*, Phys. Rev. **D63**, 124009 (2001), hep-ph/0011097.

[202] A. V. Kisselev and V. A. Petrov, Eur. Phys. J. **C36**, 103 (2004), hep-ph/0311356.

[203] A. Ringwald and H. Tu, Phys. Lett. **B525**, 135 (2002), hep-ph/0111042.

[204] M. Kowalski, A. Ringwald, and H. Tu, Phys. Lett. **B529**, 1 (2002), hep-ph/0201139.

[205] E.-J. Ahn, M. Cavaglia, and A. V. Olinto, Phys. Lett. **B551**, 1 (2003), hep-th/0201042.

[206] P. Jain, S. Kar, and S. Panda, Int. J. Mod. Phys. **D12**, 1593 (2003), hep-ph/0201232.

[207] L. A. Anchordoqui, J. L. Feng, and H. Goldberg, Phys. Lett. **B535**, 302 (2002), hep-ph/0202124.

[208] Z. Fodor, S. D. Katz, A. Ringwald, and H. Tu, Proc. of the 10th M. Grossmann Meeting (2003), hep-ph/0402102.

[209] G. Burdman, F. Halzen, and R. Gandhi, Phys. Lett. **B417**, 107 (1998), hep-ph/9709399.

[210] M. Fukugita and T. Yanagida, Phys. Lett. **B174**, 45 (1986).

[211] W. Buchmüller, Lectures given at European School of High-Energy Physics (ESHEP 2001), Beatenberg, Switzerland (2002), hep-ph/0204288.

[212] P. G. Tinyakov, Int. J. Mod. Phys. **A8**, 1823 (1993).

[213] R. Guida, K. Konishi, and N. Magnoli, Int. J. Mod. Phys. **A9**, 795 (1994), hep-ph/9311219.

[214] V. A. Rubakov and M. E. Shaposhnikov, Usp. Fiz. Nauk **166**, 493 (1996), hep-ph/9603208.

[215] N. Arkani-Hamed, S. Dimopoulos, and G. R. Dvali, Phys. Lett. **B429**, 263 (1998), hep-ph/9803315.

[216] N. Arkani-Hamed, S. Dimopoulos, and G. R. Dvali, Phys. Rev. **D59**, 086004 (1999), hep-ph/9807344.

[217] K. S. Thorne, In "J. R. Klauder: Magic Without Magic", San Francisco 1972, 231-258.

[218] AGASA, K. Shinozaki, Nucl. Phys. Proc. Suppl. **151**, 3 (2006).

[219] J. Kwiecinski, A. D. Martin, and A. M. Stasto, Phys. Rev. **D59**, 093002 (1999), astro-ph/9812262.

[220] EGRET, P. Sreekumar *et al.*, Astrophys. J. **494**, 523 (1998), astro-ph/9709257, A lower extragalactic contribution to the γ ray background, by roughly a factor two, has been proposed by Refs. [82, 83]. The cascade limit may therefore be stronger by the corresponding factor.

[221] L. A. Anchordoqui, Z. Fodor, S. D. Katz, A. Ringwald, and H. Tu, JCAP **0506**, 013 (2005), hep-ph/0410136.

[222] K. S. Capelle, J. W. Cronin, G. Parente, and E. Zas, Astropart. Phys. **8**, 321 (1998), astro-ph/9801313.

[223] S. Hannestad, Phys. Rev. **D61**, 023002 (2000), astro-ph/9911330.

[224] H. Goldberg and T. J. Weiler, Phys. Rev. **D59**, 113005 (1999), hep-ph/9810533.

[225] V. Berezinsky, A. Gazizov, and M. Kachelriess, Phys. Rev. Lett. **92**, 231101 (2006), astro-ph/0612247.

[226] P. G. Tinyakov and I. I. Tkachev, JETP Lett. **74**, 445 (2001), astro-ph/0102476.

[227] P. G. Tinyakov and I. I. Tkachev, Astropart. Phys. **18**, 165 (2002), astro-ph/0111305.

[228] H. Tu, *Ultrahigh energy cosmic neutrinos and physics beyond the Standard Model*, PhD thesis, DESY and University Hamburg, DESY-THESIS-2004-018, 2004.

Acknowledgments

I would like to take the opportunity to thank all the people who supported me during my doctoral work.

First of all, I am very grateful to my supervisor, Andreas Ringwald, for his continuous support and encouragement. It was an enjoyable and instructive time.

I would like to thank Jan Louis and Jochen Bartels for refereeing my thesis and defense. I appreciate all their effort.

Thanks to Jan "H-man" Hamann, Tobias Kleinschmidt and Lily Schrempp for carefully reading the draft of my thesis.

I am indebted to my collaborators, Luis Alfredo Anchordoqui, Haim Goldberg, Francis Halzen, Jörn Kersten, Andreas Ringwald, Huitzu Tu, and Tom Weiler, for sharing their knowledge with me and for their great support. I would also like to thank Zoltan Fodor, Jan Hamann, Steen Hannestad, Dan Hooper, Sandor Katz, Tobias Kleinschmidt, Lily Schrempp, Christian Spiering, and Frank Steffen for their support and discussions.

Thanks to office 301, Jens Kösling, Christoph "Toffi" Lüdeling, Maik Petermann, Jonas Schmidt, Jan "König" Wennekers, and Sören Wiesenfeld for the skat games and other distractions.

I would like to thank all the members of the DESY theory group for the enjoyable atmosphere.

I am extremely grateful for the love and continuous support from my family and friends.